Aus dem Bereich Medizinische Biochemie und Molekularbiologie
Theoretische Medizin und Biowissenschaften
der Medizinischen Fakultät
der Universität des Saarlandes, Homburg/Saar

Potential role of MIC25 in mitochondrial remodelling during neuronal development

Dissertation zur Erlangung des Grades eines Doktors der Medizin
der Medizinischen Fakultät der
UNIVERSITÄT DES SAARLANDES
2026

vorgelegt von: Katrin Leister
geb. am: 06.04.2000 in Backnang

Tag der Promotion: 06.05.2026
Dekan: Prof. Dr. med. dent. Matthias Hannig
Berichterstatter: Prof. Dr. Martin van der Laan
Prof. Dr. Dieter Bruns

Table of Contents

1. Summary

Mitochondria are known as organelles responsible for providing energy to the cell, to fuel all daily activities. Mitochondrial inner membranes increase surface area by forming intricate folds, the so-called cristae. Different protein distributions across cristae mark different membrane regions: oligomeric F_1F_o-ATP synthase complexes at the tips, proteins of the electron transport chain along the sides, and the mitochondrial contact site and cristae organising system (MICOS) at crista junctions that form a transition zone between cristae and the inner boundary membrane. The MICOS complex is organised into a MIC60- and MIC10-subcomplex harbouring MIC60, MIC19 and MIC25 as components of the former, and MIC10, MIC26, MIC27 and QIL1 of the latter. MICOS is required to maintain the strong negative membrane curvature at crista junctions and to form elaborate supercomplexes with proteins of the outer mitochondrial membrane. Such networks of partner proteins implicate MICOS in vital processes, like mitochondrial protein import and metabolite homeostasis.

As knowledge about the MICOS complex increases, questions about tissue-specific properties and its adaptation to special energy quests are arising. Previous data from our research group indicated that the MIC25 subunit of MICOS was explicitly upregulated in brain tissue samples of mice. This work makes use of a human neuroblastoma cell line (SH-SY5Y) to gain insights into structural, and functional changes of mitochondrial membrane shaping complexes during differentiation of SH-SY5Y cells into consecutive neuronal states. A major focus was the behaviour of the candidate protein MIC25, which was studied in SH-SY5Y as well as in human embryonic kidney cells (HEK293T) for comparison.

My data reveal significantly increased expression levels of MIC25 in SH-SY5Y cells upon differentiation in line with a role of MIC25 in mitochondrial adaptive responses during neuronal development. Remarkably, changes in MIC25 expression were found to be independent of the levels of other MICOS-subunits. Analysis of mitochondrial protein complexes by native electrophoresis and immunoprecipitation disclosed, that MIC25 was increasingly incorporated into the mitochondrial intermembrane space bridging (MIB) complex formed by MICOS and the SAM complex of the outer membrane. Bioenergetic measurements revealed that differentiated SH-SY5Y cells lacking MIC25 exhibit a reduced spare capacity for oxygen consumption, increased glycolytic activity and hyperpolarisation of mitochondrial inner membranes. By contrast, MIC25-deficient HEK293T cells showed no measurable differences in OXPHOS performance, but a moderate drop in membrane potential.

In summary, my work sheds first light on the differential behaviour and specific features of MICOS, specifically MIC25, in different cell types and tissues. It strengthens the idea that the MIC25 subunit may have a specific role in neuronal cells and/or neuronal tissue development. Further experiments will show, how loss of MIC25 affects specific cellular properties and responses during adaptive cellular processes and what triggers the strong induction of MIC25 in early developmental phases.

Zusammenfassung

Mitochondrien sind als jene Zellorganellen bekannt, die Energie für nahezu alle zellulären Prozesse bereitstellen. Die innere Membran der Mitochondrien formt Einstülpungen, die sogenannten *Cristae*, welche die Oberfläche vergrößern. Entlang dieser C*ristae* lassen sich verschiedene Proteinverteilungen feststellen: oligomerische F_1F_o-ATP Synthasen befinden sich an den Spitzen, die Proteine der Atmungskette entlang der Seiten, und der *Mitochondrial Contact Site and Cristae Organising System* (MICOS)-Komplex im Bereich der C*rista Junction*, dem Übergang zwischen C*ristae* und der inneren Grenzmembran der Mitochondrien. Der MICOS-Komplex organisiert sich in einen MIC60- und MIC10-Subkomplex. Während zum MIC60-Subkomplex MIC60, MIC19 und MIC25 gezählt werden, werden MIC10, MIC26, MIC27 und QIL1 zum MIC10-Subkomplex gerechnet. MICOS ist von Bedeutung dafür, die negative Krümmung der inneren Mitochondrienmembran im Bereich der C*rista Junctions* aufrechtzuerhalten, sowie gemeinsam mit Proteinen der äußeren Mitochondrienmembran Superkomplexe zu bilden. Darüber hinaus ist MICOS am Proteinimport sowie an der Regulation ausgeglichener metabolischer Profile beteiligt.

Mit dem Wissenszuwachs über MICOS entwickeln sich neue Forschungsfragen zu gewebsspezifischen Eigenschaften und der Anpassung an zellspezifische Energiebedarfe des Komplexes. Bereits erhobene Daten aus unserer Forschungsgruppe weisen darauf hin, dass die MIC25-Untereinheit von MICOS spezifisch in Gewebeproben von Mausgehirnen verstärkt exprimiert wird. Dabei untersucht diese Arbeit strukturelle und funktionelle Veränderungen der Mitochondrienmembran-gestaltenden Proteinkomplexe. Menschliche Neuroblastomzellen (SH-SY5Y) wurden hierfür zu adulten Neuronen differenziert. Dabei lag der Fokus auf dem Protein MIC25, dessen Eigenschaften in SH-SY5Y und *Human Embryonic Kidney Cells* (HEK293T) verglichen wurden.

Meine Arbeit zeigt eine signifikant erhöhte Expression von MIC25 in differenzierten SH-SY5Y-Zellen, die auf eine Rolle von MIC25 bei der Anpassung von Mitochondrien an die Umgebung während neuronaler Entwicklungsprozesse hindeutet. Es ist bemerkenswert, dass die verstärkte Expression von MIC25 unabhängig von den Expressionsniveaus der anderen Proteine des MICOS-Komplexes war. Die Auswertung von mitochondrellen Proteinkomplexen mittels Elektrophorese und Immunopräzipitation ergab, dass MIC25 verstärkt in den M*itochondrial Intermembrane Space Bridging* (MIB)-Komplex eingebaut wird, welcher durch MICOS und den sogenannten SAM-Komplex der äußeren Mitochondrienmembran gebildet wird. Bioenergetische Messungen ergaben, dass differenzierte SH-SY5Y Zellen mit verminderter Expression von MIC25 eine reduzierte relative Reservekapazität für den Sauerstoffverbrauch, erhöhte Glykolyseaktivität und Hyperpolarisation des Membranpotenzials der inneren Mitochondrienmembran haben. HEK293T-Zellen mit verminderter Expression von MIC25 zeigten keine Unterschiede in der Funktion der Atmungskette, allerdings eine Verminderung des Membranpotenzials.

Zusammenfassend liefert diese Arbeit erste Einblicke in die zell- und gewebespezifischen

Eigenschaften des MICOS-Komplexes im Allgemeinen und von MIC25 im Speziellen. Sie bestärkt die These, dass MIC25 eine individuelle Rolle in neuronalen Zellen und/oder deren Entwicklung spielt. Das Ziel weiterer Forschung wird es sein zu zeigen, wie der Expressionsverlust von MIC25 verschiedene Zelleigenschaften und Anpassungsprozesse beeinflusst. Eine zentrale anschließende Frage lautet, welche Faktoren die starke Expressionszunahme von MIC25 in frühen Entwicklungsstadien auslösen.

2. Introduction

2.1. Mitochondria are structurally and functionally complex organelles

When people are asked what they associate with mitochondria, the most common answer will probably be that they are the "powerhouses of the cell". Even though energy provision is a major function of mitochondria, they are also responsible for essential metabolic functions, like calcium homeostasis, signalling cascades and initiation of apoptosis [36,49,174]. Their structural and functional diversity is explained by the endosymbiont theory. It proposes that eukaryotic cells evolved from prokaryotic archaea-like cells that engulfed bacteria and developed them into mitochondria (and chloroplasts) over time [9,69,71,212]. Mitochondria possess their own circular DNA, they have their own ribosomes for protein biosynthesis and can fuse and divide independently from their host cell [9,69,71,212]. Initial phylogenetic reconstructions identified α-proteobacteria, presumably the order of Rickettsiales, as an early origin [29,70,220]. Early symbionts probably possessed more than 630 distinct protein-coding genes [50,61]. Most of these genes have been transferred from the mitochondrial DNA (mtDNA) to nuclear chromosomes [50,61]. The current human mtDNA encodes 37 genes in total, of which 13 encode mRNA, and thus polypeptides [230]. 22 genes encode tRNAs and two rRNAs [230]. Amongst the 13 protein-coding genes are the particularly hydrophobic core subunits of oxidative phosphorylation complexes I, III, IV and V (F_1F_o-ATP synthase) [230]. All encoded tRNAs and rRNAs help to establish a translational apparatus to manufacture these 13 peptides [230]. Hence, most mitochondrial proteins are encoded by nuclear DNA. Their genes are transcribed in the nucleus, and upon maturation of the encoded mRNA, the respective proteins are synthesised on free ribosomes in the cytosol [72]. For targeting to and importing into different mitochondrial compartments, they contain specific sequence information (see below).

Believed to be another relic of its procaryote origin, mitochondria are composed of two lipid bilayers forming the outer and inner mitochondrial membrane (OMM and IMM) [144]. The OMM sheathes the intermembrane space (IMS), the IMM sheathes the mitochondrial matrix [144]. Within the mitochondrial matrix, circular mitochondrial DNA is organised into nucleoids [144]. As illustrated in Figure 1, the IMM is further sub-divided into the inner boundary membrane (IBM), close to the OMM, and crista membranes (CM), that create folds with a range of sizes and shapes into the matrix [159,168]. Crista junctions (CJs) are narrow tubular constructions connecting cristae to the IBM [168]. The IBM interacts with the OMM in various ways, most notably through morphological contact sites – a structural connection able to withstand mechanical forces such as osmotic shrinkage [168,207]. Functionally, IBM and OMM contacts facilitate transport of high energy metabolites via the adenine nucleotide translocase (ANT), mitochondrial creatine kinase (mtCK) and voltage-dependent anionic channel (VDAC or porin) [49,168]. Moreover, OMM-IBM contact sites are proposed to be required for efficient remodelling of the OMM in yeast [59,168].

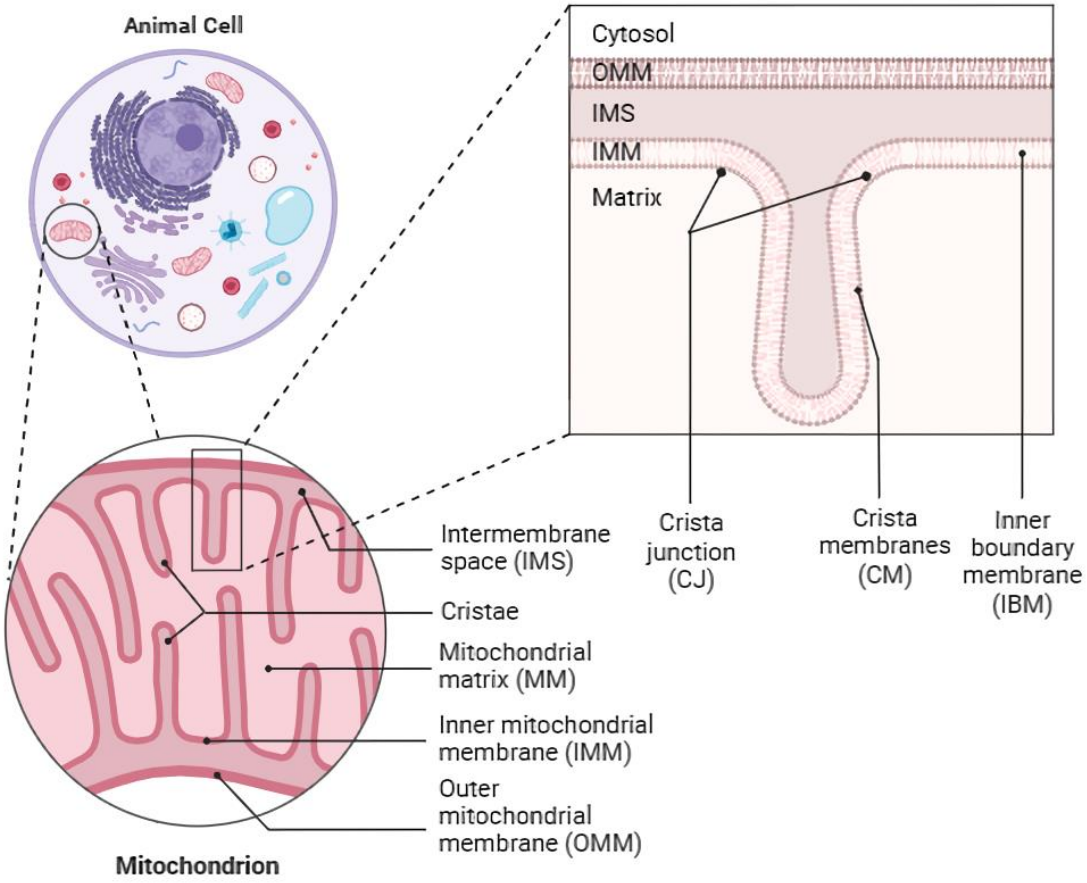

Figure 1 Organisation of mitochondrial membranes in eukaryotic cells

The organisation of eukaryotic mitochondria represents a highly ordered construct enabling structural and functional sub-compartmentalisation. The outer mitochondrial membrane (**OMM**) represents the outer barrier of mitochondria towards the cytosol; the inner mitochondrial membrane (**IMM**) encases the mitochondrial matrix at the centre of mitochondria. Both OMM and IMM enclose the intermembrane space (**IMS**). The IMM is divided further into the inner boundary membrane (**IBM**), which is closest to the OMM, and crista membranes (**CM**), that form invaginations into the matrix, called **cristae**. Crista junctions (**CJ**) encompass narrow, tubular-like structures that form the transition between IBM and CM.
Figure 1 was created with BioRender.com.

Due to compartmentalisation of the IMM, its protein composition is not uniform [207,225]. As explained above, the IBM contains proteins that are needed to facilitate preprotein transport into the IMS and matrix. Conversely, crista membranes harbour proteins of the respiratory chain complexes and F_1F_o-ATP synthase [203]. However, exchange of proteins between both IMM compartments is possible, adapting mitochondrial needs to its surrounding metabolic conditions [203]. The integral IMM protein insertase Oxa1 represents an interesting example, because in yeast cells its distribution between IBM and CM depends on the growth conditions [195,203]. During fermentation, Oxa1 is mostly present in the IBM, whereas during respiratory growth conditions it is largely found in the CM [195].

Not only protein composition differs between IBM and CM. Structurally, CMs make up the overwhelming part of the IMM by forming deep invaginations that increase the surface area

[57,126,127]. The arrangement of CMs correlates with metabolic activity of the cell – increased surface area leads to increased respiratory activity [190]. For example, in mouse mammary gland mitochondria, the change from pregnancy to lactation is accompanied by an increase in density of mitochondria reflecting IMM expansion [170]. Hence, CMs differ in packing density and/or structural composition depending on the tissue of origin and metabolic state [190]. The most prevalent shape of CMs are leaf-like extensions into the MM [190,207], but tubular (e.g., zona glomerulosa of rat adrenal cortex [216]), lamellar (e.g., zona glomerulosa of ox [161]), circular (e.g., brown fat tissue in hibernating squirrels [74]), or even triangular shapes (e.g., in bat muscle [169]) have been observed.

As mitochondria are structurally and functionally diverse, defective mitochondrial processes become apparent in a variety of ways. Collectively termed as mitochondriopathies, those defects can manifest at any age or in any tissue [231]. They can be the consequence of mutations of the nuclear genome or mtDNA, and can be inherited maternally, autosomal dominantly, autosomal recessively, or X-chromosomally [231]. Primary defects of mtDNA are inherited maternally, as mitochondria are consistently inherited through the female line, or occur sporadically [231]. Secondary defects of mtDNA arise due to mutations of the nuclear genome in genes that are essential for maintaining mtDNA [231]. These are inherited autosomally or X-linked [231]. As the majority of mitochondrial proteins are nuclear-encoded (see above), most mitochondriopathies result from mutations in the nuclear DNA [231]. These mutations can affect oxidative phosphorylation complexes, their assembly factors, mitochondrial protein synthesis and import, or phospholipid metabolism [231]. Typical mitochondriopathies are e.g., MELAS (mitochondrial encephalopathy, lactic acidosis, stroke-like episodes), LHON (Leber's hereditary optic neuropathy), KSS (Kearns–Sayre syndrome, affecting the skeletal muscle, brain, heart, and eye) and LS (Leigh syndrome, affecting the brain, eye, skeletal muscle, and peripheral nerves) [231]. Henceforth, mitochondriopathies show up with a wide range of symptoms, often delaying diagnosis [68]. Even though next generation sequencing has provided possibilities of genetic diagnosis, causative therapy remains an unsolved challenge [68].

2.2 Mitochondrial cristae exhibit sub-compartmentalisation

The extraordinary effectiveness of mitochondrial respiration is the result of the evolution of mitochondrial shape and ultrastructure [36,120,135]. According to the endosymbiont theory, intracytoplasmic membranes of α-proteobacteria, functionally responsible for harnessing energy, became cristae of todays' mitochondria [139]. Crista membranes (CMs) form small functional units that enrich molecules [128], localise proton gradients [221] and hinder the unintended release of signalling entities such as cytochrome c, which plays a major role during apoptosis [36]. Those functional units are upheld by crista junctions (CJs) that form tubular neck-like structures [207,225]. CJs separate the intermembrane space (IMS) encased by the outer mitochondrial membrane (OMM) and inner boundary membrane (IBM) from the intracristal space limited by crista membranes [207,225].

CMs harbour proteins of the respiratory chain complexes and F_1F_o-ATP synthase (see Figure 2), however, their distribution is not uniform. Components of the electron transport chain, such as NADH-ubiquinone oxidoreductase (NADH-dehydrogenase, complex I), succinate dehydrogenase (SDH, complex II), cytochrome c reductase (complex III) and cytochrome c oxidase (complex IV), are preferentially located in the flat laminar parts of CMs [42]. F_1F_o-ATP synthases concentrate at cristae rims and edges [42]. Respiratory chain complexes establish a proton gradient across the IMM by oxidising reduced co-factors, like NADH or $FADH_2$ [205]. Movement of protons along this gradient into the matrix drives ATP production by F_1F_o-ATP synthase, fuelling virtually all energy-dependent cellular functions [205].

Through blue native-polyacrylamide gel electrophoresis (BN-PAGE) experiments Schägger et al. discovered that respiratory chain complexes form supercomplexes [182]. Later, data from electron microscopy [181] and electron cryo-tomography [44] led to the identification of stable assemblies containing complexes I, III and IV. Henceforth, the existence of respiratory chain supercomplexes is now broadly recognised, but controversies about their true benefit to cells persist. In *Paracoccus dentrificans*, complex I is steadied by supercomplex formation of complex I, III and IV [197]. Therefore, co-location of free complexes and formation of supercomplexes seems to stabilise or even assists complex assembly. Different studies describe a relationship between the amount of supercomplexes present and changes of metabolic state (e.g., in heart mitochondria of mice [242]), mitochondrial shape (e.g., *in vivo* in mice and *in vitro* in HEK293T cells [35]) or mitochondrial dysfunction (e.g. in neonatal encephalomyopathy because of complex III deficiency resulting in defective supercomplex assembly [54]). However, to what extend development of these diseases can really be attributed to supercomplex assembly defects remains unclear. The hypothesis that respiratory chain supercomplexes reduce the generation of reactive oxygen species (ROS) is supported by data revealing that complex I is integrated into supercomplexes to a greater extent in neuronal cells than in astrocytes [122]. Those neurons exhibit reduced levels of ROS [122]. Another interesting proposal has been made by Blaza et al. [20]: Due to the high protein:lipid ratio in CMs, proteins are at risk of forming strong and irreversible protein-protein interactions. To prevent aggregation and consecutively loss of function, weak interactions between the single complexes might have evolved. This leads to the thought that supercomplex formation is on the one hand a result of structural properties of CMs, and on the other hand actively responsible for maintaining its structural and functional integrity.

As mentioned above, F_1F_o-ATP synthase complexes, located at cristae rims of mitochondria, contribute to cristae membrane shaping. The F_1F_o-ATP synthase is highly conserved form bacteria to eukaryotic cells, and all mammals harbour a common structure of the cytoplasmic F_1 "head" domain (9 subunits) that is connected to a membrane-bound F_o module [143,211]. F_o consists of subunits termed a and c, that ultimately transform the energy stored in the proton gradient to generate a chemical bond during ATP synthesis [143,211]. Proton movement through the IMM transmits energy to a pivot (γ, δ and ε

subunits of F_1) causing conformational changes in F_1 and ATP synthesis through ADP phosphorylation [143]. Furthermore, the role of ATP synthase and shaping of mitochondrial membranes will be assessed below.

2.3. Shaping inner mitochondrial membranes marries form with function

One of the best examples for alliance of structure and function are mitochondrial inner membranes. Their architecture supports energy metabolism, transfer of molecules and conveys communication with other organelles [157]. F_1F_o-ATP synthase does not only accumulate at rims of cristae (see Figure 2 or chapter 2.2) but is actively shaping and maintaining its compartment by forming dimers and ribbons that bend crista membranes [143]. ATP synthase dimer interfaces form conic-like shapes and induce strong bending of membranes [78,133]. Quantitative analysis of molecular simulations indicates that ribbon-formation of F_1F_o-ATP synthase dimers occurs spontaneously easing elastic tension of CMs [10]. Yeast mutants lacking F_1F_o-ATP synthase dimer interface proteins, CMs form onion-like shapes and growth rates are reduced significantly [43,154]. Additional functions of F_1F_o-ATP synthase such as maintaining the mitochondrial membrane potential and proton trapping have been described [24,41,43].

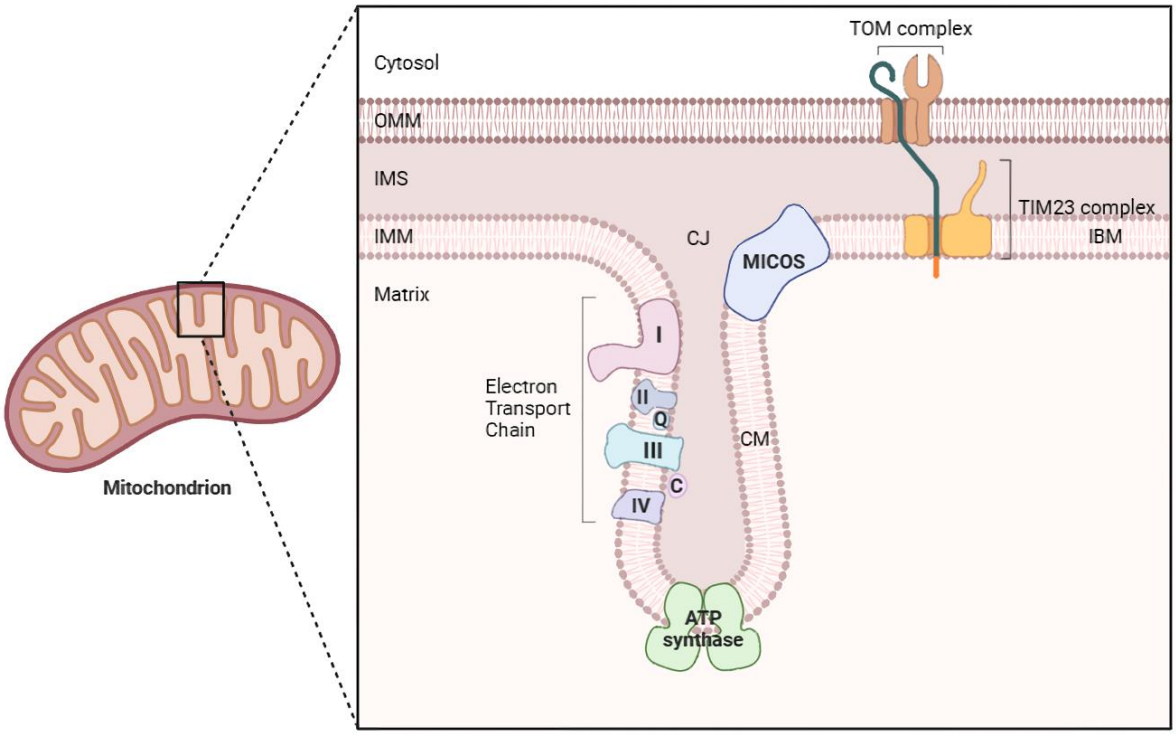

Figure 2 Organisation of protein complexes within mitochondrial membranes

Protein complexes of mitochondrial membranes are found at characteristic locations. **ATP synthase** (**green**) preferentially accumulates at cristae rims, complexes **I** (**red**), **II** (**grey**), **III** (**turquoise**) and **IV** (**purple**) together with coenzyme Q (**Q**) and cytochrome c (**C**) of the electron transport chain at crista membranes (**CM**) of mitochondrial cristae. Chiefly, the mitochondrial contact site and cristae organising system (**MICOS, blue**) is found at crista junctions (**CJ**). Protein complexes responsible for (pre-)protein import into mitochondria, the translocase of the outer membrane (**TOM, brown**) and translocase of the inner

membrane (**TIM23, yellow**), are respectively found in the outer mitochondrial membrane (**OMM**) and inner mitochondrial membrane (**IMM**), more precisely the inner boundary membrane (**IBM**), passing (pre-) proteins through the intermembrane space (**IMS**).
Figure 2 was created with BioRender.com.

The IMM hosts lipids of unique local distribution, as more than 50% of membrane lipids are cardiolipin (CL) and phosphatidylethanolamine (PE) classifying as so called "non-bilayer" phospholipids [90]. They are believed to form cone-like shapes, thereby helping to maintain high degrees of membrane curvature at minimal tension, as it is found in tips and rims of the highly folded IMM [90]. Accordingly, CL and PE are enriched in the lipid monolayer of the IMM that is negatively curved [90]. Phosphatidylcholine (PC), phosphatidylinositol (PI) and phosphatidylserine (PS) rather segregate into the positively curved monolayer [90]. This asymmetric lipid composition assists in forming stable invaginations with high degrees of membrane curvature [90]. Experiments with CL-enriched giant unilamellar vesicles acting as a model for the IMM have demonstrated, that CL-facilitated membrane bending is supported by a pH gradient [109]. As a result of local pH changes, bending progressed, halted, or regressed accordingly in this *in-vitro* study [109]. *In vivo*, the respiratory chain complexes and F_1F_O-ATP synthase are responsible for generating and consuming pH gradients [109]. Such compartmentalisation leads to locally different pH gradients that support IMM bending [109]. Another *in-vitro* study provided evidence, that negative IMM curvature and CL accumulation facilitate each other [16]. CL likely attracts conic-shaped proteins to sites of membranes with high membrane curvature [2,189]. Henceforth, bilateral influences of lipid-protein interactions seem to facilitate IMM bending in a feed forward loop, respectively driving the stepwise formation of cristae.
OPA1 (optic atrophy 1), a dynamin-like GTPase encoded by nuclear DNA, has been identified as essential for IMM bending [124]. Assembled in the cytosol and shuttled to mitochondria via a N-terminal target sequence, OPA1 exists in eight different splicing variants processed depending on tissue-specific requirements [92,124]. Two metalloproteases, YME1L and OMA1, act as regulatory knob for OPA1 by cleaving it into long- (l-) and soluble- (s-)OPA1 forms [73,83,92]. Balance between both forms is crucial for fusion and fission activity of mitochondria [124]. Mitochondrial fusion is the process by which mitochondria merge with each other to e.g. facilitate exchange of mtDNA or adapt their function to different metabolic states of the cell [210,232]. During mitochondrial fusion, l-OPA1 merges the IMM either by interacting with more l-OPA1 or with cardiolipin [64]. Mitochondrial fission is the process, where mitochondria divide into separate entities to increase their number [210,232]. Fission also fulfils an essential part in maintaining mitochondrial quality through removal of damaged mitochondria [210,232]. Processing of OPA1 is the result of metabolic states: YME1L increases cleavage with elevated oxidative phosphorylation activity [134]. Cellular stress triggers OMA1 activity leading to increased mitochondrial fission and fragmentation [52,83]. Either complete loss or excess cleavage of OPA1 destabilises the IMM by directly promoting cytochrome c release and apoptosis [98,145,153]. Discovered in 2000, the gene of OPA1 was identified as mutational locus of autosomal

dominant optic atrophy (ADOA) [4]. ADOA leads to degeneration of ganglion cells of the retina trailed by atrophy of the optic nerve manifesting clinically as progressive vision loss and scotoma within the first two decades of life [4]. Beyond affecting the retina, OPA1 mutations have also been linked to myopathy, deafness, peripheral neuropathy, and Parkinson-like characteristics [27]. Emerging evidence suggests a developmental role of OPA1. OPA1-deficient iPSCs (induced pluripotent stem cells) differentiating into dopaminergic neurons revealed mitochondrial fragmentation and neuronal loss, resembling patterns seen in neurodegeneration [101].

Different proteins, protein complexes and lipids (and their interactions!) are insurmountable for shaping the IMM, adapting it to its metabolic needs. Thus, mitochondrial morphology represents a spectrum from hyperfused, highly continuous structures to hypertubulated, fragmented structures as the result of fusion and fission activities of the OMM and IMM respectively in response to metabolic conditions [210]. Availability of nutrients, level of cellular stress and oxidative phosphorylation activity tip the tide towards mitochondrial hyperfusion or fragmentation, depending on which conditions prevail [210].

2.4. MICOS and associated proteins remodel mitochondrial crista morphology

Next to mitochondrial crista membrane tips, crista junctions are areas of high membrane curvature harbouring an evolutionary retained multi-protein complex termed mitochondrial contact site and cristae organising system (MICOS, see Figure 3) [138]. The gene of mitofilin (IMMT in mammals), later termed Mic60/MIC60, was cloned for the first time in 1994 [200]. Due to its high expression rates in heart muscle, MIC60 was initially described as a hypothetical motor protein [200]. In 2005, MIC60 was first reported to play a crucial role in organizing the IMM, as cristae of HeLa cells lacking MIC60 formed dense stacks of membrane sheets rather than the typical tubular or vesicular morphology [99]. Six years later, proteins apart from Mic60 belonging to MICOS in yeast were identified independently by three different approaches [80,87,208]. Using quantitative genetic interaction mapping of mitochondria, Hoppins et al. [87] described five proteins besides Mic60 comprising MICOS. Harner et al. [80] designed a fusion protein spanning both mitochondrial membranes to mark mitochondrial contact sites. Membrane fractions were separated by density gradients and those localising with the marker were exposed to quantitative mass spectrometry [80]. This revealed six co-localising MICOS proteins at contact sites [80]. Lastly, von der Malsburg et al. [208] Protein-A-tagged Mic60, performed differential isotope labelling followed by affinity purification and subjected the elution fractions to mass spectrometry. This approach identified six MICOS proteins interacting with translocases of the outer membrane [208]. Next to Mic60/MIC60, proteins discovered were later termed Mic10/MIC10, Mic12/QIL1, Mic19/MIC19, Mic26/MIC26 and Mic27/MIC27 in yeast/mammals respectively [80,87,158,208]. In mammals, thanks to MIC25, a paralog of MIC19, MICOS consists of at least seven genuine subunits [89,158].

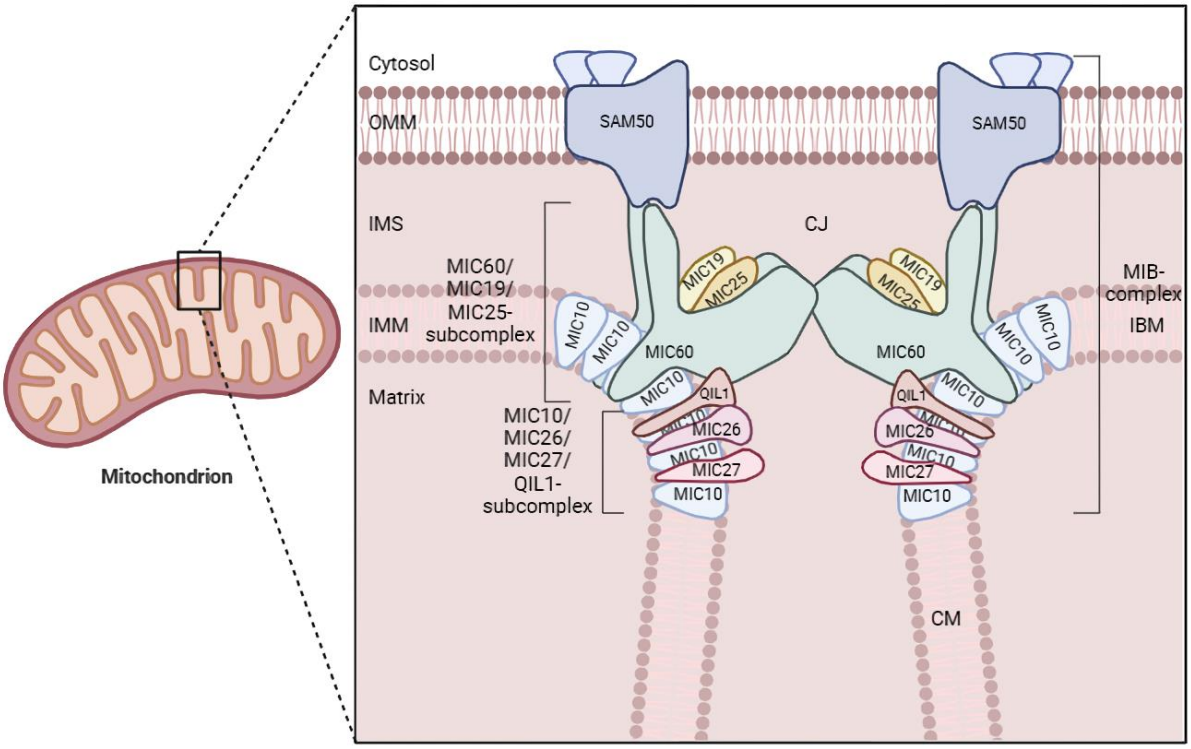

Figure 3 Organisation of MICOS-, SAM-, and MIB-complex at mitochondrial crista junctions

The mitochondrial contact site and crista organising system (MICOS) is located at mitochondrial crista junctions (**CJ**) of the inner mitochondrial membrane (**IMM**), connecting the inner boundary membrane (**IBM**) with the crista membrane (**CM**) of the inner mitochondrial membrane (**IMM**). MICOS is comprised of seven subunits in mammals, which organise in a hierarchical fashion: the core subunit MIC60 (**green**) forms a subcomplex together with MIC19 (**yellow**) and MIC25 (**orange**), the core subunit MIC10 (**light blue**) oligomerises at crista junctions and forms the second subcomplex together with MIC26 (**purple**), MIC27 (**red**), and QIL1 (**brown**). The SAM-complex (**dark blue**), located in the outer mitochondrial membrane (**OMM**), stably interacts with MICOS, thus bridging the intermembrane space (**IMS**) and forming the mitochondrial intermembrane space bridging (MIB) complex.
Figure 3 was created with BioRender.com.

MICOS is composed of two subcomplexes, the MIC60- and the MIC10-subcomplex (see Figure 3) [163,224]. MIC60 associates with MIC19 and MIC25 to form the MIC60-MIC19-MIC25 subcomplex widely accepted as bridging the IMS and interacting with protein complexes of the OMM [58,76,80,87,208,228]. MIC60 possesses an N-terminal sequence targeting it to mitochondria, which is succeeded by a segment anchoring it in the IMM and its largest, hydrophilic domain exposed to the IMS [162]. A coiled-coiled (CC) domain, lipid-binding sites, and a C-terminal domain (or mitofilin domain) are found in the IMS region [84,162]. Recently, structural insight into domains of MIC60 has been provided. MIC60 forms tetrameric arrangements, as one CC domain aligns with another CC domain in an antiparallel manner [21]. Two of such elements form an elongated X-shape, putatively spanning crista junctions [21]. Further towards the C-terminus, mitofilin domains dimerise at opposite ends of the X forming convex shapes [21]. This complements the concave shape of the IMM surface at cristae rims [21]. Furthermore, two lipid binding sites have been identified which are believed to facilitate stabilisation and shaping of crista junctions via an amphipathic profile [84]. Functions of

MIC60 in remodelling crista junctions apart from solely bridging the IMS have been described explaining homogenous diameters of crista junctions with the (adjustable) extension of MIC60-tetramers [21,84]. MIC19 likely supports tetramerisation of the CC domains and controls the dynamic remodelling of crista junctions [21,84]. The C-terminal coiled-coil helix coiled-coil helix (CHCH) domain of MIC19 binds to a region of the mitofilin domain of MIC60 further towards the N-terminus [84]. The CHCH domain encases a hairpin region by two cysteine motifs forming intramolecular disulfide bonds potentially regulating MICOS in a redox-dependent manner [177]. Now, the N-terminal region of MIC19, together with parts of MIC60, is free to form extensions connecting OMM with IMM [21]. Targets for interaction with the OMM are the general preprotein translocase of the outer membrane (TOM) and sorting and assembly machinery (SAM) complexes essentially forming mitochondrial contact sites [21,80,147,208]. Excitingly, not only OPA1 can be cleaved by OMA1, but also the N-terminal region of MIC19 provides a cleavage site for this metalloprotease activated by metabolic stress emphasising the importance of the MIC60-subcomplex in contact site formation [199].

Like MIC19, MIC25 belongs to a family of CHCH proteins, more specifically to the twin Cx9C subfamily indicating their common ancestry, as both are orthologs to Mic19 in yeast [89]. Likely, MIC19 and MIC25 are a product of whole genome duplication at the very essence of vertebrate life [89]. Revealed by pulldown assays, MIC25 interacts with both MIC60 and MIC19, forming the MIC60-MIC19-MIC25 subcomplex of MICOS [6]. As 36% of amino acids between MIC19 and MIC25 are similar, the C-terminal CHCH domain in MIC25 has been identified as binding site for MIC60, like in MIC19 [6]. Hence, MIC19 and MIC25 share characteristics, but are not identical in form and function. Of note, MIC25 does not provide an N-terminal cleavage site for OMA1 [199], but MIC25 knockdown reduces cellular ATP levels, which has not been observed for MIC19 knockdown cells in the same set of experiments [6]. Knockdown of MIC25 does not reduce cellular MIC19 levels ruling out secondary effects. Hence cellular functions must be influenced independently by MIC19 and MIC25 [6]. Crosstalk with MIC60 appears to be depending on tissue specificities, as MIC25 knockdown downregulates MIC60 in some cell types more than in others [6]. Similarly, the picture of whether and how crista morphologies are influenced by loss of MIC25, is ambivalent. An et al. [6] and Ding et al. [47] observed changes, like fewer crista junctions and lower cristae density, which are not observed by Ott et al. [148]. However, to obtain these results, different approaches were used. An et al. [6] and Ott et al. [148] both knocked MIC25 down, the former in RKO and MCF7 cells, the latter in HeLa cells. Analysing knockdown efficiency, An et al. [6] exhibited superior results. Similarly, Ding et al. [47] used HeLa cells as target cells, but performed knockout assays with great success. Hence, comparability of these studies seems to be limited. Clearly, the task of MIC25 in mitochondrial structure and function has not been determined yet and provides hypothesises for the existence of tissue-specific profiles.

The MIC10 subcomplex is constituted of MIC10, MIC26, MIC27 and QIL1, and is associated with membrane bending activity [163,224]. The MIC10 protein is characterised by the presence of two transmembrane segments, each featuring glycine-rich sequence motifs [5]. A positively charged loop

linking the adjacent transmembrane segments is responsible for topologically correct insertion into the IMM [23,203]. The positively charged loop is ultimately localised in the matrix, whereas both C- and N-terminal ends are exposed to the IMS [23,203]. Such motifs rich in glycine residues have previously been associated with dimerisation and oligomerisation activity in lipid bilayers, like in Atp20 (subunit g), a protein required for dimerisation of ATP synthase [176]. Thus, Harner et al. [80] proposed the concept of homo-oligomerisation of MIC10 next to its integration into a larger hetero-proteinaceous complex. An experimental approach exchanging the conserved glycine with alanine residues reported altered cristae membrane architecture, whereas affinity purification of these Mic10 variants still allowed detection of all MICOS subunits [23]. Hence, the lack of Mic10 glycine motifs does not abolish interaction with other MICOS proteins [23]. Oligomerisation of Mic10 and induction of negative membrane curvature were impaired leading to irregularly shaped and highly connected cristae [23]. On top of this, MIC10 does not only play a crucial role in induction and maintenance of crista membrane curvature at crista junctions as a core component of MICOS but plays a second role in interacting with F_1F_o-ATP synthase independently of its oligomerisation abilities [166]. Thus, impairment of energy metabolism and growth by cells lacking MIC10 is believed to be the result of two effects: Defects of crista architecture and reduced stability of ATP synthase dimers leading to ineffective metabolic adaptation [166].

Corresponding to MIC19 and MIC25, the paralogs MIC26 and MIC27 likely derived from duplication of genes [89]. Both proteins regulate MIC10 oligomers in an antagonising manner, as MIC27 stabilises and MIC26 destabilises them [164,238]. However, MIC27 is not essential for MIC10 oligomerisation, as complete loss of MIC27 does not fully diminish MIC10 oligomers [238]. MIC10 oligomerisation is possible with sole overexpression of MIC10 [23]. Both, MIC26 and MIC27 indicated interactions with lipids and respiratory chain complexes/ F_1F_o-ATP synthase. Early on, MIC27 was identified as cardiolipin-binding factor [213]. This proposes an interesting role of MIC27 and cardiolipin in regulating MIC10 oligomerisation, as loss of both destabilised MIC10 oligomers to a higher extend than loss of solely one of them [164]. Interestingly, double knockout of MIC26 and MIC27 resulted in impaired stability of respiratory chain complexes, supercomplexes and F_1F_o-ATP synthase [8]. This had influence on their stability possibly by altered cristae morphology and/or cardiolipin interactions [8].

QIL1, ortholog of Mic12 in yeast [89], has been identified as “link” between the MIC60- and MIC10-subcomplexes [76]. Overexpression of MIC10 in QIL1-diminished cells could not reestablish interaction with the independently stable MIC60-subcomplex [76]. A glycine-rich, N-terminal transmembrane segment and a highly conserved tryptophan-asparagine- (WN-) motif were recently identified as important interaction sites for both MIC60- and MIC10-subcomplexes [201]. The devastating effects of loss-of-function mutations in QIL1 in mammals can be seen by their relationship with early onset, fatal mitochondrial hepatopathy and encephalopathy [65,77,175,236].

Additionally, poorly understood MICOS-associated proteins like DNAJC11 [228] and SLC25A46

[192] have been discovered. DNAJC11 is defined by its highly conserved J-domain making it a constituent of the J-protein family, also called Heat Shock Protein 40 (HSP40) family. This family of co-chaperones to HSP70s supports ATP hydrolysis via its J-domain during protein folding and quality control [91,104]. Intriguingly, interactions between MIC60, MIC19, MIC25 and DNJC11 have specifically been found by mass spectrometry in the cerebrum of mice [206]. This is postulated to be the reason for crista abnormalities and ultimately motor neuron pathology in mice harbouring splicing mutations in DNAJC11 [91,206]. SLC25A46 is a member of the mitochondrial solute carrier family usually embedded in the IMM [152]. However, it has been identified as an integral protein of the OMM in mitochondria acting in a pro-fission manner [1]. Depletion of SLC25A46 led to a decrease of MIC60, almost complete loss of MIC19 and increased cleavage of OPA1 into short OPA1 forms [94]. This resulted in loss of mitochondrial cristae architecture attributing SLC25A46 to an upstream support for MICOS [94]. Clinical representations of missing SCL25A46 function are diverse, all having neuropathological phenotypes in common: optic atrophy, axonal Charcot-Marie Tooth Syndrome, cerebellar atrophy, and Leigh Syndrome have been identified [1,94]. Another protein that is believed to interact with MICOS in yeast is Aim24 [81]. Depletion of Aim24 led to dissociation of Mic10 and thus destabilisation of MICOS, but further functions in modelling cardiolipin have been proposed [81]. Hence, further work is needed to fully elucidate the role of MICOS-associated proteins, their functions and interplay to gain further insight into regulatory processes of crista architecture.

In yeast, deletion of Mic60 and Mic10 resulted in a similar IMM phenotype, as the normal tubular and vesicular structures are lost and lamellar sheets are formed that do not connect to the IBM (see above, [80,87,208]). Loss of Mic12, Mic19 or Mic27 led to a phenotype of the IMM somewhere in between, as both phenotypes are observed [208]. Recent experiments with knockout (KO) of MICOS proteins in HeLa cells revealed, that virtually all mitochondria with loss of MIC60 presented distorted structures of the IMM [193]. Knockout of MIC10, MIC19 or QIL1 led to aberrant cristae in three out of four cases [193]. Loss of MIC25, MIC26 or MIC27 resulted in normal IMM morphology in three out of four cases [193]. Interestingly, MIC10- and QIL1-KO cell lines mainly formed a large, single CM aligning with the IBM [193]. Knockout of MIC60 or MIC19 rather presented multiple, stacked CMs in concentric layers [193]. Distorted structures of the IMM recovered with re-expression of MIC60 or MIC10 respectively hinting towards MICOS as an essential player in building normal cristae morphology [193]. In this context, cristae morphology of MIC10-KO cells could resemble an intermediate form on the path towards higher structural organisation of cristae [193]. Provided by better spatial resolution images of living cells, new evidence suggests, that CMs continuously undergo membrane remodelling cycles dependent on MICOS [110]. Close apposition of cristae and subsequent fusion, as well as fission events occurred in a balanced way [110]. The rate of fusion and fission events was significantly reduced in HeLa cells lacking QIL1 [110]. Similar effects were observed for the crista junction itself: Immuno-stained MIC60 and MIC10 localised at crista junctions uncovered numerous merging and splitting events which occurred in a balanced manner and at similar rates for both visualised proteins [110].

Upon knockout of QIL1, the layout of MIC60 within CMs stayed similarly arranged, but the rates of merging and splitting events were drastically reduced [110]. Thus, a fully operational MICOS complex seems to be required for successful remodelling of crista membranes and crista junctions [110]. Experiments with actively remodelling cristae revealed, that physical diffusion barriers at certain times prevent mixing of CM proteins (here ATP5I) of different compartments [110]. Again, these processes were inhibited in QIL1-KO cells leading to the idea that MICOS might dynamically modulate protein diffusion at CJs [110]. Mobility of F_1F_O-ATP synthase between different CM compartments was demonstrated by Busch et al. [178]. This was dependent on the energy metabolism of mitochondria, as inhibition of glycolysis led to redistribution of a subpopulation of more mobile monomeric F_1F_o-ATP synthase from cristae to the IBM [178]. Accompanied by a functional shift, monomeric and F_1F_o-ATP synthase performed more ATP hydrolase than ATP synthase activity [178]. Hence, during cellular stress and decreased glucose availability, spatially and temporally separated subpopulations of F_1F_o-ATP synthase might exist providing metabolic adaptation capacity [178]. These findings underline the critical role of MICOS complex in upholding the structural integrity and remodelling CMs and CJs, which is essential for mitochondrial function and adaptation to metabolic stressors.

2.5. MICOS mediates outer-inner mitochondrial membrane contacts and protein import

It has been established, that MICOS stabilises crista junctions and is hence critical for mitochondrial architecture [22,208]. Mitochondrial protein import involves several specialised pathways, where MICOS has been described to play a pivotal role in coordinating the process [22,208]. Most nuclear encoded protein precursors destined for mitochondria are recognised at the OMM by the TOM complex, where Tom40 serves as the central entry gate [11,79,187,229]. Preproteins with an N-terminal targeting sequence are translocated through the hydrophilic channel provided by the TOM complex [79]. The N-terminal targeting sequence recruits the translocase of the inner membrane (TIM) 23 complex to the IMM [79]. This facilitates translocation of the preprotein into the IMS or matrix [79]. Even though preprotein transport into the matrix is usually managed in cooperation of both complexes, preproteins destined for the matrix can still be transported through TOM, even when transport through TIM is halted [141]. This leads to the idea that TOM- and TIM complexes are not permanently linked to each other, rather forming “dynamic translocation contact sites” [141]. TOM and TIM complexes form transient supercomplexes, which have been identified localising specifically in proximity to crista junctions [66]. MICOS, localised at crista junctions, helps to couple these complexes, enhancing protein handover [26,47]. However, the precise mechanisms of the influence of MICOS on the presequence import pathway remain unclear.

The carrier import pathway composes an alternative protein import pathway which consists of the TIM22 complex of the IMM [79,136,215]. Small chaperons in the IMS mediate the transport of preproteins from the TOM complex to the IMM [79,136,215]. This pathway is e.g. used by hydrophobic metabolite carriers lacking an N-terminal presequence [67,115,165]. MICOS has been implicated in

spatially organising the TOM-TIM22 interaction, ensuring efficient transport of these proteins [26].

Small proteins destined for the IMS are usually imported by the MIA pathway [13,14,131]. First, they are translocated through the TOM complex in the OMM and are then relayed to CHCHD4 (Mia40 in yeast) trapping them in the IMS via by oxidative folding [13,131,156,194]. For this purpose, they display conserved cysteine-rich patterns which are recognised by CHCHD4 [14,131]. Interestingly, hydrophobic interactions independent of the oxidoreductive activity of CHCHD4 have been proposed to contribute to IMS trapping [156,214]. MICOS, particularly Mic60 has a hand in preprotein import via the MIA pathway, as it was identified to transiently interact with Mia40 in yeast [204,208]. It positions Mia40 near the TOM complex helping preprotein handover [204,208]. This proposes an integral role of MICOS in spatiotemporal coupling of preprotein import into mitochondria.

β-Barrel proteins, like Tom 40, need both the TOM and the sorting and assembly machinery (SAM) for insertion into the OMM [12,86,102,217]. Following translocation into the IMS by the TOM complex, β-barrel proteins are transported via small chaperons to the SAM complex in the OMM [12,86,102]. MICOS sustains connections to both TOM and SAM complexes and deletion of MIC60 impairs β-barrel protein import and OMM membrane insertion [22]. A large hydrophilic N-terminal polypeptide transport-associated (POTRA) domain of SAM50 is required for MICOS-SAM interactions [22]. However, it remains unclear to what extend MIC60 contributes to TOM-SAM supercomplex formation, or which connection alleviates β-barrel preprotein transfer.

Newer studies suggest direct connections of SAM50 with MIC60, MIC19 and MIC25 forming the mitochondrial intermembrane space bridging (MIB) supercomplex [40,47,180,199]. The CHCH domain of MIC19 interacts with MIC60, and its N-myristoylation site interacts with SAM50 [40]. As OMA1 cleaves MIC19 N-terminally, SAM50-MIC19-MIC60 axis is disrupted leading to disassembly of the MIB supercomplex, abnormal mitochondrial structure and deficiency of crista junctions [199]. The SAM50-MIC19-MIC60 axis was partially restored by overexpression of MIC25 in MIC19 knockout cells supporting evidence of similarities in structure and function to MIC19, as MIC25 forms connections with SAM50 and MIC60 just like MIC19 [199]. During MIC19 knockout the SAM complex was destabilised, but levels of MIC60 and MIC25 were unchanged indicating a dominant role of MIC19 in maintaining MIB supercomplex [199].

2.6. MICOS proteins exhibit tissue-specific mitochondrial expression levels

To meet distinct energy and metabolic demands, mitochondria are highly specialised across different tissues. This becomes evident as they differ greatly in their mitochondrial protein composition, including key components like the electron transport chain or ribosomes, which may influence their specific function [38,88,100,150]. Morphological variations reflect this specialisation, as they are shaped by intrinsic developmental factors and extrinsic environmental cues [202]. While these differences are imminent, their functional implications remain poorly understood.

Hence, our research group has become interested in tissue-specific expression levels and/or different

isoforms of MICOS and MICOS interacting proteins. Mitochondria from heart, brain, skeletal muscle, liver, lung, and spleen of mice were isolated and analysed for expression levels of MICOS subunits and some of its associated proteins (see Figure 4). Whereas for proteins of the MIC10-subcomplex and SAM50 detected antibody intensity signals between tissues remained stable, for components of the MIC60-subcomplex, a change of isoform expression patterns of MIC60 between tissues was found. MIC60 is predicted to exist in five splicing variants in mice and four in humans [243,244]. The isoform expression levels seem to be similar in heart and skeletal muscle tissue, and similar in parenchymal organs like liver, kidney, lung and spleen. Brain tissue shows its specific predominant isoform. Moreover, an increased antibody intensity signal of MIC25 in brain tissue and to some degree in kidneys was recognised. To my best knowledge, there is no published data about their functional properties raising interesting research questions to be answered in the future. Even though MIC19 and MIC25 are orthologs (see 2.4), their expression pattern across tissues varies tremendously. Quantities of MIC25 are extensively upregulated in neuronal tissues indicating brain-specific properties of this protein. Elucidating this observation will be the goal of this thesis. Can increased expression rates of MIC25 be reproduced in human neuronal-like cells? How does presence and/or absence of MIC25 influence neuronal differentiation processes? Does this affect energy metabolism?

To assess tissue-specific roles of MIC25 in neuronal cells, a suitable human-derived neuronal cell model was necessary. In the research of neurodegenerative diseases, this requirement became essential early on. The SH-SY5Y cell line has human heritage as was sampled from a bone marrow biopsy of a four-year old girl diagnosed with metastatic neuroblastoma and is now widely used in research of Parkinson's disease [17,226]. With the help of all-trans retinoic acid (ATRA), they can be differentiated into mature, neuron-like cells, which allows direct comparisons between proliferative and post-mitotic states [113,151,172]. Prior to expression analysis of MIC25, finding a reliable marker to confirm successful differentiation was necessary and thus a major goal of this thesis.

Further hints towards an important role of tissue-specific expression of MIC25 are provided by clinical research approaches. Loss of MIC25 in heart muscle led to diminished contractility, reduced myosin and actin levels and altered mitochondrial morphology [19]. This is likely a critical driver in hypoplastic left heart syndrome, a congenital heart disease of probably oligogenic origin [19]. Likewise, knockout of MIC25 in AML12 (alpha mouse liver 12) cells resulted in a shift from oxidative phosphorylation to a glycolytic-reliant metabolism which might contribute to the progression of non-alcoholic fatty liver disease (NAFLD) [30]. A newly published study experimenting with a mouse model for ulcerative colitis, a chronic inflammatory disease of the bowel, discovered that upregulation of MIC25 during metabolic stress promoted diversification of energy sources and resistance towards cellular apoptosis [222]. Thus, tissue-specific MIC25 expression levels in heart, liver and bowel disease affect mitochondrial morphology and energy metabolism. Gaining deeper understanding of how MIC25 is regulated and what its effects are in different tissues could open new therapeutic options for conditions where mitochondrial dysfunction is vital.

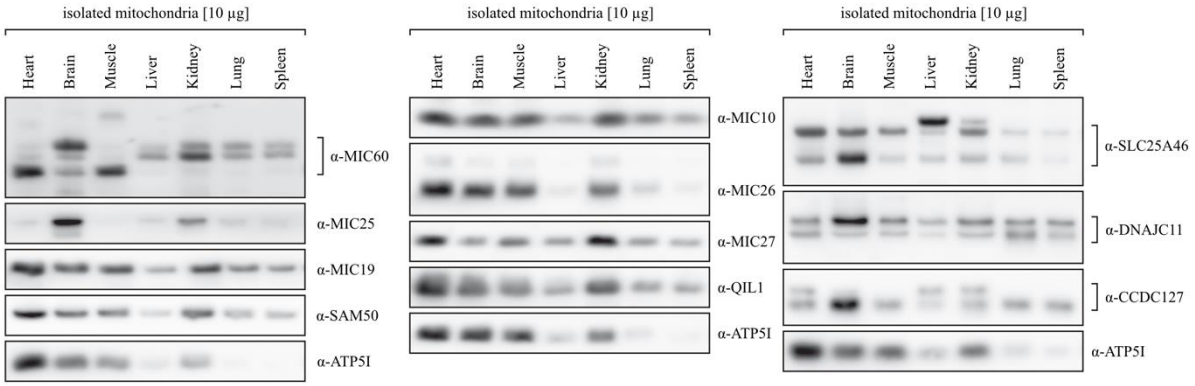

Figure 4 Tissue-specific expression of MICOS proteins in mice

Heart, brain skeletal muscle, liver, kidney, lung, and spleen tissue of mice was extracted, and mitochondria isolated. Of each tissue, 10µg isolated mitochondria were loaded, blotted on SDS-PAGE, and decorated with antibodies against MICOS proteins and MICOS-associated proteins. In brain tissue, increased expression of MIC25 and a shift in isoform patterns of MIC60 are depicted. Further neuronal specific adaptations of MICOS-associated proteins, like in SLC25A46, DNAJC11 and CCDC127 are detected. ATP5I acts as control for all depicted proteins. Its unsteady expression pattern between tissues can be explained by different degrees of ER-mitochondrial attachments leading to different degrees of purification, which needs to be considered when interpreting this figure.
Experiments labelled as Figure 4 were conducted by Sybille Jungbluth and Karina von der Malsburg.

To conclude, mitochondrial specialisation across tissues is reflected by distinct expression patterns of MICOS proteins. MIC25, as a part of MICOS, shows tissue-specific expression patterns in mice, strikingly in brain tissue. This suggests a role in neuronal-specific mitochondrial function which needs to be elucidated further and provides promising research perspectives for this thesis. Hence, it focuses on investigating the expression and potential role of MIC25 in human neuronal-like SH-SY5Y cells aiming to understand its interplay of differentiation processes with mitochondrial structure and function. This may help to gain a broader understanding of mitochondrial specialisation and its implications for tissue-specific physiology and disease.

3. Materials and Methods

3.1. Materials

3.1.1. Reagents and other crucial equipment

Table 1 Reagents and other crucial equipment

Reagents	
Reagent	**Supplier**
2-(N-morpholino)ethanesulfonic acid (MES)	Carl Roth
3-(N-morpholino)propanesulfonic acid (MOPS)	Carl Roth
3x FLAG peptide	Sigma-Aldrich
5x LiveCell Imaging Buffer	Abcam
6-Aminocaproic acid	Sigma-Aldrich
Acetic acid	Carl Roth
Acetone	Thermo Fisher
Acrylamide	Carl Roth
All-trans-retinoic acid (ATRA)	Sigma-Aldrich
AllStars Neg. Control siRNA	Qiagen
Ammonium persulfate (APS)	Carl Roth
Ampuwa Irrigation solution	Fresenius Kabi
Anti-FLAG M2 affinity gel	Sigma-Aldrich
B-27 Supplement	Gibco/Thermo Fisher
Bambanker Serum-Free Cell Freezing Medium	GC Lymphotec/Wako
Bis-Tris	Carl Roth
BN-PAGE HMW native marker kit	Cytiva
Bovine Serum Albumine (BSA)	Sigma-Aldrich
Bromphenol blue	Carl Roth
Carbonyl cyanide-p-trifluoromethoxyphenylhydrazone (FCCP)	Abcam
Coomassie brilliant blue G250	Serva
Coomassie brilliant blue R250	Carl Roth
Digitonin	Calbiochem
Dimethyl Sulfoxide (DMSO)	Carl Roth
Dithiothreitol (DTT)	Carl Roth
Dulbecco's Modified Eagle Medium (DMEM)	Gibco/Thermo Fisher
Ethanol	BCD Chemie
Ethylenediaminetetraacetic acid (EDTA)	Carl Roth
Fetal Calf Serum (FCS)	Gibco/Thermo Fisher

FlexiTube siRNA Hs CHCHD6 4	Qiagen
FlexiTube siRNA Hs CHCHD6 5	Qiagen
Fluoromount-G	Thermo Fisher
Formaldehyde 16%	Thermo Fisher
GlutaMAX Supplement	Gibco/Thermo Fisher
Glycerol	Sigma-Aldrich
Glycine	Carl Roth
HEPES	Carl Roth
Hoechst 33342	Thermo Fisher
Hydrochloric acid	Carl Roth
Isopropanol	Thermo Fisher
Lipofectamine RNAiMAX Transfection Reagent	Thermo Fisher
Mannitol	Roquette Frères/Fagron
Methanol	BCD Chemie
Milk powder (skimmed)	Sucofin
MitoTracker Red CMXRos	Thermo Fisher
N,N-Methylene bisacrylamide 2x analytical grade	Serva
Neurobasal Medium (NB)	Gibco/Thermo Fisher
Opti-MEM Serum Reduced Medium	Gibco/Thermo Fisher
PAGERuler Prestained Protein Ladder	Thermo Fisher
Phenylmethylsulfonyl fluoride (PMSF)	Carl Roth
Phosphate Buffered Saline (PBS, pH 7.2)	Gibco/Thermo Fisher
Potassium hydroxide	Carl Roth
Protease inhibitor cocktail tablets	Roche
Protein Assay Standard I (Lyophilized bovine γ-globulin)	Bio-Rad
PVDF membranes	Millipore
Rotiphorese Gel 30 (37.5:1) acrylamide solution	Carl Roth
RotiQuant Bradford reagent	Carl Roth
Seahorse XF Calibrant (pH 7.4)	Agilent
Seahorse XF DMEM Medium (pH 7.4)	Agilent
Seahorse XF Glucose	Agilent
Seahorse XF L-Glutamine	Agilent
Seahorse XF Pyruvate	Agilent
Sodium chloride	Carl Roth
Sodium dodecyl sulfate (SDS)	Carl Roth

Sucrose	MP Biomedicals
SuperSignal West Pico PLUS Chemiluminescent Substrate	Thermo Fisher
TEMED	Carl Roth
TMRE-Mitochondrial Membrane Assay Kit	Abcam
Trichloroacetic acid (TCA)	Sigma-Aldrich
Tricine	Carl Roth
Tris	Carl Roth
Triton X-100	Sigma-Aldrich
Trypan Blue stain 0.4%	Thermo Fisher
Trypsin-EDTA 0.25%	Gibco/Thermo Fisher
Tween 20	Sigma-Aldrich
Uridine	Sigma-Aldrich
β-Mercaptoethanol	Carl Roth
Equipment	
Equipment	**Supplier**
Amersham Imager 600	GE Healthcare
Blotting chamber for semidry transfer (Owl-Hep1)	Thermo Fisher
Blotting chamber for wet transfer (Mini-Trans Blot cell)	Bio-Rad
Blue Native PAGE running apparatus (SE600X)	Hoefer
Cell culture microplate, 96 well, flat bottom, black	Greiner bio-one
Counting chamber BLAUBRAND® Neubauer improved, w/o clips double ruling	Brand
Leica DFC3000 G CCD camera and a 63x/1.40 objective	Leica
Leica DMi8 fluorescent microscope	Leica
Microplate reader (Spark 10M)	Tecan
SDS-PAGE running apparatus (Mini-Protean system)	Bio-Rad
Seahorse XF Cell Mito Stress Test Kit	Agilent
Seahorse XF96 Cell Culture Microplates	Agilent
Seahorse XF96 Extracellular Flux Assay Kit	Agilent
Seahorse XFe96 Analyzer	Agilent
Spin columns	MoBiTec
Software	
Software	**Supplier**
Affinity Designer 1.10.1	Serif
Affinity Photo 1.10.1	Serif

BioRender.com (web version)	BioRender
Excel	Microsoft
Fiji/ImageJ 2.1.0	(Schindelin et al, 2012 [183])
Huygens Essential	Scientific Volume Imaging
Illustrator CC	Adobe
Photoshop CC	Adobe
Prism v8.0	GraphPad
Seahorse XF Imaging and Normalization System	Agilent
SPSS statistics 28.0.1.1	IBM
Word	Microsoft

3.1.2. Antibodies

Table 2 Antibodies

Antibodies against human proteins			
Target	**Identifier or cat. number**	**Source or Supplier**	**Dilution**
α-ATP5I	ab122241	abcam	1:500
α-BiP		Zimmermann laboratory	1:500
α-CCDC127	HPA045052	Sigma-Aldrich	1:500
α-DNAJC11	ab183518	abcam	1:500
α-FLAG M2	F1804	Sigma-Aldrich	1:500
α-FLAG R	F7425	Sigma-Aldrich	1:500
α-GAPDH	60004-1-Ig	PTG	1:2000
α-HSPA9	ab227215	abcam	1:500
α-MFN1	ab57602	abcam	1:500
α-MFN2	11925	CST	1:500
α-MIC10	5032	Laboratory of Nikolaus Pfanner (University of Freiburg) & Martin van der Laan	1:500
α-MIC19	HPA042935	Sigma-Aldrich	1:500
α-MIC25	HPA051975	Sigma-Aldrich	1:500
α-MIC26	HPA003187	Sigma-Aldrich	1:500
α-MIC27	HPA000612	Sigma-Aldrich	1:500
α-MIC60	5041	Laboratory of Nikolaus Pfanner (University of Freiburg) & Martin van der Laan	1:500
α-mtTFA	ab276558	abcam	1:500
α-Neurofilament H	2836	CST	1:1000
α-OMA1	sc-515788	Santa Cruz	1:500
α-OPA1	612607	BD Biosciences	1:500
α-PSD95	2507S	CST	1:1000
α-QIL1	5033	Laboratory of Nikolaus Pfanner (University of Freiburg) & Martin van der Laan	1:500
α-SAM50	ab246987	abcam	1:750
α-SAP97	ab134156	abcam	1:1000
α-SLC25A46	ab237760	abcam	1:500

α-Synaptophysin	ab52636	abcam	1:500
α-Synaptophysin	ab8049	abcam	1:500
α-TOM22	ab179826	abcam	1:500
α-TOM40	ab185543	abcam	1:500
total OXPHOS (α-ATP5A; α-UQCRC2; α-MTCO1; α-SDHB; α-NDUFB8)	ab110413	abcam	1:1000
α-Tubulin α	ab7291	abcam	1:500
Secondary antibodies			
Target	**Identifier or cat. number**	**Source or Supplier**	**Dilution**
Goat α-mouse IgG (H+L) Highly Cross-Absorbed Secondary Antibody, Alexa Fluor Plus 488	A-11029	Thermo Fisher	1:3000
Goat α-mouse IgG antibody coupled to peroxidase	DC02L	Merck	1:3000
Goat α-rabbit IgG antibody coupled to peroxidase	AP132P	Merck	1:5000

3.1.3. Cell lines

Table 3 Mammalian cell lines

Cell line	**sgRNA or retroviral construct**	**Source/created by**
HEK293T	-	Laboratory of Michael T. Ryan, Melbourne, Australia (Stroud et al, 2016 [198])
HEK293T MIC25-12	sgRNA: 5'-GGTGTCCTTCGGAGTGGACGCGG-3'	Laboratory of Michael T. Ryan, Melbourne, Australia (Stroud et al, 2016 [198])
SH-SY5Y	-	Laboratory of Barbara Niemeyer, CIPMM, Saarland University, Germany
SH-SY5Y + FLAG-SAM50	SH-SY5Y transduced with ^{FLAG}SAM50 (non-clonal population)	Alexander von der Malsburg, Saarland University, Germany

3.2. Methods

3.2.1. Biochemical assays

3.2.1.1. Isolation of mitochondria

SH-SY5Y cells were grown on 145 mm cell culture dishes at 37 °C and 5% CO_2 and harvested. Thus, cells were rinsed with PBS, trypsinised with 1 ml Gibco Trypsin-EDTA 0.25%, taken up in 37 °C DMEM medium (see 3.2.2.1), pelleted at 500 x g for 5 min, resuspended in PBS (room temperature) and centrifuged again at 500 x g for 5 min. Those cells were stored at -80 °C. On ice, cells were resuspended in buffer A (83 mM Sucrose, 10 mM HEPES-KOH pH 7.2) and blended in a glass-teflon dounce homogeniser. The same volume of Buffer B (250 mM Sucrose, 30 mM HEPES-KOH pH 7.2) was added and the cell suspension was equally distributed into micro tubes which were subsequently centrifuged at 1000 x g for 5 min at 4 °C. The supernatant was taken off and centrifuged 12000 x g, 2 min at 4 °C. Now the crude mitochondria pelleted down were resuspended in buffer C (320 mM Sucrose, 1 mM EDTA pH 8, 10 mM Tris pH 7.4) and their protein concentration was determined using a Bradford assay by adding 900 µl 1x Rotiquant to 2 µl mitochondria in 98 µl H_2O and contrasting the absorbance at 595 nm to an IgG standard curve. Makeshift mitochondria aliquots were preserved at temperatures of -80 °C.

3.2.1.2. SDS-PAGE and immunoblotting

Isolated mitochondria or cell lysates, depending on the experiment, were added to a SDS sample buffer (Laemmli buffer, [116]) containing 2% [w/v] SDS, 10% [v/v] glycerol, 60 mM Tris pH 6.8, 1% [v/v] β-mercaptoethanol and 0.01% [w/v] bromphenole blue. Samples were incubated at 95 °C for 5 min or 65 °C for 15 min to denature proteins and inactivate proteases. Bis-Tris SDS polyacrylamide gels were cast using a 3x BisTris gel buffer (1 M BisTris-HCl pH 6.4), acrylamide (37.5:1), 10% APS and TEMED and gels ran at a constant voltage of 120 V either using MES low-molecular weight running buffer (50 mM MES, 50 M Tris, 1 mM EDTA, 0.1% [w/v] SDS) or MOPS high-molecular weight running buffer (50 mM MOPS, 50 mM Tris, 1 mM EDTA, 0.1% [w/v] SDS). Next, proteins were transferred to PVDF membranes either using a semidry blotting system with semidry transfer buffer (20 mM Tris, 150 mM glycine, 0.02% [w/v] SDS, 10-20% [v/v] ethanol) at a constant current of 350 mA for 120-150 min or a wet blotting system with a wet blot transfer buffer (25 mM Tris pH 8.3, 192 mM glycine, 10% [v/v] ethanol) at a constant voltage of 100 V for 60 min. To appraise whether proteins were loaded equally PVDF membranes were dyed with Coomassie brilliant blue R250 (0.2% [w/v] in 40% [v/v] ethanol, 10% [v/v] acetic acid) and decolourised with destaining solution (40% [v/v] ethanol, 10% [v/v] acetic acid) followed by taking pictures with a CCD camera system (Amersham Imager 600). The PVDF membranes were marked and horizontally sectioned for immuno-decoration with multiple antibodies, and destained with methanol to remove any excess Coomassie brilliant blue. PVDF membrane snippets were washed with TBS-T (20 mM Tris-HCl pH 7.5, 125 mM

NaCl, 0.1% [v/v] Tween 20) and blocked with TBS-T containing 5% [w/v] skimmed milk powder (TBS-T-M) 30-60 min at room temperature or overnight at 4 °C. Subsequently, the membrane snippets were incubated with primary antibodies diluted in TBS-T-M for at least 60 min or overnight at 4 °C, washed 3x with TBS-T and incubated with peroxidase-coupled secondary antibodies for at least 45 min and washed again with TBS-T. Ultimately detection was achieved by enhanced chemiluminescence by incubating membrane snippets in SuperSignal West Pico PLUS Chemiluminescent Substrate for a few seconds and capturing images using a CCD camera system (Amersham Imager 600). For better visual representation tonal corrections were carried out using Affinity Photo.

3.2.1.3. BN-PAGE [223]*: Examination of mitochondrial protein complexes*

Mitochondria were isolated, pelleted by centrifugation (10000-20000 x g for 10 min at 4 °C) and the supernatant was discarded. Pelleted mitochondria were solubilised in BN-PAGE digitonin solubilisation buffer (1% [w/v] digitonin, 20 mM Tris-HCl pH 7.4, 50 mM NaCl, 0.1 mM EDTA, 10% [v/v] glycerol, 1 mM PMSF) at a concentration of 1 µl/µg by gently pipetting up and down and incubating on ice for 15 min. Afterwards, mitochondrial lysates were centrifuged (10000-20000 x g for 10 min at 4 °C) and 5 µl 10x BN-PAGE LoadingDye (5% [w/v]Coomassie brilliant blue G250, 500 mM 6-aminocaproic acid, 100 mM Bis-Tris HCl pH 7.0) was added to the supernatant. To sediment any Coomassie brilliant blue G250 particles, samples were spun 10000-20000 x g for 0.5 min at 4 °C and ultimately loaded on self-made BN-PAGE 4%-13% gradient gels where the gel buffer contained 66.7 mM 6-amiocaproic acid and 50 mM Bis-Tris HCl pH 7.0. Gels were run at 600 V, 25 mA in a water-cooled (5 °C) Hoefer gel chamber with 4 litres of anode buffer (50 mM Bis-Tris HCl pH 7.0) and cathode buffer blue (50 mM Tricine-HCl pH 7.0, 15 mM Bis-Tris HCl pH 7.0, 0.02% [w/v] Coomassie brilliant blue G250). When about 15 min later the samples entered the gel, the blue cathode buffer was substituted by a dye-free cathode buffer (50 mM Tricine-HCl pH 7.0, 15 mM Bis-Tris HCl pH 7.0) continuing the run until the blue front reached the end of the gel about 45 min later. The gel was transferred into SDS running buffer (250 mM Tris, 1.91 M glycine and 10% [w/v] SDS) and incubated for 10 min, then relocated into semidry transfer buffer (20 mM Tris, 150 mM glycine, 0.02% [w/v] SDS, 10-20% [v/v] ethanol) and blotted at a constant current of 350 mA for 120-150 min to PVDF membranes followed by antibody decoration as described in 3.2.1.2.

3.2.1.4. FLAG immunoprecipitation

To facilitate detection, purification, and stoichiometric analysis of the MICOS complex, SAM50 was N-terminally tagged with a FLAG-epitope (^{FLAG}SAM50). This artificial peptide was fused to SAM50 and thus expressed in SH-SY5Y cells. Mitochondria containing ^{FLAG}SAM50 were isolated as described in 3.2.1.1. 500 µg mitochondria of each condition of interest were previously isolated, thawed and pelleted at 20000 x g for 5 min at 4 °C. Removal of supernatant is required to resuspend pellets

remaining in the micro tube in 500 µl 1% Digitonin SILAC solubilisation buffer (1% [w/v] digitonin, 20 mM Tris-HCl pH 7.4, 50 mM NaCl, 0.1 mM EDTA, 10% [v/v] glycerol, 2 mM PMSF) and incubating them on ice for 30 min. This step is necessary to extract mitochondrial proteins from their membranes while preserving their functionality. To get rid of any debris, centrifuge 20000 x g for 5 min at 4 °C. Remove 50 µl supernatant ("total", thus containing the whole scope of mitochondrial proteins enabling to act as control), mix it with 50 µl 2x SDS sample buffer (see section 3.2.1.2) in a fresh micro tube to denature proteins and inactivate proteases, and incubate at 65 °C for 10 min. TCA precipitate "total", if necessary (refer to standard protocols for TCA precipitation). To equilibrate affinity gel, add 40 µl of anti-FLAG M2 affinity gel together with 250 µl 0.3% Digitonin SILAC solubilization buffer (0.3% [w/v] digitonin, 20 mM Tris-HCl pH 7.4, 50 mM NaCl, 0.1 mM EDTA, 10% [v/v] glycerol, 2 mM PMSF) to MoBiTec spin columns, and centrifuge 100 x g at 4 °C for 2 min. Then, transfer the remaining supernatant of extracted mitochondrial proteins to columns and incubate with gentle rotation at 4 °C for 2 h (hours) to allow binding of ^{FLAG}SAM50 to anti-FLAG affinity gel. Eight washing steps were consecutively performed by adding 500 µl 0.3% Digitonin SILAC wash buffer (0.3% [w/v] digitonin, 20 mM Tris-HCl pH 7.4, 60 mM NaCl, 0.5 mM EDTA, 10% [v/v] glycerol) each time to the spin columns containing ^{FLAG}SAM50 bound to affinity gel. Each of the eight washing steps is followed by spinning at 50 x g at 4 °C for 1 min, to allow removal of unbound proteins. As a next step, proteins bound to affinity gel within the spin columns were eluted with 50 µl elution buffer (0.3% Digitonin SILAC wash buffer containing 100 µg/ml 3xFLAG peptide) by rotating them at 100 x g at 4 °C for 5 min. After centrifuging at 100 x g 1 min, a second elution is performed by adding 46 µl 0.3% Digitonin SILAC wash buffer containing 100 µg/ml 3xFLAG peptide. After spinning again at 100 x g for 1 min, combine elutions from both elution steps. As a last step, add 32 µl 4x SDS sample buffer (see section 3.2.1.2) to the eluate now containing ^{FLAG}SAM50 and all proteins it forms a stable connection with. The eluate was denatured at 65 °C for 10 min and subsequently analysed by SDS-PAGE and immunoblotting as described above.

3.2.2. Generation and culture of human cell lines

3.2.2.1. Tissue culturing

SH-SY5Y WT, HEK293T WT and KO cells were cultivated in a humidified incubator at 37 °C and 5% CO_2. Culturing medium was Dulbecco's modified eagle medium (DMEM) encompassing 4.5 g/l glucose, L-glutamine and Pyruvate supplemented with 10% [v/v] FCS and 50 µg/ml uridine. Cells were subcultured at 90% cell density by rinsing them with PBS at room temperature, trypsinising and resuspending in DMEM at 37 °C into new cell culture dishes. To be able to store cells, cells were harvested, pelleted at 500 x g 5 min, resuspended in Bambanker freezing medium and stored at -80 °C.

3.2.2.2. Counting cells

After washing with PBS, trypsinising and resuspending in DMEM medium and transferring into a falcon, cells were counted using Neubauer hemocytometry. 10 µl of each cell suspension were taken off and diluted 1:2 with Trypan Blue stain 0.4%. The Neubauer chamber was humidified, the cover slip placed and checked for Newton's rings. Those should be visible after adding 10 µl suspension to top and bottom counting area each. When now placed under a microscope using 10x objective, complete corner squares should be visible. All four corner squares of the top and bottom counting area were counted and the average cell number calculated and if numbers weren't homogenous enough, counting was repeated. The cell number per millilitre was calculated by multiplying the average cell number with the dilution factor of Trypan Blue stain 0.4% (here factor 2) and 10^4. The volume of cell suspension needed for a specific cell number was calculated by the rule of proportion and thus plated in the according dishes.

3.2.2.3. Conditions for differentiation

SH-SY5Y cells, undifferentiated neuroblast-like, can be differentiated into more mature human sympathetic neurons using a variety of methods [188] resulting in a variety of phenotypes. Neurobasal medium containing 2% [v/v] B-27 supplement, 1% [v/v] GlutaMAX Supplement, 50 µg/ml uridine, and all-trans-retinoic acid (ATRA) in a final concentration of 10 µM were added to cells plated 24 h prior in DMEM culturing medium to achieve differentiation into a chiefly cholinergic phenotype [113]. While replacing Neurobasal medium and ATRA (10 µM) after 48 h, cells grew for a total of five days before being harvested.

3.2.2.4. siRNA knockdown

Cells destined for transfection with siRNA were plated at least 24 h prior to transfection to reach 60-80% confluency. For transfection of a single 6-well, 9 µl Lipofectamine RNAiMAX and 3 µl (30 pmol) of 10 µM siRNA were each diluted in 150 µl Opti-MEM Medium containing HEPES, 2.4 g/l sodium

bicarbonate and L-glutamine. Diluted siRNA was added to diluted Lipofectamine RNAiMAX in a ratio of 1:1. After incubating at room temperature for 5 min, 250 µl siRNA-lipid complexes were added to a single 6-well leading to a final of 25 pmol siRNA and 7,5 µl Lipofectamine RNAiMAX used. Cells were incubated for at least 24 h before changing medium.

3.2.3. *Assays of mammalian cells*

3.2.3.1. *Analysis of cell lysates*

SH-SY5Y cells were grown and harvested as described in 3.2.1.1. After centrifuging, PBS was withdrawn and the cell pellet resuspended in lysis buffer (20 mM Tris-HCl pH 7.4, 150 mM NaCl, 1 mM DTT, 0.5% [v/v] Triton X-100, Roche protease inhibitor). The volume was adapted individually according to the size of the pellet. After incubating 30 min on ice, the lysate was spun at 845 x g for 5 min to pellet the nucleuses and the supernatant was taken off to a new micro tube to determine the protein concentration using a Bradford assay by adding 900 µl 1x Rotiquant to 2 µl cell lysate in 98 µl H_2O and comparing the absorbance at 595 nm to an IgG standard curve. The supernatant was analysed by SDS-PAGE and immunoblotting.

3.2.3.2. *Fluorescence microscopy analysis of mitochondrial morphology*

Cells were grown on cover slips with a diameter of 18 milimeters. MitoTracker Red CMXRos was diluted using DMSO to a stock concentration of 1 mM and added 1:20000 to DMEM medium which was placed onto the cover slips after removing PBS and incubated for 10 min at 37 °C at 5% CO_2. After medium removal, cover slips were rinsed with PBS 3x and cells fixated using Paraformaldehyde (PFA) (4% [v/v] Formaldehyde, 10% [v/v] 10x PBS). The incubation period was 20 min at room temperature. Cells were washed, incubated with 0.1% Triton X-100 diluted in PBS for 10 min at room temperature and washed again with PBS 3x. Cover slips were transferred on a droplet of 2% [w/v] BSA diluted in PBS cells facing the solution. Following another washing step with PBS, cover slips were transferred onto a droplet of primary antibody solution diluted in 2% [w/v] BSA in PBS, incubated for an hour, washed again, and transferred onto secondary antibody solution and Hoechst 33342 (20 mM stock, 1:500 end concentration) diluted in 2% [w/v] BSA in PBS for another hour. Cover slips were rinsed with PBS and plain water before relocating onto 8 µl Fluoromount-G mounting medium placed on a glass slide. To congeal, glass slides were, shielded from light, incubated over night at room temperature. Pictures of the cells were taken with a Leica DMi8 fluorescence microscope with a Leica DFC3000 G CCD camera and a 63x/1.40 objective. Huygens Essential software made deconvolution of Z-stacks possible and with Fiji/ImageJ images were projected by maximum intensity. For better visual representation, contrast corrections were performed using Adobe photoshop.

3.2.3.3. *Membrane potential measurements*

Cells were seeded into a black flat-bottom 96-well cell culture plate and let grown for at least 24 h. On the day of the assay, medium was removed from all wells. Half of the seeded wells for each condition need to be used as a control and thus were treated with 20 µM FCCP in DMEM without FCS. All the other wells were treated solely with DMEM without FCS, and all together were incubated at 37 °C 5% CO_2 for 10 min. After removing media TMRE staining was conducted (500 nM TMRE, 2 µM Hoechst

33342 in DMEM without FCS but with 20 µM FCCP for all control wells). Cells were incubated at 37 °C at 5% CO_2 for 20 min and washed with 100 µl PBS. 1x LiveCell Imaging Buffer was added and the resulting fluorescence signal was measured by Tecan microplate reader (fluorescence excitation/emission wavelengths 549/575 nm) for TMRE and Hoechst 33342 each. To determine protein levels, cells were dissoluted in 1x Rotiquant and Bradford assay at 595 nm was performed.

3.2.3.4. Measurement of mitochondrial metabolic function

Metabolic function of undifferentiated, differentiated and with siRNA transfected knockdown SH-SY5Y cells, as well as HEK239T WT and KO cells, was measured with the Seahorse XFe96 Analyzer. The Extracellular Flux Analyser works by forming 7 µl micro-chambers with limited diffusion to measure oxygen consumption rates (OCR) in pmol/min and extracellular acidification rates (ECAR) in mpH/min with fluorescent sensors that are attached to a biocartridge that is placed over the cell culture plate and lowered to 200 µm above the cells [55]. Each fluorescent sensor for every well is circled by four injection ports where all types of agents can be delivered to the cells [55]. Here, oligomycin, FCCP and rotenone/antimycin A, all interfering with oxidative phosphorylation, were used. OCR and ECAR were measured every 3 minutes, and this allowed obtaining real-time data which was then normalised to protein quantity by Bradford assay. This was necessary to minimise confounding because even though the optimal seeding density for each condition was established at 20.000 cells (30.000 cells for HEK293T WT and KO), cells grew at different rates leading to a potentially uncontrollable variable. One day prior to the assay, into the wells of the utility plate of the Extracellular Flux Assay Kit, 200 µl of sterile water were added and the sensors of the sensor cartridge were submerged in the water and placed in a non-CO_2 incubator at 37 °C. To prevent evaporation, the Extracellular Flux Assay Kit was wrapped in plastic. On the day of the assay, Seahorse XF Assay Medium (1 M [v/v] Seahorse XF Glucose, 100 mM [v/v] Seahorse XF Pyruvate, 200 mM [v/v] Seahorse XF L-Glutamine, Seahorse XF DMEM Medium pH 7.4) was prepared and pre-warmed to 37 °C. Cells seeded at least 24 h prior into Seahorse XF Cell Culture Microplate were washed with 100 µl XF Assay Medium and incubated with 180 µl XF Assay Medium each well for 45-60 minutes in a non-CO_2 incubator at 37 °C. Water was removed from the Extracellular Flux Assay Kit, the wells filled with 200 µl prewarmed XF Calibrant and also incubated in a non-CO_2 incubator at 37 °C for 45-60 minutes. This time was used to prepare inhibitors from Seahorse XF Cell Mito Stress Test Kit. Oligomycin, FCCP and rotenone/antimycin A were solubilised in XF Assay Medium to create stock concentrations of 100 µM oligomycin and FCCP and 50 µM rotenone/antimycin A. Final concentrations were 1,5 µM oligomycin, 1 µM FCCP and 0.5 µM rotenone/antimycin A each well. Working solutions were prepared shortly before loading ports followed by running the assay.

4. Results

4.1. SH-SY5Y cells act as a model for human neuronal cells

To evaluate the tissue-specific effects of MICOS proteins, specifically MIC25, a human neuronal-like dopaminergic cell model primarily used in research of Parkinson`s disease was used [226]. So-called SH-SY5Y cells were obtained in the early 1970s, after the SK-N-SH line was subcloned three times [17]. They derived from neuroblastoma, the most prevalent solid tumour outside the skull in children under the age of five [34]. It originates from neuronal crest cells and hence can develop anywhere in the peripheral sympathetic nervous system; thus, clinical symptoms vary according to the location of the tumour [34]. Therefore, it is unsurprising that SH-SY5Y cells themselves can firstly be differentiated and secondly display a catecholaminergic phenotype, as they exhibit tyrosine hydroxylase activity and basal noradrenaline release in a differentiated state [151,172]. But those cells are not purely catecholaminergic, as moderate activity of dopamine-β-hydroxylase was described indicating a dopaminergic phenotype [18]. Originally, only marginal levels of acetylcholinesterase and choline acetyltransferase were observed, usually indicating a cholinergic phenotype [18]. Alternate differentiation protocols besides the most common one with 1% retinoic acid (RA), like the concomitant use of RA and brain-derived neurotrophic factor (BDNF), reported increases in enzymes typical for cholinergic properties [45]. This opened their use as neuronal-like cell model in other neurodegenerative diseases like Alzheimer's [45]. Typically, to enhance dopaminergic phenotype, phorbol esters in combination with RA are added [160]. Thus, SH-SY5Y cells do not exhibit just one single phenotype but display mixed phenotypes with varying dominants depending on differentiation method. For this thesis, differentiation was conducted solely with RA, as a specific phenotype resembling some disease was not particularly necessary.

For my study it was greatly paramount, that SH-SY5Y cells differentiate upon treatment with RA and thus display a phenotype of mature neurons and a mature neuronal marker expression pattern accordingly. Only then, expression levels of MIC25 can be compared between both states and ultimately analysed for MIC25 function. Undifferentiated SH-SY5Y cells, like cancerous cells, proliferate indefinitely making them easily culturable [151]. Outgrowth of extensive, meticulous neurites resembling axons and/or dendrites and triangular shaped cell bodies, as well as detection of neuronal proteins including neuron specific enolase (NSE) define differentiated SH-SY5Y cells [113]. Markers like MAP2, Synaptophysin and neuronal nuclei antigen (NeuN) were described to identify differentiated SH-SY5Y cells by SDS-PAGE [31,121], but in my experience the ones tested were not suitable, as their detection levels were too low (data not shown). To be able to test the hypothesis of increased MIC25 expression in differentiated SH-SY5Y cells, identifying a neuronal marker reliably recognising differentiated SH-SY5Y cells was a priority of this thesis. Figure 5A shows a titration experiment where different concentrations of all-trans retinoic acid (ATRA) were added to different cell culture dishes. The expression levels of Neurofilament H in undifferentiated and differentiated

cells, as well as for 30 and 50 µg SH-SY5Y lysate, were compared, and expression levels of Tubulin α (control for cell expression) and ATP5i (control for mitochondrial expression) were considered. It is evident that expression levels of Neurofilament H increase in differentiated SH-SY5Y cells compared to undifferentiated cells, but the effect of increased ATRA exposure seem to be negligeable. Regarding the published norm of using concentrations of 10 µM ATRA for differentiating SH-SY5Y cells [45,113,188], it has been decided to apply to this in the future. Loading 30 µg SH-SY5Y lysate is sufficient to confirm differentiation.

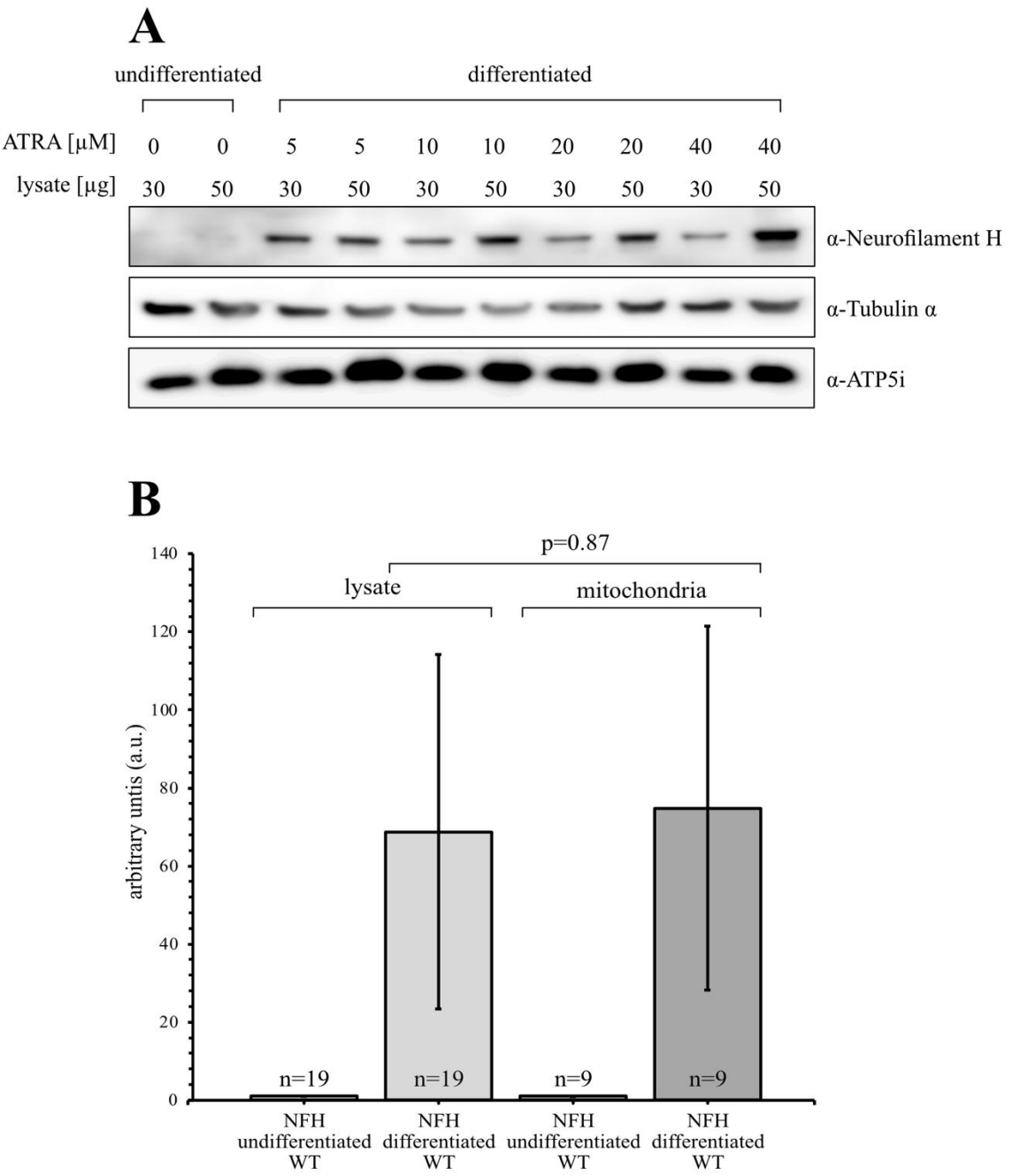

Figure 5 Differentiation of SH-SY5Y cells and Neurofilament H (NFH) expression

A. SH-SY5Y cells were treated with increasing amounts of all-trans retinoic acid (ATRA), lysed, loaded at

30 and 50 µg and western blotted detecting NFH and controls. **B.** Quantification of NFH using Fiji/Image J in undifferentiated and differentiated SH-SY5Y lysates (n=19) and isolated mitochondria (n=9). Error bars indicate standard deviation (SD). A two-sided T-test assuming equal variances was performed to compare NFH expression in differentiated SH-SY5Y lysates with differentiated SH-SY5Y isolated mitochondria. The mean value of differentiated SH-SY5Y lysates (M = 68.78, SD = 90.72) was not significantly different from the mean value of differentiated SH-SY5Y isolated mitochondria (M = 74.84, SD = 93.37); t (26) = -0.16, p = 0.87.

Figure 5B demonstrates a dramatic increase of NFH levels in differentiated SH-SY5Y cells quantified via Fiji/ImageJ from Western blots. Using undifferentiated SH-SY5Y cells as baseline (1x), NFH expression rises 69-fold in differentiated cell lysates and 75-fold in differentiated isolated mitochondria. There is no significant difference between NFH increase in differentiated lysates and mitochondria (p=0.87). This identifies NFH as a robust marker of neuronal differentiation. It suggests that separate lysate validation may be unnecessary when examining protein expression in isolated mitochondria despite NFs being cytoplasmic proteins [235].

Interestingly, the lack of NFH depletion specifically during mitochondrial isolation suggests that a subpopulation of mitochondria may specifically associate with neurofilaments. Neurofilaments (NFs) – neuron-specific intermediate filaments (IFs) - support asymmetrical structure and conduction of electric signals in neurons [235]. Phosphorylation and dephosphorylation mediate aggregation, turnover and disintegration of complex networks, usually held in a parallel array [235]. Perpendicular extending side-arms keep a minimum distance from the individual NFs making axonal radial growth possible [235]. NFs are heteropolymers composed of different subunits, Neurofilament H (NFH) is known as the heavy polypeptide chain [234]. When NFH knockout mice are compared to wild-type controls, conduction velocity of electric signals and outward rectification is significantly decreased [114].

In conclusion, SH-SY5Y cells were chosen as neuronal cell model, as they proliferate indefinitely and are hence easily culturable [151]. They are human-like, thus expressing markers and exhibiting properties not easily found in a non-human model making them my choice for assessing the rate of MIC25 expression, its biochemical consequences on MICOS and MIB complex, its morphological consequences on neuronal mitochondria and ultimately its functional implications regarding membrane potential and shifts in energy metabolism. NFH acts as a reliable differentiation marker in SH-SY5Y cells, its increased expression in differentiated lysates and isolated mitochondria compared to undifferentiated samples is stable. Moreover, NFH detection is sufficient at loading quantities of 30 µg and expression is stable at different ATRA concentrations (here, 10 µM ATRA are the concentration of choice), making the differentiation protocol less susceptible to error.

4.2. SH-SY5Y cells show increased MIC25 expression when differentiated

It is poorly understood how tissue-specific expression levels of mitochondrial proteins facilitate brain-specific morphology and function. The mitochondrial contact site and cristae organising system (MICOS), among other protein complexes, supports formation, sustainment, and adaptation of the inner mitochondrial membrane (IMM) to the cell`s need [137]. MIC25, a protein belonging to the MIC60-subcomplex of MICOS [163], shows increased expression rates in isolated brain tissue of mice compared to other organ samples (see Figure 4). To be able to test the hypothesis of increased MIC25 expression in differentiated neuronal tissue, SH-SY5Y neuroblastoma cells act as a model for morphology, function, and processes during neurogenesis (see chapter 4.1.). Cell culture conditions allow for dividing or differentiation as necessary whereas limitations such as impossible further propagation of primary neurons as soon as they are fully differentiated do not apply [113].

To investigate the effects of differentiation on MICOS and MICOS-related proteins, Figure 6A shows Western blot images of SH-SY5Y cell lysates and isolated mitochondria, 30 µg each. All displayed proteins belonging to the MIC60- and MIC10-subcomplex, except for MIC25, show stable expression levels when comparing undifferentiated and differentiated samples in lysates and mitochondria separately. The same applies to SAM50 and TOM22 as MICOS-related proteins. When differentiated, solely MIC25 shows persistent increase in protein detection, both in lysates and isolated mitochondria, hence indicating an enlargement of the MIC25 protein pool exclusively in mitochondria. Enriched protein detection of ATP5i, but depleted protein detection of Tubulin α and GAP-DH in isolated mitochondria compared to lysates gives a hint that the isolation protocol decreases the number of cytosolic proteins present while NFH detection in differentiated cells remains sufficient to provide evidence for successful differentiation.

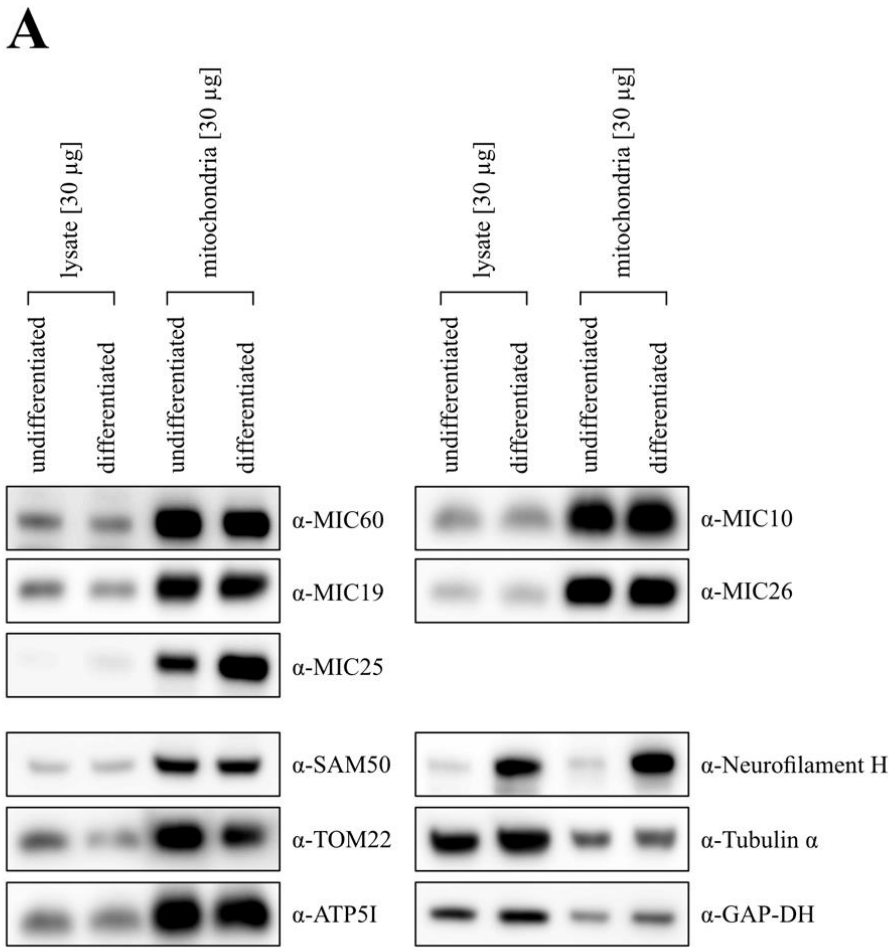
A
lysate [30 µg]
mitochondria [30 µg]
undifferentiated
differentiated
α-MIC60
α-MIC19
α-MIC25
α-MIC10
α-MIC26
α-SAM50
α-TOM22
α-ATP5I
α-Neurofilament H
α-Tubulin α
α-GAP-DH

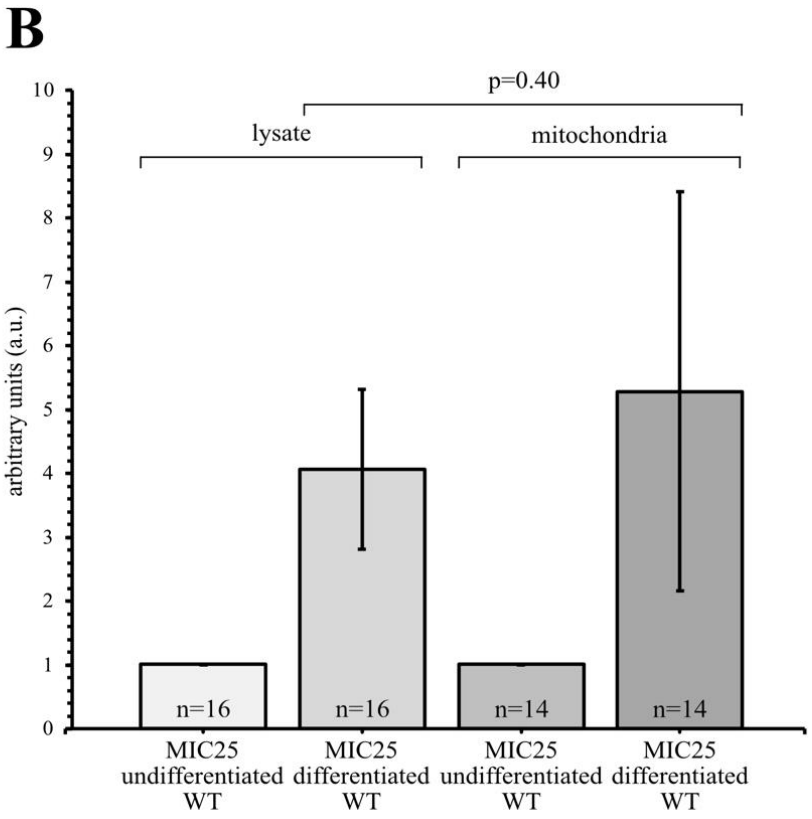
B
p=0.40
lysate
mitochondria
arbitrary units (a.u.)
0
1
2
3
4
5
6
7
8
9
10
n=16
n=16
n=14
n=14
MIC25 undifferentiated WT
MIC25 differentiated WT
MIC25 undifferentiated WT
MIC25 differentiated WT

Figure 6 Differentiation of SH-SY5Y cells and MIC25 expression

A. Expression rates of MICOS and MICOS-related proteins were compared on a western blot of undifferentiated and differentiated SH-SY5Y lysates on the one hand and undifferentiated and differentiated SH-SY5Y isolated mitochondria on the other hand. **B.** Quantification of MIC25 using Fiji/Image J in undifferentiated and differentiated SH-SY5Y lysates (n=16) and isolated mitochondria (n=14). Error bars indicate standard deviation (SD). A two-sided T-test assuming unequal variances was performed to compare MIC25 expression in differentiated SH-SY5Y lysates with differentiated SH-SY5Y isolated mitochondria. The mean value of differentiated SH-SY5Y lysates (M = 4.11, SD = 2.42) was not significantly different from the mean value of differentiated SH-SY5Y isolated mitochondria (M = 5.65, SD = 6.30); t (16.17) = -0.86, p = 0.40.

To show the impact of differentiation on MIC25 expression in SH-SY5Y WT, immunoblots were quantified using Fiji/ImageJ (Figure 6B). When using MIC25 protein detection in undifferentiated SH-SY5Y WT in lysate and mitochondria as a reference and setting it 1, MIC25 protein detection in differentiated lysate increases 4.1, in differentiated mitochondria 5.7 times. There is no significant difference between MIC25 protein levels in lysates and mitochondria (p=0.4) supporting the claim of increased MIC25 expression within the mitochondrial pool of proteins.

To sum up, tissue specific expression patterns of MIC25 are not restricted to isolated mouse brain samples but can be reproduced using SH-SY5Y cells. When comparing undifferentiated SH-SY5Y lysates and isolated mitochondria to differentiated samples, there is a persistent increase in MIC25 expression rates, but not for other MICOS and MICOS related proteins. This directs toward tissue specific functions of MIC25, possibly for adult neurons or during differentiation processes themselves. What is going to happen to MICOS and MICOS-related proteins when MIC25 is downregulated? The next chapter is going to assess this question.

4.3. siRNA knockdown of MIC25 in differentiated SH-SY5Y cells leads to stable expression of other MICOS proteins

As the previous chapter states, there is an increase of MIC25 expression in differentiated SH-SY5Y cells, in lysates and isolated mitochondria, when compared to undifferentiated SH-SY5Y cells, whereas the expression rates of other MICOS and MICOS-related proteins remain constant. This chapter explores the consequences of siRNA knockdown of MIC25 on expression rates of MICOS and MICOS-related proteins. Previously it has been observed that knockdown of single MICOS proteins influences other MICOS components, the effects depending on the importance of the protein for the complex [147]. Depletion of MIC60 in HeLa cells leads to loss of MIC19, MIC25, MIC10, MIC26, MIC27 as well as SAM50; depletion of MIC19 reduced the levels of MIC60, MIC10, MIC26, MIC27 and SAM50, whereas MIC25 is unaffected [148]. One study reported that the knockdown of MIC25 leaves other MICOS components or SAM50 untouched [148]. MIC25 siRNA knockdowns were conducted to test whether knockdown in neuronal-like SH-SY5Y cells shows tissue specific effects on MICOS components. Knockdowns were performed as described in 3.2.2.4. Two different types of MIC25 siRNA (siRNA MIC25-4, siRNA MIC25-5), apart from siRNA control having no silencing capacity working as negative control and checking for any adverse effects of the transfection agents, were introduced, both showed excellent knockdown efficiency estimated for about 90% (Figure 7). This is remarkable regarding the fact that a full differentiation cycle of 5 days with no additional transfection was conducted afterwards. Looking at cell lysates, Figure 7 compares MICOS components in undifferentiated, differentiated (siRNA control) and differentiated knockdown (MIC25-4 and MIC25-5 siRNA) samples. As described in chapter 4.2, MIC25 expression increases when comparing differentiated with undifferentiated samples. Samples containing MIC25 siRNA are depleted of MIC25, but not depleted of either MIC60, MIC19, MIC10, or MIC26. Mitochondrial transcription factor A (mtTFA) plays a vital part in the regulation machinery of replication of mitochondrial DNA (mtDNA) and is as such proportional to its levels [33,239]. This makes up the perfect control for the expression rates of mitochondrial proteins and as depicted in Figure 7, stays constant across all samples. On top of this, mtTFA, together with Tubulin α, acts as control for NFH, which confirms differentiation by increased display in all differentiated probes in comparison to the undifferentiated probe. Notably, there is a slight increase in detection levels of NFH when MIC25 is knocked down in comparison to differentiated WT cells (see chapter 5.1).

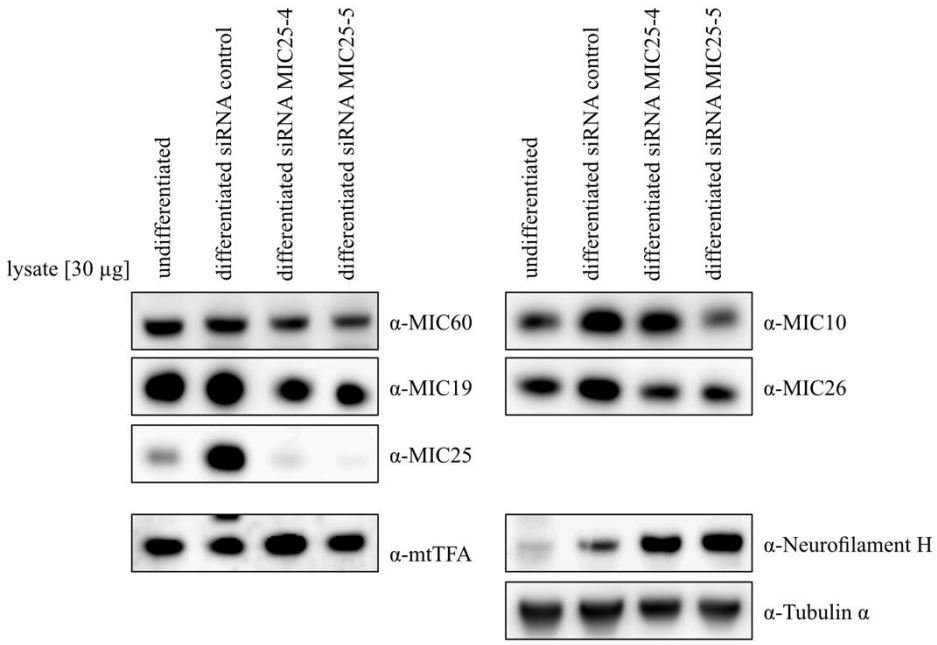

Figure 7 Expression of MICOS proteins in MIC25 knockdown SH-SY5Y lysates
Expression of MICOS proteins in undifferentiated SH-SY5Y lysates were compared to expression in differentiated siRNA control, siRNA MIC25-4 and siRNA MIC25-5 lysates by being loaded at 30 µg on a SDS gel subjected to western blotting.

To conclude, siRNA knockdown of MIC25 does not have any consequences on expression levels of other MICOS proteins in different SH-SY5Y lysates. Even though both siRNAs show excellent knockdown efficiency, in the following experiments knockdowns will be performed using MIC25-5 siRNA, as only using one siRNA provides the more time- and money efficient approach. Chapter 4.4 is going to examine the role of MIC25 not only on the level of the single protein and its effect on other MICOS proteins, but also its role within multiprotein complexes, the MICOS and MIB complex.

4.4. In SH-SY5Y cells, MIC25 is part of the MIB complex and within increasingly detected when differentiated

Strong data supports that MICOS proteins are organised into a MIC60- (MIC60, MIC19, MIC25) and MIC10- (MIC10, MIC26, MIC27, QIL1) subcomplex [58,76,148,238]. To uphold cristae membrane architecture, the MIC60-MIC19-SAM50-axis is indispensable, whereas the accessory subunits are not essentially necessary [148]. Though, Tang et al. [199] describes direct interactions of MIC25 with MIC60 and SAM50; when investigating MIC19 knockout in HeLa cells, MIC25 is partially able to preserve the functionality of mitochondrial intermembrane space bridging complex (MIB). When introducing $\mathrm{MIC25^{FLAG}}$ into HeLa WT and MIC19 knockout cells, MIC25 or $\mathrm{MIC25^{FLAG}}$ is incorporated into MICOS and MIB complexes to a greater extend [199]. As MIC25 is stronger expressed in differentiated SH-SY5Y cells than in undifferentiated SH-SY5Y cells, Figure 8 assesses the effects of differentiation of SH-SY5Y cells on MICOS and MIB complex behaviour. It was anticipated that increased MIC25 expression in mitochondria of differentiated SH-SY5Y cells would lead to a size shift of the MICOS complex due to its supposedly higher molecular weight, which should be detectable via BN-PAGE. Surprisingly, no shift in detection of MIC60, MIC19, MIC25, MIC10 or QIL1 in mitochondria of differentiated SH-SY5Y cells occurred (Figure 8), only detection of MIC25 was consistently stronger. This is emphasised by TOM40, acting as control for loading equal amounts of mitochondria, which rather falters in mitochondria of differentiated SH-SY5Y cells. The idea that simply all MICOS proteins are increasing is not supported, as only MIC25 shows increased protein detection. Since none of the other MICOS proteins show reduced levels, it is unlikely that one of them has been exchanged (by MIC25), even though decreased incorporation of MIC19 into MICOS and MIB complexes when $\mathrm{MIC25^{FLAG}}$ was overexpressed has been described [199]. Interestingly, when using the SAM50 antibody, two complexes are detected. On the one hand (according to literature [147]) the SAM complex at approximately 250 kDa, on the other hand the MIB complex well above 700 kDa. Within the bands of the MIB complex, SAM50 exhibits a constantly increased presence in differentiated isolated SH-SY5Y mitochondria.

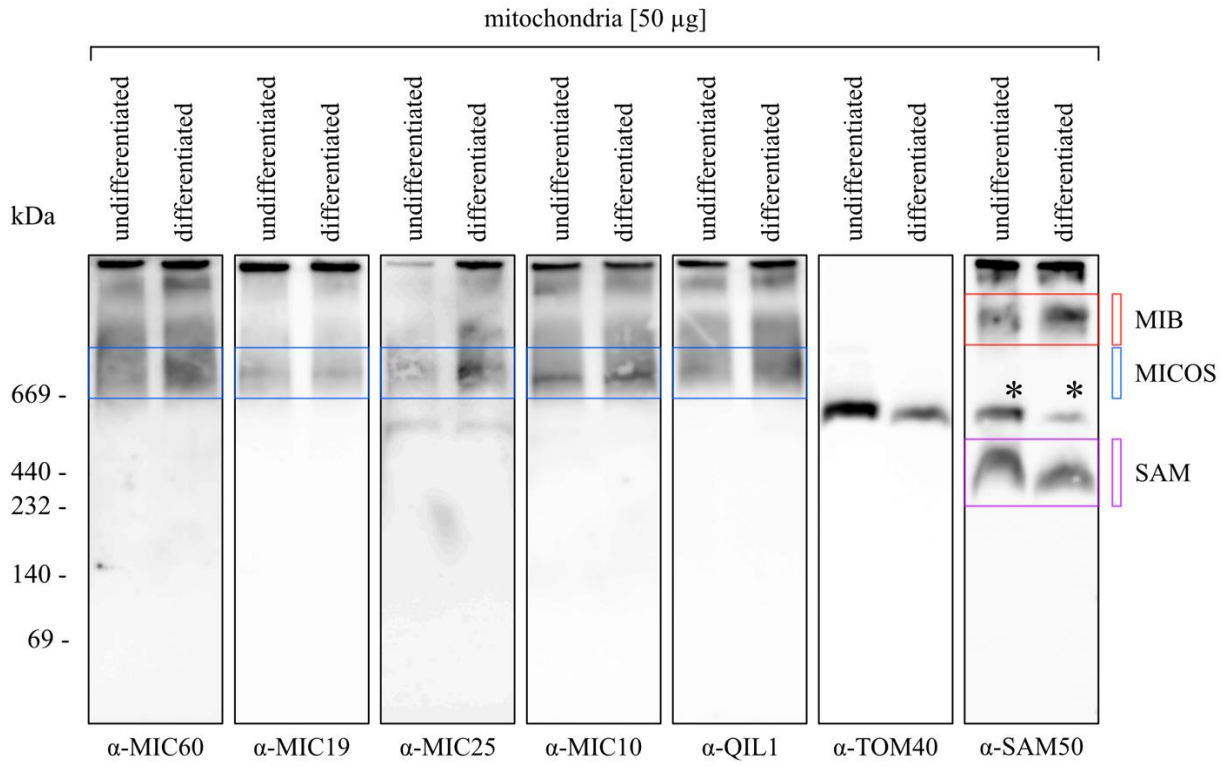

Figure 8 Behaviour of MICOS proteins and SAM50 on blue native-PAGE
BN-PAGE analysis of 50 µg undifferentiated and differentiated isolated SH-SY5Y mitochondria using antibodies against MICOS subunits, TOM40 and SAM50. Different complexes were colour-labelled: MIB-complex in red, MICOS complex in blue and SAM50 complex in pink. * Membrane slip of TOM40 antibody was redecorated with SAM50 antibody so the original TOM40 bands are still visible.

To further assess the possible connection between MIC25 and the MIB complex, SAM50 was N-terminally tagged with a FLAG-peptide (^{FLAG}SAM50) and co-expressed together with endogenous SAM50 within SH-SY5Y cells to be able to perform FLAG-immunoprecipitations. Figure 9 compares SDS-PAGE bands of isolated mitochondria of SH-SY5Y WT and ^{FLAG}SAM50 cells, both undifferentiated and differentiated. The antibody against SAM50 detects a double band in both undifferentiated and differentiated ^{FLAG}SAM50 mitochondria, even though detection of the endogenous SAM50 in ^{FLAG}SAM50 cells is reduced. This indicates that both endogenous and FLAG-tagged SAM50 are expressed and detectable. This is further proven by FLAG protein detection in the row below for mitochondria of undifferentiated and differentiated ^{FLAG}SAM50 cells (Figure 9). Outer membrane protein TOM22 serves as loading control. Furthermore, successful differentiation was confirmed by the detected increase in NFH expression. Again, Tubulin α acts as cytosolic loading control, detection being depleted as when comparing to lysate samples (see Figure 7).

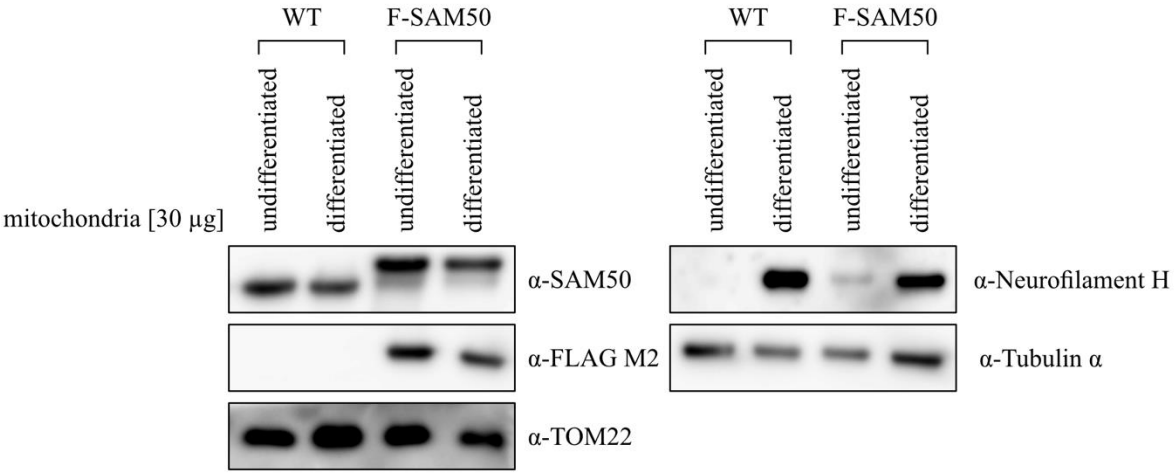

Figure 9 Introduction of SH-SY5Y ^{FLAG}SAM50 cell line
N-terminally FLAG-tagged SAM50 was introduced into the SH-SY5Y cell line and co-expressed with endogenous SAM50. Undifferentiated and differentiated SH-SY5Y WT and ^{FLAG}SAM50 mitochondria were isolated and analysed by SDS-PAGE and western blot.

Acting as a mild detergent, digitonin was added to isolated mitochondria of WT and ^{FLAG}SAM50 SH-SY5Y cells at a final concentration of 1%. FLAG-tagged proteins were bound to anti-FLAG-beads, excess proteins were washed off, and samples were subjected to two consecutive elution steps using triple FLAG peptide. Total and eluate samples of both WT and ^{FLAG}SAM50 mitochondria, each undifferentiated and differentiated, were loaded on SDS-PAGE. When assessing the lanes that represent WT eluates, it becomes clear that no bands are visible since no FLAG construct entered those cells and consequently no FLAG elution was possible (Figure 10A). The opposite is true for ^{FLAG}SAM50 eluates: Bands are present for all MICOS proteins and, except for MIC25, to similar extents, concluding that the complex did not fall apart during the purification process. SAM50 and FLAG protein detection provide evidence for the presence of ^{FLAG}SAM50 in ^{FLAG}SAM50 eluates. Small amounts TOM22 can be immunoprecipitated together with MICOS, thus ATP5i acts as negative control in all lanes where eluates were loaded. MIC25, as expected, shows in all differentiated total lanes increased protein levels. Additionally, when immunoprecipitating ^{FLAG}SAM50, there is more MIC25 protein eluted when comparing differentiated to undifferentiated mitochondria.

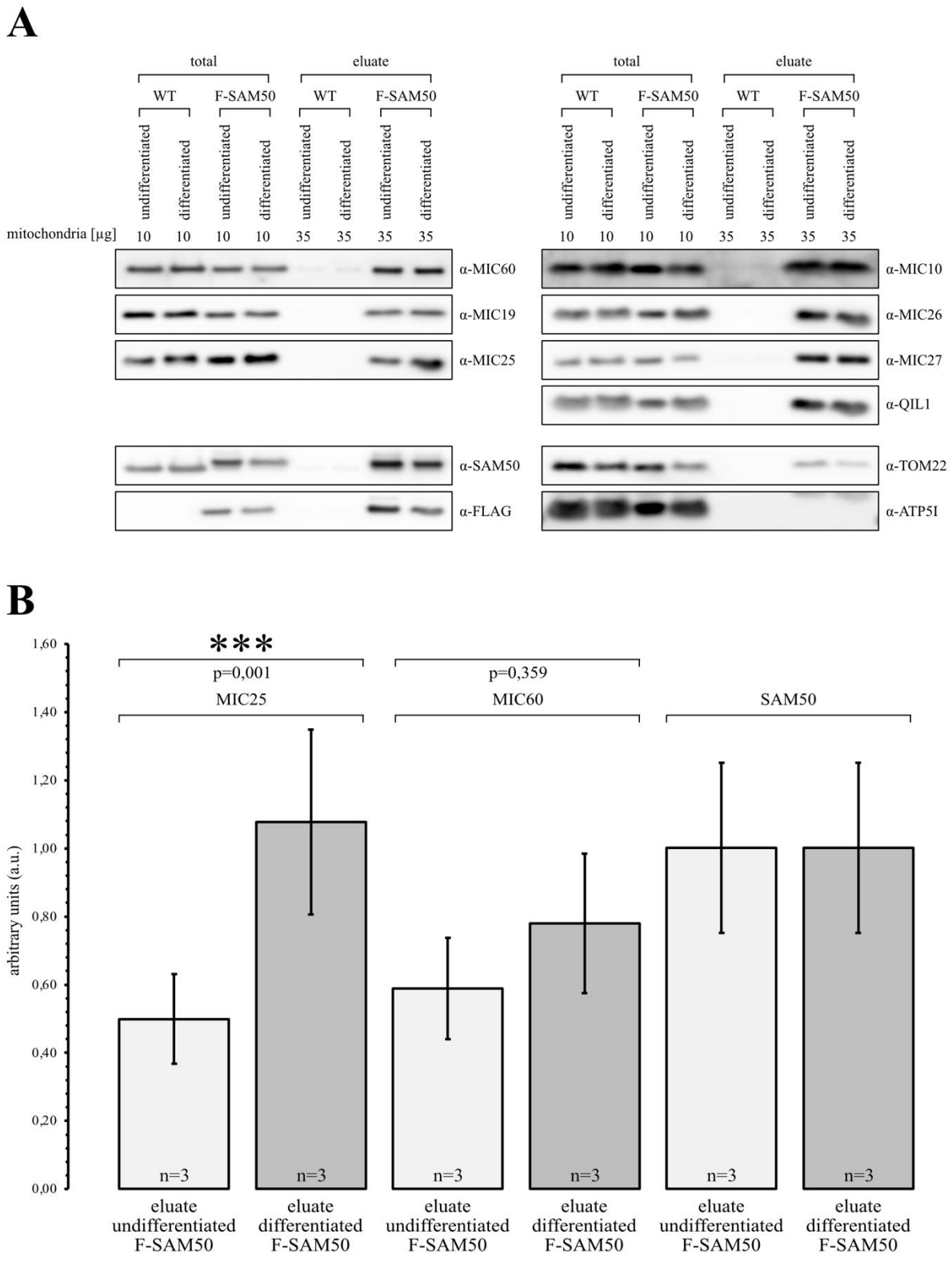

Figure 10 Immunoprecipitation of SH-SY5Y ^{FLAG}SAM50 and quantification

A. Immunoprecipitations of isolated WT and ^{FLAG}SAM50 mitochondria were performed, in undifferentiated and differentiated conditions each. Next to totals, eluates, were digitonin acted as mild detergent at a final concentration of 1%, were loaded on SDS gels, and subjected to immunoblotting. **B.** Bands of undifferentiated and differentiated eluates of MIC25, MIC60 and SAM50 were quantified using Fiji/Image J and values of SAM50 taken as reference for relative changes of MIC25 and MIC60 pulldown between undifferentiated and differentiated eluates. Error bars indicate standard deviation (SD). A one-way ANOVA

was performed to compare the effect of differentiation on MIC25 and MIC60 elution quantity in ^{FLAG}SAM50 SH-SY5Y cells. There was a statistically significant difference in elution quantity between at least two groups (F (3, 8) = 17.28, p = 0.001). Post-hoc Bonferroni correction for multiple comparisons found that the mean value of relative elution quantity was significantly different between undifferentiated MIC25 eluate and differentiated MIC25 eluate (p = 0.001, 95% C.I. = -0.88, -0.28). There was no statistically significant difference between undifferentiated MIC60 eluate and differentiated MIC60 eluate (p = 0.359, 95% C.I. = -0.49, 0.11).

Figure 10B illustrates quantification data of three ^{FLAG}SAM50 immunoprecipitations such as shown in Figure 10A. Eluate protein levels of MIC25, MIC60 and SAM50 were quantified, using SAM50 as a reference to determine relative changes in MIC25 or MIC60 pulldown. Thus, SAM50 immunoprecipitation rates were in mitochondria of undifferentiated and differentiated cell eluates set as 1. Depicted pulldown quantity of MIC25 was significantly higher in mitochondria of differentiated than in undifferentiated ^{FLAG}SAM50 cells (p=0.001) whereas pulldown quantity of MIC60 between mitochondria of differentiated and undifferentiated ^{FLAG}SAM50 cells was not statistically significant (p=0.359). This correlates with the results shown in Figure 8, where only the presence of MIC25 within the MICOS complex is increased.

Taken together, MIC25 reveals increased expression levels within MICOS complex on blue native-PAGE when examining mitochondria of differentiated SH-SY5Y cells. All other MICOS proteins are expressed at stable rates. Among the components of the MIB complex, only SAM50 exhibits enhanced protein detection. When performing ^{FLAG}SAM50 immunoprecipitations, MIC25 reveals itself as part of MIB complex. Quantitative data indicates that MIC25 pulldown increases, when analysing differentiated SH-SY5Y mitochondria compared to undifferentiated ones. MIC25 appears to play a dynamic, differentiation-dependent role in mitochondrial architecture, specifically in differentiated SH-SY5Y cells. Its increased incorporation into both MICOS and MIB complexes suggests that MIC25 may act as regulatory linker between the complexes, contributing to neuronal remodelling during differentiation. However, excess of MIC25 could still be explained by other roles than by its role within MICOS complex, as metabolic data indicates (chapters 4.6 and 4.7), and chapter 5.3 discusses. How differentiation processes and presence/absence of MIC25 influence mitochondrial networks of SH-SY5Y cells, the next chapter will elaborate.

4.5. Immunofluorescence reveals structural changes of mitochondrial networks when differentiating SH-SY5Y cells

When SH-SY5Y cells differentiate, their features change: Clustering, non-polarised cell bodies mature into cells with long extensions resembling features of primary neurons [113]. How do mitochondrial structural networks relate to pyramid-shaped cell bodies and neurite outgrowth? For example, high levels of mitochondrial fission in a post-mitotic phase of neuronal stem cells promote the path towards adult neurons, whereas fusion activity destines towards preserved self-renewal capacity [93]. As MIC25 reveals itself as part of the MIB complex, this chapter analyses the mitochondrial networks of undifferentiated, differentiated and MIC25 knockdown SH-SY5Y by immunofluorescence microscopy. For this purpose, as described in 3.2.3.2, Mitotracker dye was added to DMEM culture medium, to allow accumulation dependent on membrane potential in energised mitochondria. Thus, Mitotracker dye stains mitochondria in Figure 11B-E red. Staining for Tubulin α (green) and nucleoli (Hoechst33342, blue) were conducted after fixation. Additionally, all staining was merged into one image depicted in the colourful picture on the right. This staining was conducted for four different conditions: undifferentiated SH-SY5Y WT (Figure 11B), differentiated SH-SY5Y WT (Figure 11C), undifferentiated SH-SY5Y MIC25 siRNA knockdown (Figure 11D) and differentiated SH-SY5Y MIC25 siRNA knockdown (Figure 11E). For each condition cells were lysed and analysed via Western blot to confirm successful differentiation by NFH increase in differentiated samples and MIC25 knockdown in samples treated with MIC25-5 siRNA (Figure 11A). Hence, Tubulin α acts as control for cytosolic expression rates and ATP5i as control for expression rates of mitochondrial proteins.

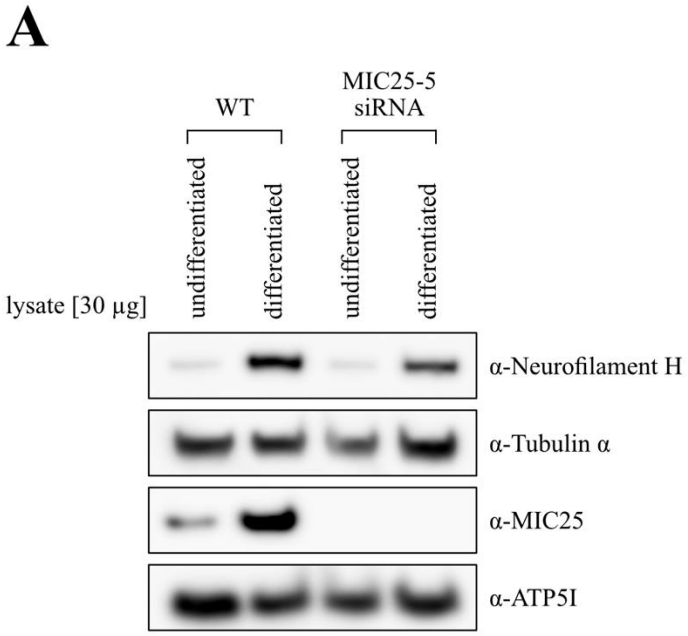

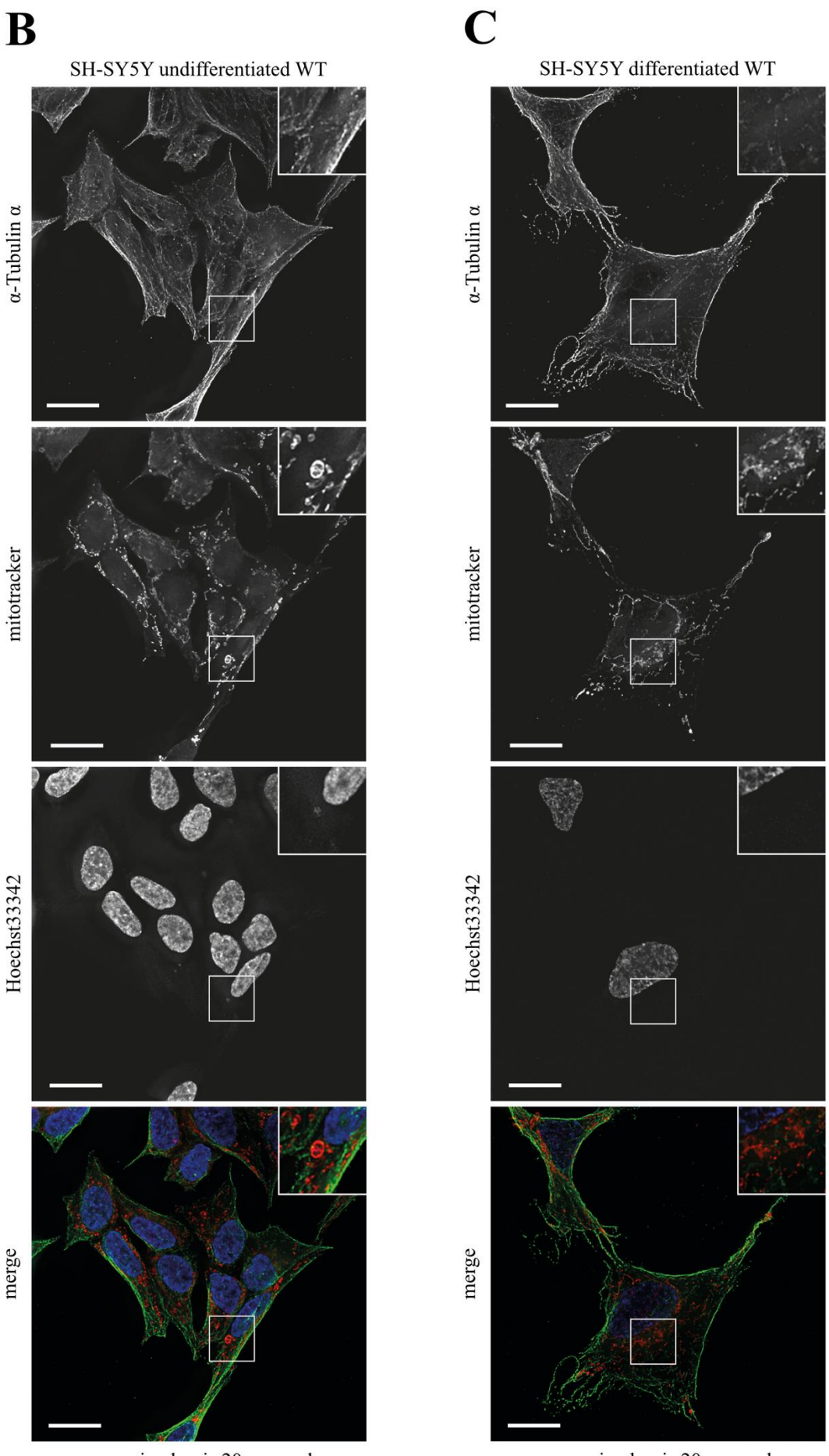
B
SH-SY5Y undifferentiated WT
α-Tubulin α
mitotracker
Hoechst33342
merge
measuring bar is 20 μm each
C
SH-SY5Y differentiated WT
α-Tubulin α
mitotracker
Hoechst33342
merge
measuring bar is 20 μm each

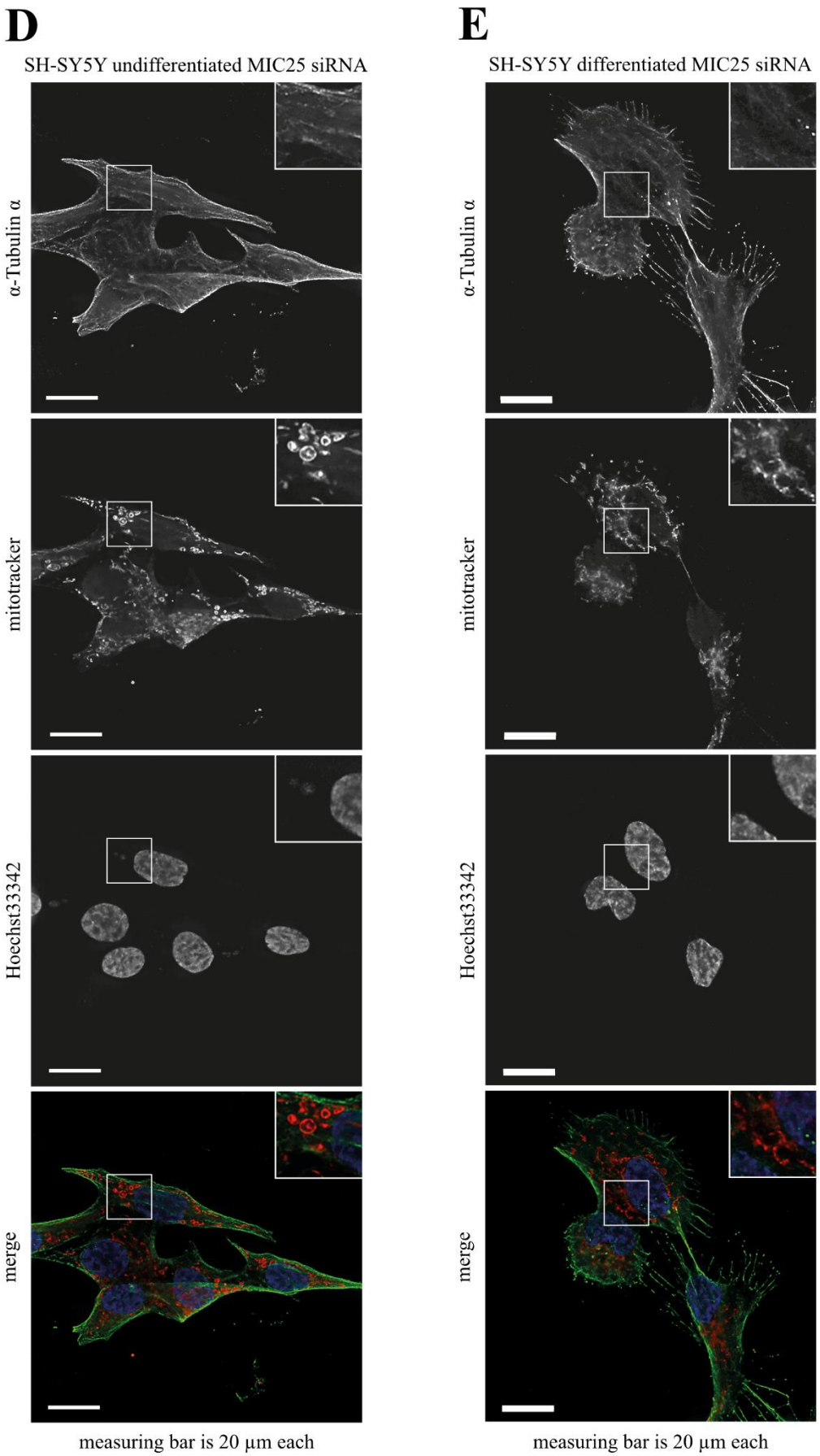
D
SH-SY5Y undifferentiated MIC25 siRNA
α-Tubulin α
mitotracker
Hoechst33342
merge
measuring bar is 20 µm each
E
SH-SY5Y differentiated MIC25 siRNA
α-Tubulin α
mitotracker
Hoechst33342
merge
measuring bar is 20 µm each

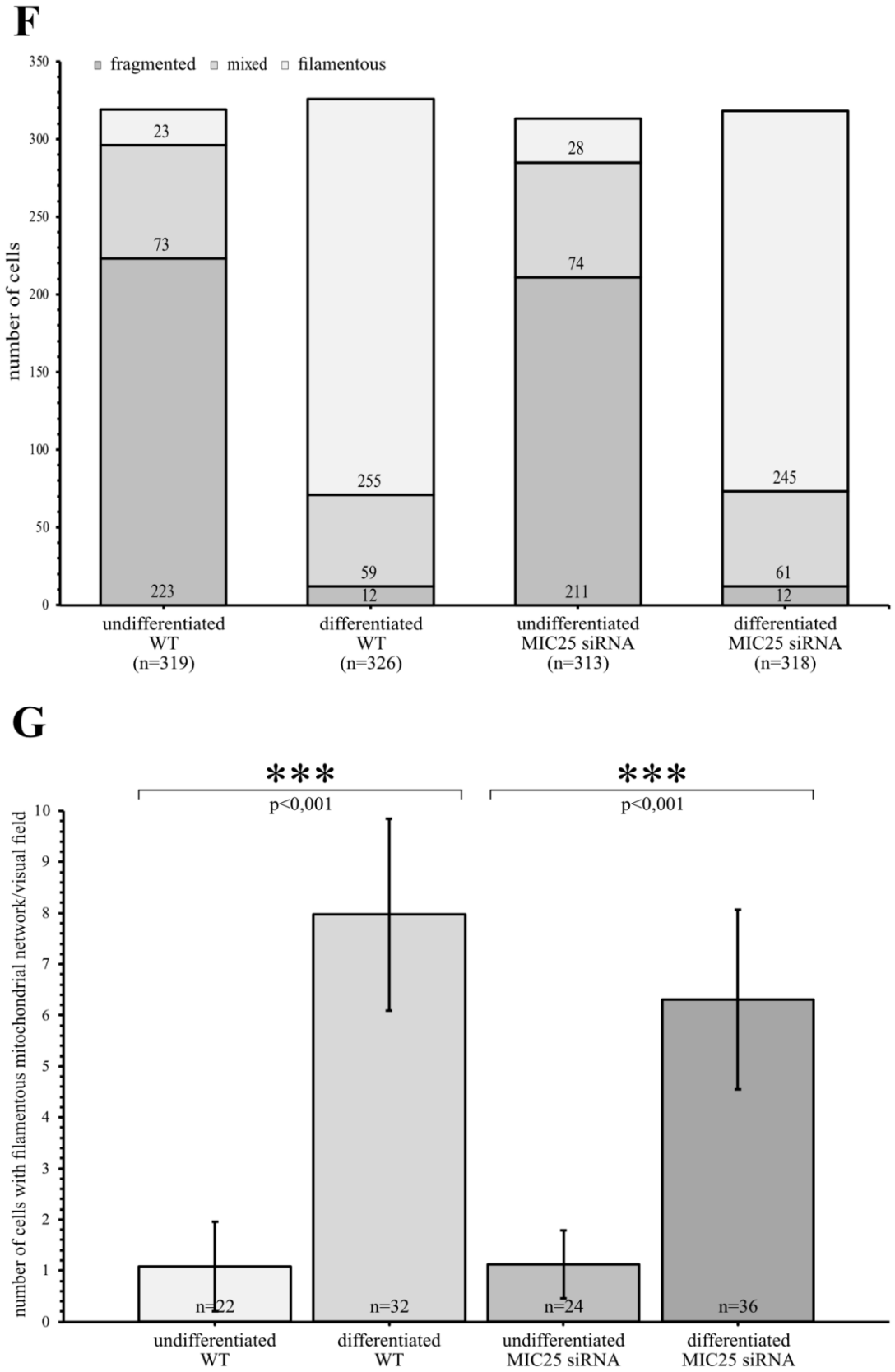

Figure 11 Analysing SH-SY5Y mitochondrial networks using immunofluorescence
A. Lysates of undifferentiated and differentiated SH-SY5Y WT and MIC25-5 siRNA knockdown cells were analysed by a western blot to confirm differentiation and depletion of MIC25 for B-E. **B-E.** Representative immunofluorescence images of undifferentiated and differentiated WT cells, as well as

undifferentiated and differentiated MIC25-5 siRNA knockdown cells. Mitochondrial morphology was analysed using an antibody against Tubulin α (left, green), mitotracker accumulating within negatively charged mitochondria (middle left, red), and Hoechst33342 to stain nucleoli (middle right, blue). All staining was merged in one picture (right). Pictures were taken with a Leica DFC3000 G CCD camera and a 63x/1.40 objective. Scale bar is 20µm each. **F.** From three independent experiments as depicted representatively in B-E, at least 100 cells each were counted and categorised into mainly "fragmented", "mixed", or "filamentous" mitochondrial networks. **G.** The number of cells with filamentous mitochondrial networks/visual field (1296 x 966 px; 3.75 µm × 3.75 µm pixel size) were analysed statistically. Error bars indicate standard deviation (SD). A nonparametric Kruskal-Wallis Test was conducted to examine the differences in filamentous cells numbers in WT and MIC25-5 siRNA knockdown cells according to differentiation status. Significant differences (Chi square = 71.09, $p = 0.000$, df = 3) were found among the four compared categories. Post-hoc Bonferroni correction for multiple comparisons found that the mean number of cells with filamentous mitochondrial networks was significantly different between undifferentiated WT and differentiated WT cells ($p < 0.001$). There also was a statistically significant difference between undifferentiated MIC25 siRNA knockdown and differentiated MIC25 siRNA knockdown cells ($p < 0.001$).

To analyse the structure of mitochondrial networks, at least 100 cells of each condition for each of the three independent experiments were counted and categorised into mainly "fragmented", "mixed," or "filamentous" mitochondrial network morphologies. As Figure 11F illustrates, mitochondrial networks in undifferentiated WT and MIC25 siRNA knockdown cells formed predominantly spherical shapes, whereas networks in differentiated WT and MIC25 siRNA knockdown cells preferred filamentous structures. Out of 319 counted undifferentiated WT and 313 counted undifferentiated MIC25 siRNA knockdown cells, only 23 and respectively 28 cells showed predominantly filamentous mitochondrial structures. Out of 326 differentiated WT and 318 differentiated MIC25 siRNA knockdown cells, 255 and respectively 245 exhibited predominantly filamentous mitochondrial networks.

Thus, the difference in cells with filamentous mitochondrial networks per visual field between undifferentiated and differentiated SH-SY5Y WT cells on the one hand and undifferentiated and differentiated SH-SY5Y MIC25 siRNA knockdown cells on the other hand is statistically significant (both $p<0.001$, Figure 11G). Filamentous mitochondrial networks seem to be a preferred feature of differentiated SH-SY5Y cells, no matter whether WT or MIC25 siRNA knockdown. This leads to the assumption that depletion of MIC25 does not influence the arrangement of mitochondrial networks greatly in SH-SY5Y cells, no matter whether undifferentiated or differentiated.

In summary, mitochondrial networks seem to behave differently in undifferentiated and differentiated SH-SY5Y cells. In undifferentiated cells, mitochondria rather form fragmented arrays which are only scarcely found in differentiated cells. There, filamentous networks are predominantly present. This distribution is not substantially different when MIC25 is knocked down using siRNA. Mitochondrial networks thus seem to adapt to changes in neuronal maturation processes. Even though MIC25 is part of MICOS and MIB complex and shows increased expression when differentiating SH-SY5Y cells, its absence does not seem to drastically influence mitochondrial network formation and adaptation. As this

observation is limited by the resolving capacity of immunofluorescence microscopy, the role of MIC25 in MICOS-SAM contacts stays unresolved. This work will now focus on the metabolic status of SH-SY5Y cells while undifferentiated and differentiated, as well as the presence or absence of MIC25.

4.6. Differentiation status and presence of MIC25 influence metabolic states of SH-SY5Y cells

For mature neurons, mitochondria are highly important organelles to meet their bioenergetic demands, whereas swiftly dividing cells, especially stem cells and cancer cells, rely on glycolysis as their primary energy source [125]. It is important for neurons to perform oxidative phosphorylation and ATP production at a rate sufficient to fulfil their bioenergetic needs, but to have an additional spare capacity to ramp up energy production under stress conditions [32]. Knockouts of MIC26 and MIC27 as proteins of the MIC10-subcomplex in HeLa cells indicate reduced basal respiratory capacity and FCCP could only increase maximal respiration rates marginally compared to control cells [111]. As a study with human colorectal cancer (RKO) cells presents, MIC25 knockdown severely reduces total, glycolytic and mitochondrial ATP production, as well as oxygen consumption rates (OCR) [6]. This raises questions about OCRs in undifferentiated and differentiated SH-SY5Y cells regarding their MIC25 expression status.

In Figure 12A OCR was measured by Seahorse XFe96 Analyzer as described in 3.2.3.4 and graphed for four conditions: undifferentiated WT (red), undifferentiated MIC25-5 siRNA (yellow), differentiated WT (green) and differentiated MIC25-5 siRNA (blue). Basal respiratory rates, the OCR of cells in untreated conditions, was highest for undifferentiated WT cells and is substantially lower for differentiated WT cells. This gap cannot be seen for undifferentiated and differentiated MIC25 siRNA knockdown cells (Figure 12B).

To study how OCRs change, inhibitors of the electron transport chain and ATP synthase were added sequentially. First, for each condition oligomycin was added at a final concentration of 1.5 µM. Oligomycin blocks the proton channel of ATP synthase which massively reduces the flow of electrons through the electron transport chain [97]. As a result, any change in OCR after adding oligomycin directly reflects the oxygen used for ATP production by ATP synthase. After oligomycin treatment, oxygen consumption levels in all four conditions at similar rates. This indicates that ATP production capacity by ATP synthase is highest in undifferentiated WT cells, lower in differentiated WT, and similarly reduced in both undifferentiated and differentiated MIC25 siRNA knockdown cells (see Figure 12C). The difference between the initial (basal) respiratory rate and the OCR after oligomycin represents the proton leak, which is independent of the activity of ATP synthase.

To measure maximal respiratory capacity, FCCP at final concentrations of 1 µM was added to each condition. FCCP acts as uncoupler, thus channelling protons through the inner mitochondrial membrane following their concentration gradient which has previously been created by complex I-IV of the electron transport chain before they can be used by oxidative phosphorylation to supply energy in form of ATP [62]. Subtracting basal respiration from maximal respiration yields spare respiratory capacity, reflecting the cells' vigour and ability to respond to environmental stressors [75]. In absolute numbers, spare respiratory capacity is highest in undifferentiated WT cells, followed by differentiated WT and

differentiated SH-SY5Y MIC25 siRNA knockdown cells. Undifferentiated MIC25 siRNA knockdown cells show no significant spare respiratory capacity ($p<0.001$; Figure 12D). When analysing Figure 12E, which divides maximal respiration by basal respiration and multiplies it by 100, the picture shifts: While undifferentiated WT cells were able to increase their basal respiratory rate by 266%, differentiated WT cells could do this by 399%. Differentiated MIC25 siRNA knockdown cells increased their basal respiratory rate by 274%, while for undifferentiated MIC25 siRNA knockdown cell, basal respiratory rate could not be upheld by FCCP addition (94%). Therefore, undifferentiated WT cells show highest basal and maximal respiration rates but differentiated WT cells were able to achieve the highest relative increase in spare capacity. For both MIC25 knockdown variants, relative spare respiratory capacity was reduced when comparing it to its WT counterpart, but for undifferentiated MIC25 siRNA knockdown cells, the effect was most devastating.

At last, 0.5 µM rotenone/antimycin A, inhibitors of complex I and complex III of the electron transport chain [171], were added to each condition. This enables shutting down the electron transport chain completely unveiling rates of non-mitochondrial oxygen consumption [171]. Thus, all measurements level out at minimal OCRs (Figure 12A).

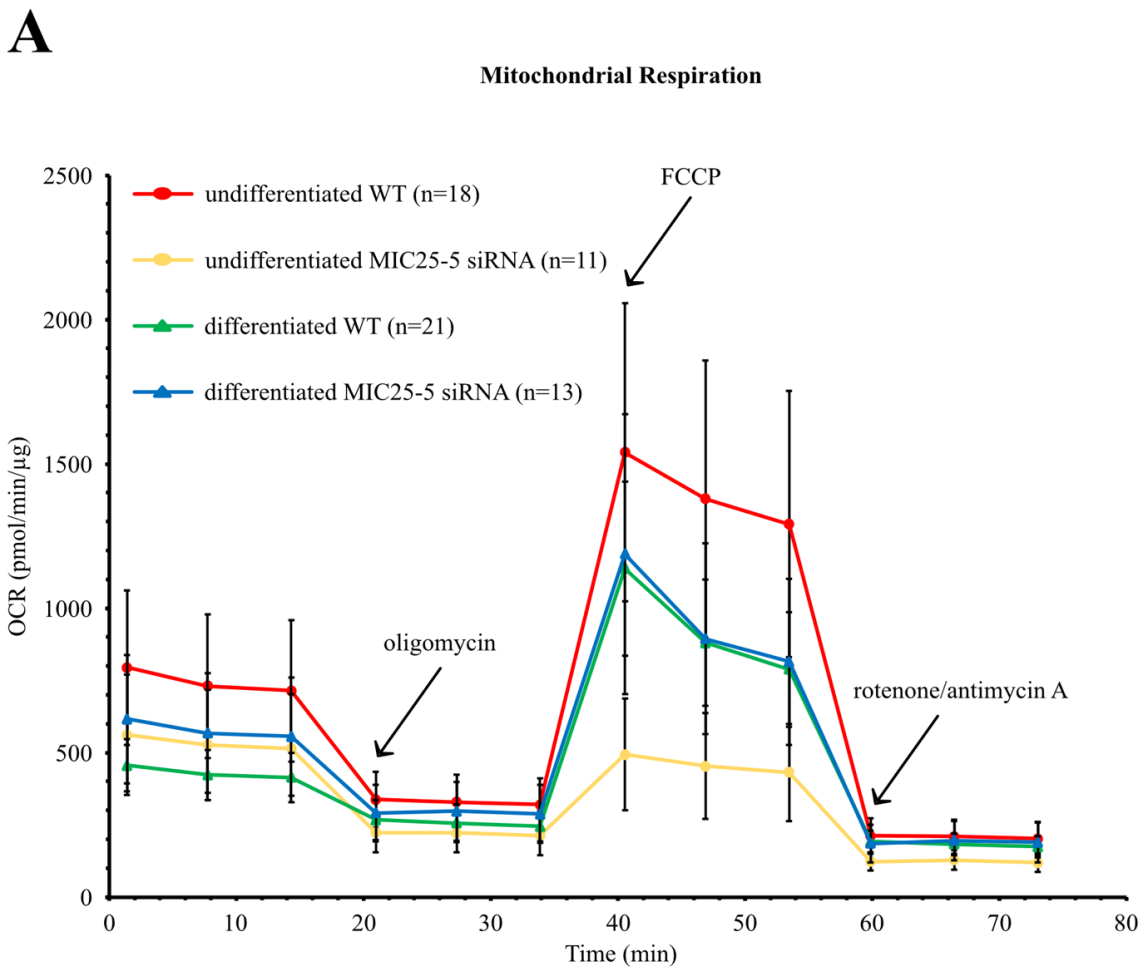

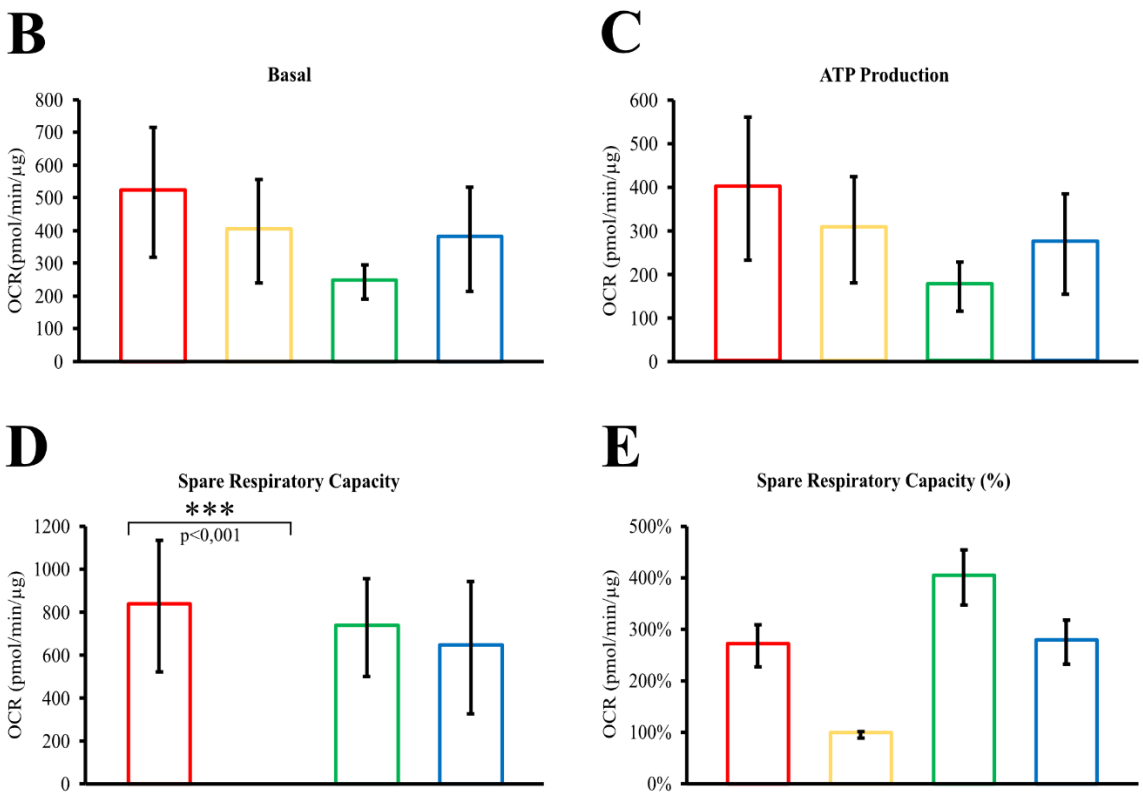

Figure 12 Influence of differentiation status and MIC25 presence on oxygen consumption of SH-SY5Y cells

A. Oxygen consumption rates of SH-SY5Y cells were measured by Seahorse XFe96 Analyzer and Mito Stress Test Kit over time in four different conditions: undifferentiated WT (red), undifferentiated MIC25-5 siRNA (yellow), differentiated WT (green) and differentiated MIC25-5 siRNA (blue). Obtained data was normalised for protein quantity (y-axis pmol/min/µg protein). Error bars indicate two standard deviations. **B-E.** Basal oxygen consumption rate, ATP production, absolute respiratory capacity and relative respiratory capacity were graphed for the same experiment and the same conditions as depicted in A. Undifferentiated WT in red, undifferentiated MIC25-5 siRNA in yellow, differentiated WT in green and differentiated MIC25-5 siRNA in blue. Error bars indicate two standard deviations (SD). A nonparametric Kruskal-Wallis Test was conducted for measurements of spare respiratory capacity (**D**). Significant differences (Chi square = 29.575, $p < 0.001$, df = 3) were found among the four compared categories. Post-hoc Bonferroni correction for multiple comparisons found that the spare respiratory capacity of cells was significantly different between undifferentiated WT and undifferentiated MIC25-5 siRNA cells ($p < 0.001$).

To maintain steady intracellular pH levels, cells translocate protons out of their cell bodies into the extracellular space which can be indirectly correlated to the intracellular emergence of protons [48]. While converting glucose to ATP, the cell produces acidic by-products: lactate by glycolysis (1 proton/ATP) or bicarbonate (0.18 protons/ATP) by oxidative phosphorylation [48]. Lactate production by glycolysis and acidification of the extracellular space not only correlate under basal conditions, but also when glycolytic activity is enhanced by e.g. hypoxia or ceases with e.g. impaired glucose uptake of the cell [48].

The Seahorse XFe96 Analyzer can measure extracellular acidification rates (ECAR) correlating to the

cellular lactate production by glycolysis. Again, four conditions were assessed, each at basal rates and following the introduction of oligomycin, FCCP and rotenone/antimycin A. The difference between ECAR when oligomycin is added and basal ECAR can be referred to as spare glycolytic capacity.
In Figure 13A, undifferentiated WT cells show spare glycolytic capacity enabling them to switch from oxidative phosphorylation to increased glycolysis as soon as oligomycin inhibits the ATP synthase. MIC25 siRNA knockdown cell lines only show spare glycolytic capacity marginally whereas differentiated WT cells do not seem to switch to glycolytic activity at all. Interestingly, their basal ECAR is lowest throughout the experiment indicating that those cells heavily bank on oxidative phosphorylation to meet their energy demands. Conversely, undifferentiated WT cells seem to be more adaptable for example to glucose scarcity enabling them to keep proliferating even in dire conditions. As MIC25 siRNA knockdown measurements both show similar curves, the basal ECAR is already higher than in undifferentiated WT cells. From the beginning, those cells rely more on glycolysis. Henceforth, they cannot largely increase their glycolytic activity when oligomycin makes ATP synthesis via oxidative phosphorylation impossible. These findings suggest that knockdown of MIC25 might reduce metabolic adaptivity in both undifferentiated and differentiated cells.

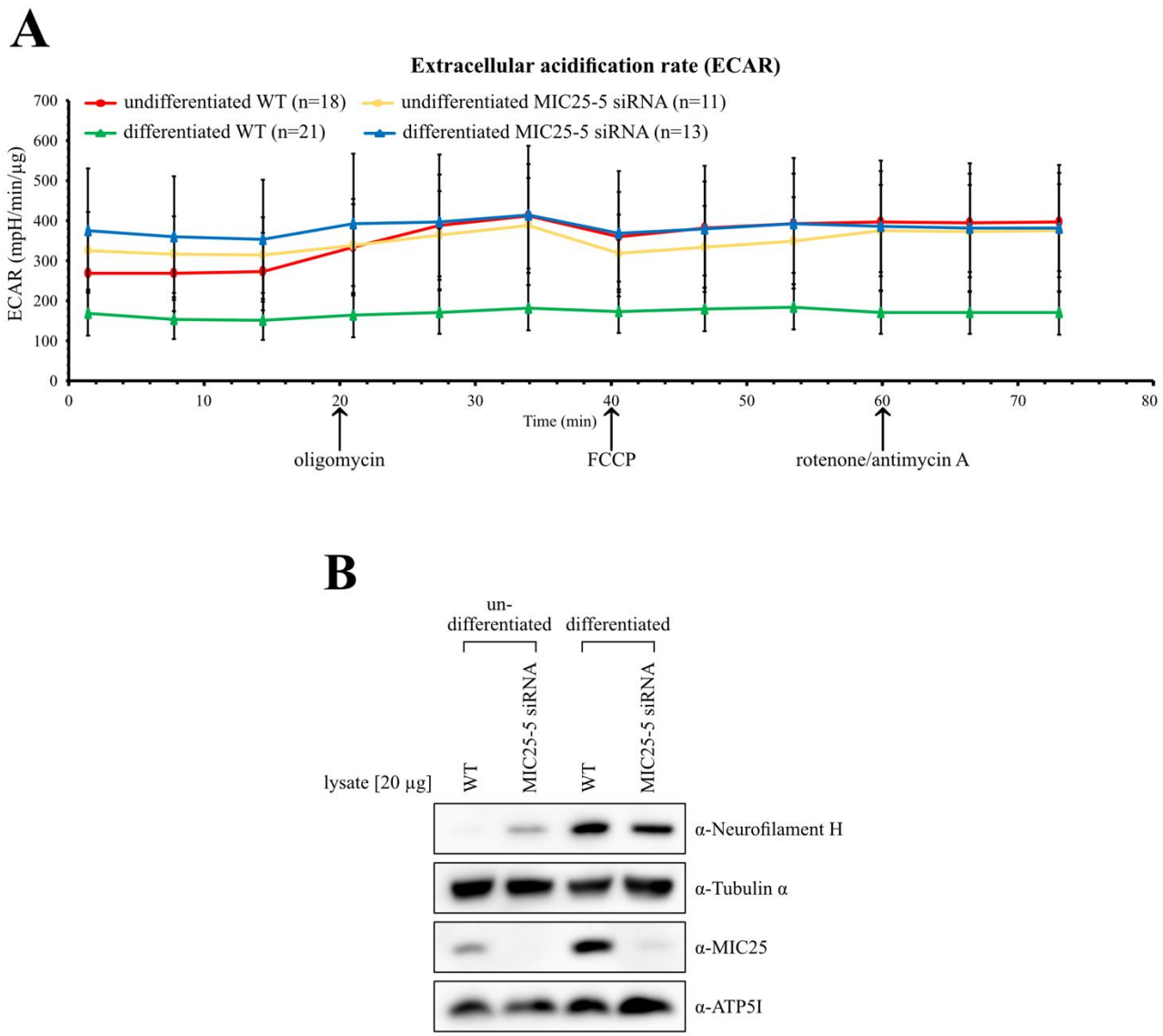

Figure 13 Influence of differentiation status and MIC25 presence on extracellular acidification of SH-SY5Y cells

A. Extracellular acidification rates of SH-SY5Y cells were measured by Seahorse XFe96 Analyzer and Mito Stress Test Kit over time in four different conditions: undifferentiated WT (red), undifferentiated MIC25-5 siRNA (yellow), differentiated WT (green) and differentiated MIC25-5 siRNA (blue). Obtained data was normalised for protein quantity (y-axis mpH/min/µg protein). Error bars indicate two standard deviations. **B.** Undifferentiated and differentiated SH-SY5Y lysates of WT and MIC25-5 siRNA knockdown cells were analysed by a western blot to confirm differentiation and depletion of MIC25 for Figure 12A-E and Figure 13A.

To confirm differentiation and MIC25 knockdown, cell lysates were loaded on a SDS gel and blotted (Figure 13B). High intensity antibody detection for NFH in lanes with differentiated cells and faint bands for undifferentiated cells confirms differentiation, even though loss of MIC25 in undifferentiated SH-SY5Y cells leads to increased detection of NFH when compared to undifferentiated WT cells (see

chapter 5.1). Tubulin α acts as control for cytoplasmic expression and its bands are similar across all conditions. Undifferentiated and differentiated samples treated with MIC25 siRNA only show marginal MIC25 detection, confirming efficient knockdown. Here, ATP5i is the control of choice for expression of mitochondrial proteins, the band detection density is similar across all four conditions as well.

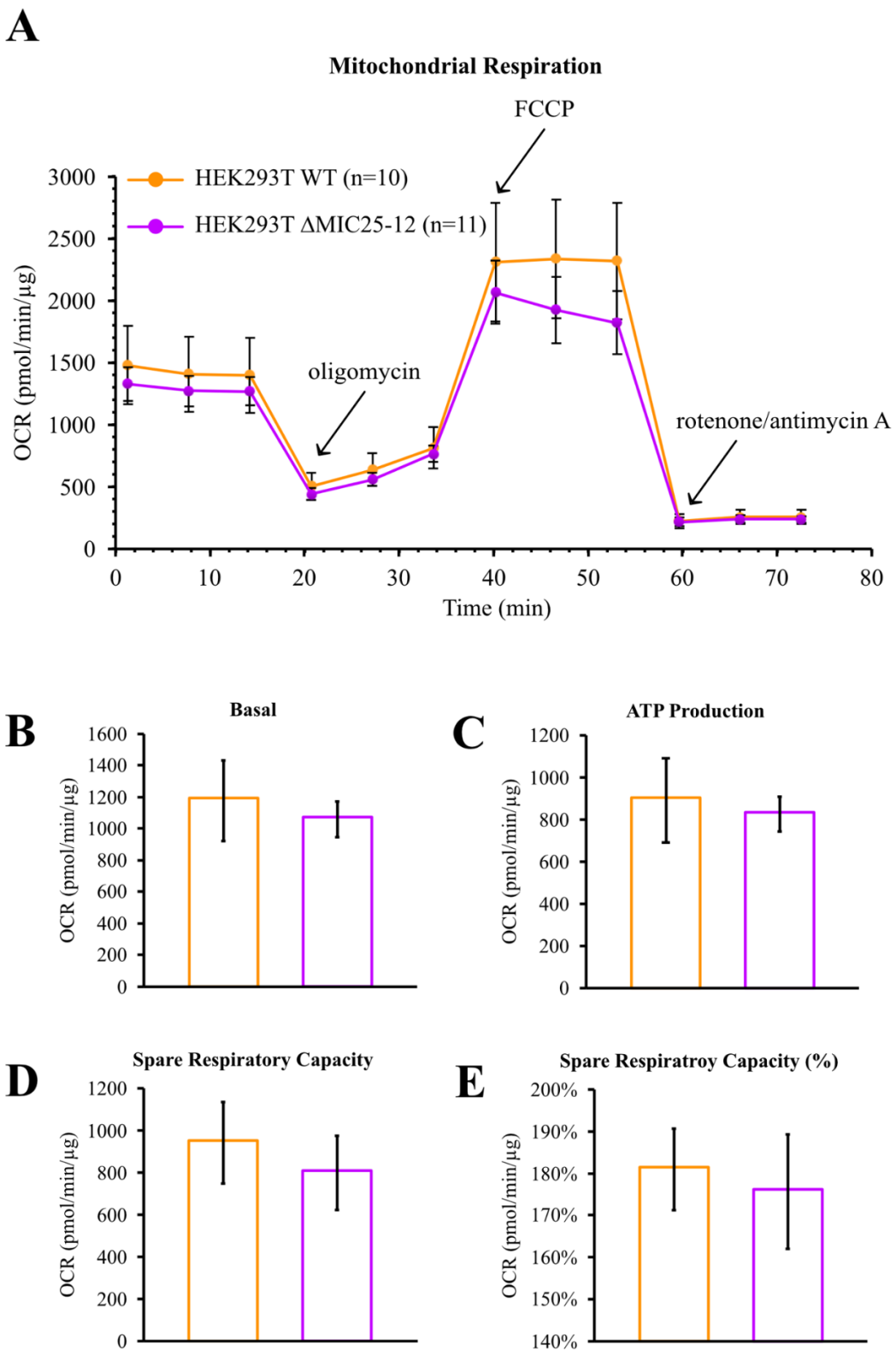

Figure 14 MIC25 presence and oxygen consumption of HEK293T cells
A. Oxygen consumption rates of HEK293T WT (orange) and ΔMIC25-12 (purple) were measured by Seahorse XFe96 Analyzer and Mito Stress Test Kit over time. Obtained data was normalised for protein quantity (y-axis pmol/min/µg protein). Error bars indicate two standard deviations. **B-E.** Basal oxygen consumption rate, ATP production, absolute respiratory capacity and relative respiratory capacity were graphed for the same experiment and the same conditions as depicted in A. HEK293T WT in orange, HEK293T ΔMIC25-12 in purple. Error bars indicate two standard deviations (SD).
Experiments labelled as Figure 14 A-E were conducted by Sybille Jungbluth and Karina von der Malsburg.

Human embryonic kidney (HEK) cells, as they resemble progenitor kidney cells, do not show any neuronal features such as the capacity to grow axons or dendrites. Henceforth, measurements of oxygen consumption rates for HEK293T WT and HEK293T MIC25-12 knockout (KO) cells were carried out to inquire effects of MIC25 presence/absence outside the neuronal prerequisite (Figure 14A). After sequentially adding oligomycin, FCCP and rotenone/antimycin A, basal respiratory rate, ATP production rate and absolute and relative spare capacity (Figure 14B-E) were not substantially different when MIC25 was knocked out compared to its HEK293T WT. This is particularly interesting when reconciling that MIC25 expression seems to increase selectively in brain tissue of mice (see Figure 4) leading to the assumption that MIC25 might be needed in neurons selectively to accommodate to metabolic needs of the undifferentiated and differentiated cell.
Concluding this chapter, MIC25 expression rates seem to be linked to tissue specific metabolic needs. Whereas in HEK293T cells, MIC25 knockout does not greatly influence oxygen consumption rate at any given condition, the picture shifts for SH-SY5Y cells. Firstly, differentiation processes lead to lower basal respiration, maximal respiration, and ATP production rates, but those cells can increase their relative spare respiratory capacities most efficiently. Secondly, MIC25 knockdown in undifferentiated and differentiated cells leads to similar rates of basal respiration and ATP production, both lower than in undifferentiated WT, but higher than in differentiated WT. Whereas differentiated MIC25 knockdown cells do still show increases in absolute and relative spare capacity, even though lower than differentiated WT, undifferentiated MIC25 knockdown depletes both completely. Thirdly, only undifferentiated WT cells can increase glycolytic activity when ATP production by ATP synthase is not possible. Thus, MIC25 seems to be indispensable for on the one hand tissue specific metabolic adaptation, on the other hand the ability to respond to stress. Here, another factor will be discussed in the following chapter: The mitochondrial membrane potential as driving force of ATP production [37].

4.7. The absence of MIC25 in differentiated SH-SY5Y cells reveals hyperpolarisation of mitochondrial membrane potential

The mitochondrial membrane potential $\Delta\psi_m$ is the result of the ability of the complexes of the electron transport chain to pump protons [37]. This leads to a net alkaline and negatively charged mitochondrial matrix of -180 mV and is thus the main driver for oxidative phosphorylation by ATP synthase [37]. Maintaining the mitochondrial membrane potential at a healthy medium level is crucial for minimising generation of reactive oxygen species (ROS) and ultimately for the cells' survival [103]. In this approach, TMRE, which is highly positively charged, accumulates in areas with net negative charges in a linear manner. Thus, mitochondria with rather depolarised membrane potentials accumulate less TMRE than mitochondria with hyperpolarised membrane potentials. Figure 15A shows the accumulation of TMRE within mitochondria of living SH-SY5Y cells normalised for protein quantity for four conditions: Undifferentiated WT, differentiated WT, undifferentiated MIC25 siRNA and differentiated MIC25 siRNA. For each condition, TMRE fluorescence signal was measured in two different states: with and without adding 20 µM FCCP. As FCCP acts as uncoupling protein, protons pass from the intermembrane space of mitochondria into the mitochondrial matrix. This reduces the net negative charge across mitochondrial membranes disrupting the electrochemical gradient which is needed to accumulate TMRE. Thus, cells where FCCP was added, act as negative control. Henceforth, all measurements are relative values displayed as the multiple of 1, as the measurements where FCCP was added were averaged and used as reference point (and thus are 1 for each condition). This methodology allows comparison of net increased accumulation of TMRE and thus increased mitochondrial membrane potential with a FCCP-induced baseline of nearly maximally depolarised mitochondria. Firstly, and not surprisingly, all cells show higher membrane potentials without FCCP present which is resembled by columns bigger than 1. When comparing undifferentiated and differentiated WT mitochondrial membrane potentials as well as undifferentiated and differentiated MIC25 siRNA mitochondrial membrane potentials, there is no significant difference ($p > 0.05$). Moreover, between undifferentiated WT and undifferentiated MIC25 siRNA mitochondrial membrane potentials, no significant difference is detectable ($p > 0.05$). Though, there is a statistically significant difference between differentiated WT and MIC25 siRNA cells ($p = 0.001$). Thus, when MIC25 is absent due to siRNA knockdown in differentiated cells, mitochondrial membrane potential increases. This indicates that the electrochemical gradient between the mitochondrial intermembrane space and matrix becomes steeper, possibly due to maximal proton pumping activity of the electron transport chain as the result of a response to cellular and mitochondrial stress that could lead to impaired mitochondrial function and ultimately cellular demise.

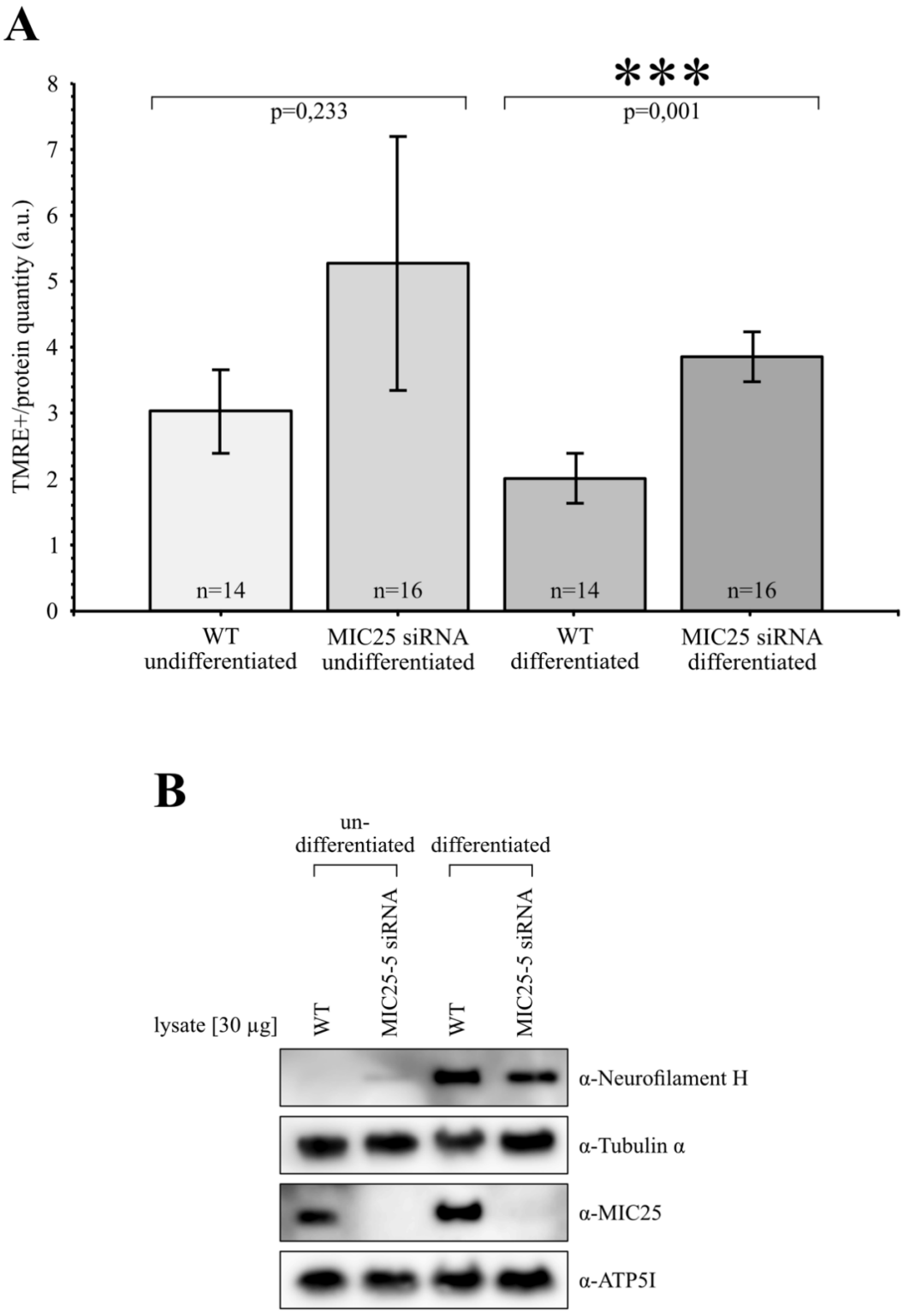

Figure 15 Influence of differentiation status and MIC25 presence on mitochondrial membrane potential of SH-SY5Y cells

A. Mitochondrial membrane potential was analysed by accumulation of TMRE (highly positively charged) in the mitochondrial matrix (usually negatively charged) and its fluorescence signal measured. Each condition was measured with and without the addition of FCCP which acts as negative control as the membrane potential collapses and sequestering TMRE becomes impossible. Therefore, each condition is depicted as relative value to the multiple of 1, where the average of measurements where FCCP was added

acts as reference point (and is hence 1 for each condition). Error bars indicate one standard deviation (SD). A nonparametric Kruskal-Wallis Test was conducted to examine the differences in mitochondrial membrane potential in WT and MIC25-5 siRNA knockdown cells according to differentiation status. Significant differences (Chi square = 16.85, p = 0.000, df = 3) were found among the four compared categories. Post-hoc Bonferroni correction for multiple comparisons found that the mean mitochondrial membrane potential was significantly different between differentiated WT and differentiated MIC25-5 siRNA cells (p = 0.001). There was no statistically significant difference between undifferentiated WT and undifferentiated MIC25 siRNA cells (p > 0.05). **B.** Undifferentiated and differentiated SH-SY5Y lysates of WT and MIC25-5 siRNA knockdown cells were analysed by a western blot to confirm differentiation and depletion of MIC25.

Figure 15B confirms differentiation by depicting NFH expression in differentiated WT and MIC25-5 siRNA knockdown cells. Notably, NFH expression slightly increases, and undifferentiated MIC25-5 siRNA knockdown cells compared to WT cells (see chapter 5.1). Tubulin α antibody, which shows similar expression in all lanes, acts as cellular control. Similarly, stable expression of ATP5i in all samples acts as control for expression of mitochondrial proteins. Therefore, missing MIC25 antibody detection in both undifferentiated and differentiated MIC25-5 siRNA knockdown cells seems to be an effect of siRNA knockdown and hence did not happen by chance.

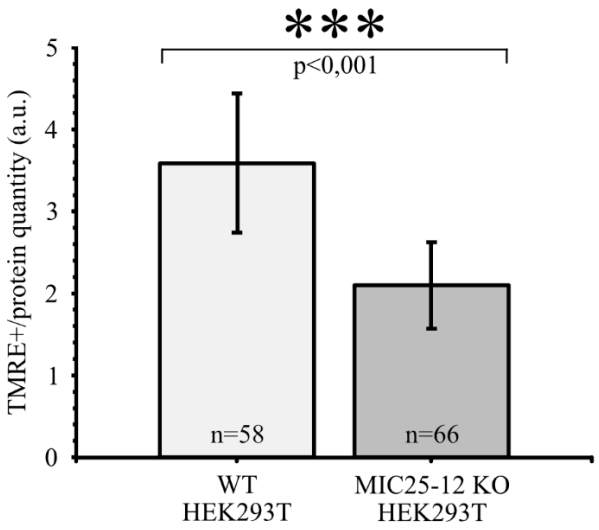

Figure 16 Influence of MIC25 presence on mitochondrial membrane potential of HEK293T cells

Mitochondrial membrane potential was analysed by accumulation of TMRE (highly positively charged) in the mitochondrial matrix (usually negatively charged) and its fluorescence signal measured. Each condition was measured with and without the addition of FCCP which acts as negative control as the membrane potential collapses and sequestering TMRE becomes impossible. Therefore, HEK293T WT and HEK293T MIC25-12 KO are depicted as relative values to the multiple of 1, where the average of measurements where FCCP was added acts as reference point (and is hence 1 for each condition). Error bars indicate standard deviation (SD). A two-sided T-test assuming unequal variances was performed to examine the differences in mitochondrial membrane potential in HEK293T WT and MIC25-12 KO cells. The mean value of HEK293T WT (M = 3.59, SD = 1.70) was significantly different from the mean value of HEK293T MIC25-12 KO (M = 2.09, SD = 1.06); t (93.36) = 5.80, p < 0.001.

Like in chapter 4.6, results of mitochondrial membrane potential measurements in undifferentiated and differentiated SH-SY5Y cells with or without MIC25 were compared with data from HEK293T WT and HEK293T MIC25-12 KO (Figure 16). Again, mitochondrial membrane potential was measured once with the addition of 20 µM FCCP and once without. By collapsing the mitochondrial membrane potential, its uncoupling effect prevents TMRE accumulation, establishing a baseline for minimal membrane potential. Wielded as negative control, measurements with FCCP are averaged and used as reference point with the value 1 for describing all measurements without FCCP for each condition as the multiple of 1. This identical approach makes Figure 15A and Figure 16 comparable in relative terms. Astonishingly, significant differences were observed between both conditions. Mitochondrial membrane potentials in HEK293T MIC25-12 KO are significantly lower than in WT cells ($p < 0.001$). While for undifferentiated and differentiated SH-SY5Y cells lacking MIC25, membrane potentials are on average about 5 times/4 times as high as the baseline, the membrane potential in HEK293T cells lacking MIC25 only increases by two-fold indicating different cellular responses to removal of MIC25. Taking this together, differentiation status of SH-SY5Y cells does not have a significant impact on the mitochondrial membrane potential. But loss of MIC25 due to siRNA knockdown in differentiated SH-SY5Y cells significantly increases mitochondrial membrane potential. Loss of MIC25 in differentiated SH-SY5Y cells could be an explanation for induction of cellular stress responses leading to maximal activity of the electron transport chain. Though, cell type and differentiation status in combination with lack of MIC25 greatly influences mitochondrial membrane potential in unexpected ways. While in HEK293T cells without MIC25, the membrane potential significantly decreases, in undifferentiated SH-SY5Y cells lacking MIC25, no significant effect was observed, and in differentiated SH-SY5Y cells lacking MIC25, significant hyperpolarisation is observed. This pinpoints highly versatile effects of MIC25 depending on tissue and cellular state which will be further discussed in chapter 5.3.

5. Discussion

5.1. As part of the MIB complex, MIC25 expression increases in differentiated SH-SY5Y cells

Aim of this thesis was to gain better insight into tissue specific effects of MIC25 as a MICOS protein at mitochondrial cristae junctions. Previous data from our research group has indicated that MIC25 is upregulated in isolated adult brain tissue of mice (see Figure 4). To be able to perform biochemical analysis of MIC25 in relation to the differentiation status in neuronal tissue, two requirements had to be met: (1) finding a suitable cell model for human neuronal cells and (2) establishing reliable neuronal differentiation markers. Of course, the best model to study the effects of MIC25 would be to culture primary human neurons. However, inaccessibility and lack of proliferation makes this technically difficult. Inaccessibility can be overcome by using primary neurons of rodents, but their lack of proliferation stands. For this thesis, SH-SY5Y cells were used as a human-like neuronal cell model as they were retrieved from a four-year old with metastatic neuroblastoma by bone marrow biopsy [17]. Their cancerous origin lets them replicate in cell culture whereas their origin from the sympathetic nervous system allows differentiation processes to take place [113] making comparisons of MIC25 presence or absence between undifferentiated and differentiated cellular states possible. Many other neuronal-like cells that are easy to cultivate, such as PC12 and Neuro-2a, are generated form non-human species [226].

It has been reported that differentiation of SH-SY5Y cells leads to identification of several neuronal markers, like MAP2, Synaptophysin, neuronal nuclei antigen (NeuN) and others [31,121]. The challenge was to find a marker that provided reliable detectability on SDS-PAGE with low loading quantities and validity not only for lysed cells, but also for isolated mitochondria. Neurofilament H (NFH) provided all those requirements (Figure 5A, Figure 5B, Figure 6A). Even though NFH has mostly been used as target for immunofluorescence to confirm axonal outgrowth during differentiation [25,53], there is evidence that NFH has previously been used to corroborate differentiation [82] in a successful manner. Numerous pieces of evidence point towards interaction of mitochondria and NFs [85,117,118]. Overly et al. [149] observed the motility of dendritic and axonal mitochondria: Mitochondria located in dendrites preferably stayed stationary and when moving, where shipped shorter distances compared to mitochondria in axons which correlated to increased metabolic activity in dendrites but decreased metabolic activity in axons. Additionally, in vitro data suggests, that highly phosphorylated NFH side-arms preferentially bind mitochondria with high membrane potential [209]. This indicates a role of NFs in controlling localisation and state of mobility of mitochondria [209], that may help to explain the slight NFH increase upon MIC25 knockdown (see Figure 7, Figure 13 and Figure 15), as loss of MIC25 is associated with increased mitochondrial membrane potential (see chapter 4.7 and chapter 5.3).

As cell model and differentiation marker are decided on, providing evidence for increased MIC25 expression in differentiated SH-SY5Y cells was the next step (Figure 6A). Quantitative analysis of MIC25 expression in SH-SY5Y cells (Figure 6B) demonstrates that the increased MIC25 levels observed upon differentiation are not only observed in whole-cell lysates but also in isolated mitochondria. Moreover, the extent of this increase is similar when comparing MIC25 levels in differentiated and undifferentiated cells in both lysate and mitochondria. This leads to the conclusion that MIC25 is increasing in its mitochondrial compartment, and the same protein pool can be detected when cells are lysed. To answer questions about MIC25 behaviour in its natural environment, the MICOS and MIB complex, biochemical approaches were used. Blotting for other MICOS and MICOS-related proteins on SDS-PAGE in differentiated SH-SY5Y cells does not reveal any increased or decreased protein detection apart from increased MIC25 itself when comparing to undifferentiated SH-SY5Y cells. An et al. [6] explored the effects of exogenously expressed HA-S-tagged MIC25 (CHCHD6/CHCM1) next to endogenous MIC25 in RKO colon cancer cells. This model of MIC25 overexpression revealed increased protein abundance of endogenously expressed MIC60 (mitofilin) postulating tight regulation and crosstalk of MIC25 and MIC60 [6]. As increased MIC25 expression in differentiated SH-SY5Y cells does not lead to increased MIC60 levels as in RKO cells, this clearly demonstrates how tissue specific the effects of MIC25 levels can be. This finding is subject to limitations, as MIC25 in differentiated SH-SY5Y cells is endogenously overexpressed, thus not genetically modified and introduced externally reducing exogenous errors.

The organisation of MICOS proteins into two subcomplexes has been clearly illustrated in previous studies, as downregulation of one protein can lead to instability of other components of the respective protein (sub-)complex depending on how crucial that protein is for the overall stability [7,76,110,119,147,148,199]. In HAP1 cells, depletion of MIC60 leads to loss of MIC19 and MIC25, as well as loss of all proteins of the MIC10-subcomplex, MIC10, MIC26, MIC27 and QIL1 [110]. Knockout of MIC10 primarily leads to loss of QIL1, MIC26 and MIC27, an effect of selective destabilisation of the MIC10-subcomplex [110]. Loss of MIC25 or MIC26 in HeLa cells did not affect expression levels of other MICOS components [148]. This alludes to the observation that MIC25 siRNA knockdown in undifferentiated and differentiated SH-SY5Y lysates does not influence other MICOS and MICOS-related proteins (Figure 7). As attempts to produce SH-SY5Y MIC25 knockout cells failed, knockdowns using siRNA were chosen to achieve MIC25 depletion. Thus, effects of MIC25 depletion in isolated mitochondria of undifferentiated and differentiated SH-SY5Y cells, instead of crude lysates, were not retrievable due to the large number of transfected cells that would have been needed to isolate enough mitochondria. Hence, this observation is limited to the compartment of a whole cell, even though discussed data from one paragraph above (or see Figure 6B) does not indicate a second pool of MIC25 outside of mitochondria.

A recent study overexpressed MIC25 by introducing $MIC25^{FLAG}$ to HeLa cells and observed increased affiliation of endogenous MIC25 or exogenous $MIC25^{FLAG}$ into MICOS and MIB complexes on BN-

PAGE [199]. Similar results can be observed for SH-SY5Y cells, as increased MIC25 expression in differentiated mitochondria compared to undifferentiated mitochondria can be seen as a form of endogenous MIC25 overexpression. The protein detection of MIC25 in differentiated isolated mitochondria within MICOS complex is increased compared to undifferentiated isolated mitochondria (Figure 8). MIC25 thus seems to be increasingly incorporated into the MICOS complex. This does not seem to be true for other MICOS proteins, as their detection levels remains stable. Conversely, Tang et al. [199] reports a decrease of endogenous MIC19 in MICOS complex when overexpressing $MIC25^{FLAG}$ in HeLa cells. In MIC19 KO cells, overexpression of $MIC25^{FLAG}$ restored other MICOS proteins, normal mitochondrial shape was preserved, and MIC25 increasingly incorporated into the MICOS complex [199]. This led to the conclusion that MIC25 acts as partial alternative for MIC19 in building and maintaining MIC60-MIC19-SAM50 axis which is crucial in forming contacts between outer and inner mitochondrial membrane constructing and controlling mitochondrial ultrastructure [199]. Structurally, MIC25 and MIC19 have great similarities, as they are disclosed as twin CX_9C proteins, are similar in size and exhibit 36% sequence identity [237]. Experimental approaches have provided evidence for binding of MIC19 to MIC60 via its CHCH domain and to SAM50 via its N-terminus in a myristylation-dependent manner [39,47]. Similarly, MIC25 directly interacts with MIC60 via its C-terminus (including its CHCH domain) and with SAM50 via its N-terminus [6,47]. Additionally, direct interactions between MIC60 and SAM50 have been reported [47]. However, MIC25 seems to be dispensable for a stable connection of MICOS and SAM [47,199], whereas MIC19 proves to be vital in this connection [39,199]. To what extent this holds true for neuronal-like cells or what other purpose increased MIC25 incorporation into MICOS might serve still needs to be elucidated by further inquiries. It is arguable, that BN page itself (like in Figure 8) is not the optimal method for detection of increased MIC25 incorporation into MICOS complex in differentiated SH-SY5Y cells, as a) there are sensitivity and detection limits of size shifts of the protein complexes, b) MIC25 could be incorporated sub-stoichiometrically, or c) MIC25 might incorporate into alternate assemblies possibly with MIC19 and/or SAM50.

To follow these thoughts, co-immunoprecipitations of ^{FLAG}SAM50 in mitochondria of undifferentiated and differentiated SH-SY5Y cells were performed. MIC25 was eluted in both conditions, but to an increased extend in differentiated ^{FLAG}SAM50 eluates (Figure 10). This adds evidence that increased MIC25 detection in differentiated SH-SY5Y cells is not restricted to MICOS itself but is also discernible in MIB complex. Interestingly, in differentiated isolated SH-SY5Y mitochondria, SAM50 detection within MIB complex on BN-PAGE increases, but not within SAM complex itself, which is detectable at a lower molecular weight (Figure 8). It has been observed that co-expression of ^{FLAG}SAM50 together with endogenous SAM50 reduces the amount of endogenous SAM50 detectable (see Figure 9). At first sight, this does not seem to be inherently coherent, but hypothetically the total amount of SAM50 within a cell could be limited. This could be explained by the predicament that certain proteins do need to assemble with other proteins for their long-term stability, as increased

stability of proteins due to heteromeric complex assembly is well documented [179,184,199]. Thus, increased presence of MIC25 could supposedly increase the limit of the SAM50 protein pool in a cell. Henceforth, MIC25 might play, together with SAM50, a neuronal-specific role in stabilisation and maintenance of the contact of the outer and inner mitochondrial membrane. To further test this, co-immunoprecipitation assays of ^{FLAG}SAM50 in MIC60-depleted mitochondria of undifferentiated and differentiated SH-SY5Y cells could be performed in the future. Would the increase in detection rates of MIC25 in differentiated conditions persist?

Evidence suggests that reduction of SAM50 in HeLa cells leads to loss of cristae architecture on top of a distorted, rather spherical mitochondrial structure [147]. Its function in maintaining mitochondrial ultrastructure is independent of sorting and assembly of β-barrel proteins crediting its role as part of the MIB complex, next to MIC60, MIC19 and MIC25, working as gantry to maintain cristae architecture [147,199]. However, differences in distribution patterns of SAM50 across cell types were found. In fibroblasts, SAM50 is described as evenly distributed across the mitochondrial surface [96], whereas in astrocytes, SAM50 seemed to form networks unevenly distributed across the intermembrane space, only overlapping partially with crista junctions [180]. When overlapping distribution patterns of SAM50 with those of MIC19, other sites of association apart from exclusively the crista junctions were proposed [180]. Whether there might be contacts of MIC25 and SAM50 on other sites than the crista junction in neuronal-like cells remains highly speculative but provides further research perspectives.

5.2. Mitochondrial networks of SH-SY5Y cells adapt according to their differentiation status

First and foremost, neurons are cells. As every cell, they match their structure to their function by growing long and delicate extensions from their large cell bodies in forms of axons and dendrites to make transferral of information in form of electric signals and neurotransmitters via synapses from cell to cell possible. Due to this exceptional structure, neurons face challenges to metabolically supporting their needs. Therefore, finding differences of mitochondrial networks before and after differentiation of SH-SY5Y cells is reasonable. While undifferentiated SH-SY5Y cells show fragmented mitochondrial formations, differentiated SH-SY5Y possess dominantly filamentous mitochondrial arrays. SH-SY5Y cells, like neurons, adapt their structure to their function while differentiating, their retracted, scattered cell bodies outgrow elongated processes making connections to neighbouring cells forming clustered arrays [188]. Thus, filamentous mitochondrial networks seem to support metabolic demands of differentiated SH-SY5Y cells better than spherical ones.

Changes of mitochondrial shape have been well described as the effect of two antagonistic systems: fusion and fission [63,233]. Fusion and fission activities are the effects of GTP hydrolysis by high-molecular weight GTPases: Mitofusin 1 and 2 (MFN1, MFN2) of the outer mitochondrial membrane assist outer mitochondrial membrane fusion and OPA1 as protein of the inner mitochondrial membrane expedites IMM fusion; dynamin-related protein 1 (DRP1) is a cytoplasmic protein that is mobilised to the outer mitochondrial membrane to promote mitochondrial fission [106,146]. Additionally, dispersion of mitochondria in the cell is the result of bidirectional transport along microtubules and their associated motor proteins kinesin and dynamin [28]. Interestingly, fusion and fission dynamics influence axonal transport, as both, extreme fusion (hyperfusion) and extreme fission (fragmentation) can hamper with mitochondrial axonal trafficking [51,56,186]. Neither hyperfusion nor fragmentation is found when knocking down MIC25 and repeating mitochondrial network analysis in undifferentiated and differentiated SH-SY5Y cells. Lacking MIC25, SH-SY5Y cells seem to behave like undifferentiated and differentiated SH-SY5Y WT cells in terms of their mitochondrial network structure leading to the conclusion that differentiation status plays a greater role than presence or absence of MIC25 in forming adept networking structures. Whether shifts from fragmented to filamentous arrays happen later or are more prolonged when MIC25 is absent would need further evaluation by repeating this experimental approach at different steps of differentiation. It is thinkable, that the sub-cellular location of mitochondrial networks in SH-SY5Y cells shifts regarding to MIC25 expression levels. For example, filamentous structures of differentiated SH-SY5Y cells could be concentrated around the nucleus or dispersed into axon-like protrusion. To answer this question, further immunofluorescence assays with an alternative evaluation focus could be a next step. Further limitations arise due to the inability to evaluate the effect of MIC25 at sub-mitochondrial structures. In which way mitochondrial inner boundary membrane, crista junction and cristae tubules might

structurally be affected can only be revealed by higher resolution microscopy such as electron transmission microscopy. Published data draws an ambivalent picture: Ott et al. [148] observed no altered cristae morphology when HeLa cells lacked MIC25 but Ding et al. [47] noted lesser cristae junctions and reduced cristae density, and An et al. [6] described clearly altered mitochondrial cristae structure when eliminating MIC25 in RKO, MCF-7 and A375 cells raising further data to support the stance of cell-type specific effects of MIC25.

During embryonic neurogenesis, morphological changes of mitochondria have been observed to play a crucial role in determining the fate of neuronal stem cells. Mils et al. [132] observed neurogenesis in the spinal cord of mice and chicken. Mitochondria in mitotic cells were small and round, in the interphase they were short and thick [132]. In differentiating neurons, mitochondrial length increased accompanied by increased complexity of mitochondrial networks enabling those cells to become a more efficient energy provider to fulfil changing energetic demands of differentiating neurons [132]. Changes of mitochondrial networks have therefore been shown to not accompany, but direct metabolic changes from glycolysis to oxidative phosphorylation as well as stem cell fate [107,108]. Due to mild, acute mitochondrial fragmentation, neuronal stem cells appear to become committed progenitors at the expense of their ability to self-renew by retrograde mitochondrial-to-nuclear signalling activating transcription genes and silencing self-renewal genes [107]. However, like observed in many neurodegenerative diseases, a shift of mitochondrial networks toward chronic states of fragmentation, diminishes neuronal ability to self-renew and reduces the stem cell pool [107]. Henceforth, differences in mitochondrial networks of undifferentiated and differentiated SH-SY5Y cells could play an important role in guiding and accompanying the physiological process of neurogenesis and facilitate shifts in energy provision at different developmental stages.

5.3. MIC25 has tissue specific effects on membrane potential and metabolism of SH-SY5Y cells

As chapter 5.1 discusses MIC25 on a protein-focused level using biochemical approaches, this chapter will broaden the horizon and elaborate on MIC25 in context of cellular and mitochondrial metabolism. It has been demonstrated that MIC25 expression increases in differentiated SH-SY5Y cells within its multiprotein complexes MICOS and MIB, thus hypothesising how those structural differences might correlate to functional dissimilarities is not farfetched. In the following, results of extracellular flux assays and membrane potential measurements will be discussed along three major bullet points: Differences between undifferentiated and differentiated SH-SY5Y cells, differences between MIC25 presence and absence, and differences in SH-SY5Y cells compared to other cell types.

Mounting evidence suggests that differentiation processes of neuronal stem cells into adult neurons are accompanied by a metabolic shift towards increased mitochondrial activity, alongside a corresponding decrease in glycolysis and fatty acid oxidation [3,15,196,241]. For example, proteins associated with glycolysis such as hexokinase 2 (HK2) and lactate dehydrogenase isoform A (LDHA), are downregulated during differentiation [241]. These changes are reflected in Figure 13A, where differentiated SH-SY5Y cells exhibit limited glycolytic activity. Only in undifferentiated cells, inhibition of ATP synthase leads to increased glycolytic activity. This reflects their higher basal glycolytic activity and greater capacity for upregulation, which in turn points towards their metabolic reliance on glycolysis. In contrast, when looking at oxygen consumption rates, differentiated SH-SY5Y cells have lower basal respiratory activity, maximal respiratory activity and ATP production rates compared to undifferentiated SH-SY5Y cells (Figure 12A-E), despite mitochondrial membrane potentials being about the same (Figure 15A). An explanation could be that undifferentiated SH-SY5Y cells are more proliferative, whereas differentiated SH-SY5Y cells tend to exit the cell cycle [227]. Moreover, differentiated SH-SY5Y cells exhibit enhanced spare respiratory capacity, highlighting an improved ability to adjust mitochondrial ATP production to cellular demands and thus use mitochondrial energy more efficiently. In contrast, undifferentiated SH-SY5Y cells rely heavily on glycolysis to meet their energy demands. This shift suggests metabolic adaptation of differentiated SH-SY5Y cells allowing them to provide sustained energy production in basal conditions and increase it when necessary, e.g. due to changing conditions. The relative contribution of glycolysis versus alternative substrates like acetyl-CoA to oxygen consumption remains unclear; further experiments using 2-deoxyglucose that blocks glycolysis could provide insight [105,191]. All-trans retinoic acid (ATRA), which triggers differentiation and inhibits the cell-cycle, is primarily responsible for metabolic changes brought upon SH-SY5Y cells during and after differentiation [130]. By inducing differentiation, ATRA indirectly promotes the metabolic shift from glycolysis towards oxidative phosphorylation, as reflected in differentiated SH-SY5Y cells [130]. This remodelling in a broader sense includes shifts in signalling pathways, structural adaptations and enhanced mitochondrial

proliferation [130]. Notably, ATRA is currently being used clinically to treat cancers such as acute promyelocyte leukaemia and paediatric neuroblastoma [95,142].

Loss of MIC25 points towards altered mitochondrial metabolism and function. Hyperpolarised mitochondrial membrane potentials in differentiated SH-SY5Y MIC25 knockdown cells are a sign of increased creation of reactive oxygen species (ROS) and thus cellular stress [103]. Experimental studies have demonstrated that a mitochondrial membrane potential surpassing 140 mV prompts an exponential increase in ROS production [112,173] making tight governance of the membrane potential vital to keep it in physiological ranges of approximately 80 to 140 mV [103]. To further test this, ROS production could be measured in undifferentiated and differentiated SH-SY5Y cells with normal and depleted MIC25 levels. Commonly used methods include fluorescent probes sensitive to different oxidants that can be analysed by plate-based fluorescent assays, fluorescent microscopy or flow cytometry, and electron paramagnetic (spin) resonance (EPR/ESR) allowing straightforward identification of free radicals [60,140]. In SH-SY5Y cells with depleted MIC25 levels, findings of higher basal glycolytic activity and trouble to further increase it under oligomycin stress support that MIC25 is essential for metabolic adaptability under compromised mitochondrial activity (Figure 13). In line with previous studies [6,185], knocking down MIC25 in undifferentiated SH-SY5Y cells reduces their oxygen consumption rates and, as a result, lowers their spare respiratory capacity compared to its WT counterpart. A similar, but less pronounced effect is seen in differentiated SH-SY5Y cells lacking MIC25. Their spare respiratory capacity is reduced in comparison to differentiated SH-SY5Y WT cells, but their basal respiration and ATP production remain mainly unchanged. This is surprising given that MIC25 expression naturally increases during differentiation, suggesting it plays a more critical role in mature neurons. One would expect not only impaired spare respiratory capacity but also basal bioenergetic parameters (see chapter 4.1 and 5.1 for reference). Hypothetically, there could be a shift in the role of MIC25. In differentiated cells, influence of MIC25 on mitochondrial bioenergetics could become secondary to other tasks. A recent paper proposes a connection between MIC25, and a protein closely related to Alzheimer's disease (AD), the β-amyloid precursor protein (APP) [185]. One of the key features of Alzheimer's pathology is the accumulation of plaques in the brain consisting of β-amyloid (Aβ) protein aggregates [240]. The transmembrane protein APP can be cleaved by different secretases: β- and γ-secretases sequentially cleave APP which generates Aβ among other products (amyloidogenic processing) [240]. α-Secretases cleave APP molecules within the Aβ domain which impedes Aβ formation (non-amyloidogenic processing) [240]. Following conventional knowledge, the plasma membrane is a major processing site of APP [218]. It is lesser known, that the endoplasmic reticulum (ER), the trans-Golgi apparatus and endosomes also have been identified as APP processing sites, especially for the amyloidogenic processing pathway [218]. On top of that, mitochondria and mitochondria-associated membranes have been demonstrated as localisation and processing sites of APP [46,155,219]. Shang et al. [185] proposes a model, where MIC25 and APP stabilise each other in the mitochondrial membranes. As soon as this balance is disrupted by the pathological increase of APP,

MIC25 expression is transcriptionally downregulated leading to less MIC25-APP-links [185]. Consecutively, APP in the mitochondrial outer membrane is increasingly processed into Aβ, which in turn further suppresses MIC25 transcription [185]. This feedback loop propagates APP processing and Aβ accumulation fuelling pathological plaque formation [185]. Furthermore, Wilkins et al. [219] describes an inverse relationship between APP co-localisation to mitochondrial membranes and Aβ secretion, depending on the mitochondrial membrane potential. Depolarisation observes more APP in the mitochondrial outer membranes while Aβ secretion stalls, hyperpolarisation diminishes APP in mitochondrial outer membranes while Aβ secretion increases [219]. Differentiated SH-SY5Y cells lacking MIC25, compared to their WT respectively, display a significantly higher membrane potential (Figure 15). According to Wilkins et al. [219], this would lead to reduced APP levels in the outer mitochondrial membrane and mitochondria-associated membranes, while Aβ secretion into the extracellular space would increase. As reported by Shang et al. [185], this would further reduce MIC25 transcription rates. Hence, inherently increased MIC25 expression levels in differentiated SH-SY5Y cells could hypothetically provide an intrinsic buffer from pathological APP build up and Aβ plaque formation after cleavage by β- and γ-secretases.

Regarding data depicting selective MIC25 increase in isolated brain tissue of mice (see Figure 4 and chapter 2.6), but not in other mouse tissues (heart, skeletal muscle, liver, kidney, lung, and spleen) comparing metabolic data of neuronal-like SH-SY5Y cells with data of human embryonic kidney cells (HEK293T) was particularly interesting. When examining oxygen consumption and ATP production in HEK293T WT and MIC25 KO cells, there is virtually no difference across conditions (see Figure 14). This is not the case for SH-SY5Y cells lacking MIC25, supporting the idea that MIC25 has tissue-specific metabolic functions. The effect is especially strong in the undifferentiated state, were both oxygen consumption rate and ATP production are massively reduced (see Figure 12). Similarly, significant reductions are seen in RKO colorectal cancer cells with MIC25 knocked out [6]. This leaves room for debate of how changes in MIC25 expression relate to its specific roles in other tissues than the brain. Even in HEK293T cells, naturally expressing lower MIC25 rates than differentiated neuronal tissues (see Figure 4 and 2.6), loss of MIC25 is not entirely without effect: mitochondrial membrane potentials decrease significantly when compared to WT (Figure 16). The permeability transition pore (PTP) is a protein megacomplex that forms a channel spanning all mitochondrial membranes [123]. Ablation of the mitochondrial membrane potential has been associated with increased PTP permeability which is proposed to trigger apoptosis [123]. PTP opening is regulated by the mitochondrial membrane potential and matrix pH, as lower membrane potentials increase opening probability, while matrix acidification decreases it [123]. Short, transient PTP openings release ROS and calcium, which act as signalling molecules that either inhibit PTP or promote mitochondrial biogenesis [174]. This ultimately protects against apoptosis, and the membrane potential is quickly restored [174]. Only full, sustained opening of PTP leads to membrane potential collapse and halts oxidative phosphorylation by disrupting the proton gradient [174]. Hence, reduced membrane potentials in HEK293T MIC25 KO cells lower

thresholds and could bring the cells on the brink of apoptosis. However, this conclusion is not supported by measurements of oxygen consumption, ATP production or glycolysis rates, which remain stable. Hypothetically, reduction of membrane potential is significant, but not immediately functionally relevant, as the cell is able to vindicate normal cellular function. But it is thinkable, that reduction of MIC25 makes HEK293T cells more susceptible to mitochondrial dysfunction, mitophagy and apoptosis. Thus, an approach could be to induce apoptosis in both HEK293T WT and MIC25 KO cells and measure the release of cytochrome c and/or changed expression of regulatory proteins or caspases by western blotting [129] at frequent time intervals. With such a method, great temporal resolution could be achieved, as simultaneous activation of pro- and anti-apoptotic factors can be identified at an early stage, but processes cannot be observed for a single cell overt time, as cell integrity is destroyed in the course [129]. Moreover, loss of the mitochondrial membrane potential in HEK293T MIC25 KO cells is diametral to the tendency of differentiated SH-SY5Y cells lacking MIC25 to hyperpolarise. At present, I can only bring this to reason in a context of highly specialised, tissue-specific functions of MIC25, where in neuronal tissues, energy metabolic effects become inferior to maintaining poorly understood proteinaceous interactions like in the context of Alzheimer's disease [185]. To fathom these, affinity chromatography could be performed. It is highly sensitive and thus could show interactions we do not anticipate yet, and all sample proteins could in turn be tested equally [167]. However, high sensitivity always produces false positives, hence cross-referencing with immunoprecipitations and consecutive western blots are helpful, as previously anticipated interactions can be verified with the appropriate antibody [167].

To summarise, this chapter explores the intricate relationships between MIC25 and SH-SY5Y cell differentiation status, its tissue specificity, cellular energy metabolism, mitochondrial membrane potential and its potential role in neurodegenerative diseases such as Alzheimer's. Induction of SH-SY5Y cell differentiation with the help of ATRA leads to lower oxygen consumption rates and glycolytic activity possibly which may reflect a shift from cellular proliferation to cellular maintenance. At the same time, relative spare respiratory capacity increases, suggesting improved metabolic adaptability to changing conditions. Knockdown of MIC25 leads to changes in oxygen consumption rates, spare respiratory capacity, and mitochondrial membrane potentials partially consistent and partially inconsistent with existing literature [6,185] emphasising the need to interpret the role of MIC25 in a tissue-specific manner. This is underlined by comparisons with effects in HEK293T cells, where oxygen consumption and ATP production remain stable when MIC25 is taken away, but membrane potentials significantly decrease, where in differentiated SH-SY5Y cells, it hyperpolarises. To fully understand increased MIC25 levels in differentiated neuronal cells, aspects apart from metabolic effects need to be considered, as interplay with the amyloid precursor protein of Alzheimer's disease in mitochondrial membranes has been discovered [185]. However, tissue-specific function of MIC25 warrants further investigation, as this protein and its neuronal interactions remain poorly understood.

5.4. Conclusion

The outcomes of this research project have provided insight into biochemical, structural and metabolic implications of MIC25, a subunit of MICOS. The MICOS complex shapes crista junctions and builds intricate connections to the outer mitochondrial membrane (see chapters 2.4 and 2.5). Discovery of tissue-specific expression levels of MIC25 upon the extraction of different mouse tissues (see chapter 2.6) led to the hypothesis that this might correlate to tissue-specific function and might provide unexpected insight into the characterisation of crista junctions. Hence, SH-SY5Y cells were utilised as human neuronal-like cell model due to their abilities to replicate indefinitely in culture but differentiate when needed.

Increased expression levels of MIC25 in neuronal tissue upon successful neuronal differentiation could only be verified and reproduced upon employment of Neurofilament H acting as reliable differentiation marker. However, biochemical analysis of other MICOS and MICOS-related proteins did not reveal any changes upon (natural) upregulation or downregulation (via knockdown) of MIC25 in differentiated SH-SY5Y cells. Nonetheless, MIC25 was increasingly incorporated into MICOS and MIB complex when SH-SY5Y cells were differentiated providing evidence for a role in stabilisation of the outer and inner mitochondrial membrane with the help of SAM complex. Are there neuronal-specific MIC25-SAM interactions? How do they influence mitochondrial ultrastructure and differentiation processes? Further research might provide answers.

Further inquiries into mitochondrial ultrastructure via immunofluorescence microscopy disclosed that differentiation status of SH-SY5Y cells was dominant to the presence or absence of MIC25 for the formation of adept mitochondrial networks. Due to low resolution, impacts on crista ultrastructure could not be determined, but as preexisting data draws an ambivalent picture (see [6,47,148]), further investigation across varying tissues seems like a promising approach. However, primary effects of differentiation status on mitochondrial network formation can also be interpreted inversely, as mitochondrial networks might coordinate processes of neuronal differentiation. How does the timeline for those changes look like? Which mitochondrial effectors are involved and how is upstream regulation organised? We do not know the solutions to those questions.

To further fathom the role of increased MIC25 expression in neuronal tissue, analysis of the cell's energy metabolism needed to be conducted and compared with its effects on other tissues. Lack of MIC25 in differentiated SH-SY5Y cells leads to reduced relative spare respiratory capacity, increased glycolytic activity and hyperpolarisation of mitochondrial membranes indicating reduced ability to adapt to changing environments and increased ROS production. Nevertheless, in HEK293T cells loss of MIC25 surprisingly reduces the mitochondrial membrane potential hinting towards decreased thresholds for apoptosis, as all other parameters stay on similar levels. These findings point toward tissue-specific roles of MIC25 expression that may go beyond a straightforward involvement in energy metabolism, given the complexity and occasional inconsistency of the data. Newest research associates

MIC25 directly with the amyloid precursor protein described in the pathology of Alzheimer's disease, as they stabilise each other and form regulatory feedback loops (see 5.3 and [185]). Therefore, in differentiated neuronal cells, an increased presence of MIC25 could provide an intrinsic buffer protecting from amyloid accumulation in the brain. However, further work is needed to fully understand tissue-specific expression patterns of mitochondrial proteins in the context of neurogenerative diseases and to explore how this knowledge could translate into innovative treatment options.

6. References

1. Abrams AJ, Hufnagel RB, Rebelo A, Zanna C, Patel N, Gonzalez MA, Campeanu IJ, Griffin LB, Groenewald S, Strickland A V., Tao F, Speziani F, Abreu L, Schüle R, Caporali L, La Morgia C, Maresca A, Liguori R, Lodi R, Ahmed ZM, Sund KL, Wang X, Krueger LA, Peng Y, Prada CE, Prows CA, Schorry EK, Antonellis A, Zimmerman HH, Abdul-Rahman OA, Yang Y, Downes SM, Prince J, Fontanesi F, Barrientos A, Németh AH, Carelli V, Huang T, Zuchner S, Dallman JE (2015) Mutations in the UGO1-like protein SLC25A46 cause an optic atrophy spectrum disorder. Nat Genet 47:926
2. Acehan D, Malhotra A, Xu Y, Ren M, Stokes DL, Schlame M (2011) Cardiolipin affects the supramolecular organization of ATP synthase in mitochondria. Biophys J 100:2184–2192
3. Agostini M, Romeo F, Inoue S, Niklison-Chirou M V., Elia AJ, Dinsdale D, Morone N, Knight RA, Mak TW, Melino G (2016) Metabolic reprogramming during neuronal differentiation. Cell Death Differ 23:1502
4. Alexander C, Votruba M, Pesch UEA, Thiselton DL, Mayer S, Moore A, Rodriguez M, Kellner U, Leo-Kottler B, Auburger G, Bhattacharya SS, Wissinger B (2000) OPA1, encoding a dynamin-related GTPase, is mutated in autosomal dominant optic atrophy linked to chromosome 3q28. Nature Genetics 2000 26:2 26:211–215
5. Alkhaja AK, Jans DC, Nikolov M, Vukotic M, Lytovchenko O, Ludewig F, Schliebs W, Riedel D, Urlaub H, Jakobs S, Deckers M (2012) MINOS1 is a conserved component of mitofilin complexes and required for mitochondrial function and cristae organization. Mol Biol Cell 23:247
6. An J, Shi J, He Q, Lui K, Liu Y, Huang Y, Sheikh MS (2012) CHCM1/CHCHD6, Novel Mitochondrial Protein Linked to Regulation of Mitofilin and Mitochondrial Cristae Morphology. J Biol Chem 287:7411
7. Anand R, Strecker V, Urbach J, Wittig I, Reichert AS (2016) Mic13 Is Essential for Formation of Crista Junctions in Mammalian Cells. PLoS One 11:
8. Anand R, Kondadi AK, Meisterknecht J, Golombek M, Nortmann O, Riedel J, Peifer-Weiß L, Brocke-Ahmadinejad N, Schlütermann D, Stork B, Eichmann TO, Wittig I, Reichert AS (2020) MIC26 and MIC27 cooperate to regulate cardiolipin levels and the landscape of OXPHOS complexes. Life Sci Alliance 3:
9. Andersson SG, Kurland CG (1999) Origins of mitochondria and hydrogenosomes. Curr Opin Microbiol 2:535–541
10. Anselmi C, Davies KM, Faraldo-Gómez JD (2018) Mitochondrial ATP synthase dimers spontaneously associate due to a long-range membrane-induced force. J Gen Physiol 150:763
11. Backes S, Hess S, Boos F, Woellhaf MW, Gödel S, Jung M, Mühlhaus T, Herrmann JM (2018) Tom70 enhances mitochondrial preprotein import efficiency by binding to internal targeting sequences. J Cell Biol 217:1369–1382
12. Baker MJ, Webb CT, Stroud DA, Palmer CS, Frazier AE, Guiard B, Chacinska A, Gulbis JM, Ryan MT (2009) Structural and functional requirements for activity of the Tim9-Tim10 complex in mitochondrial protein import. Mol Biol Cell 20:769–779
13. Banci L, Bertini I, Cefaro C, Cenacchi L, Ciofi-Baffoni S, Felli IC, Gallo A, Gonnelli L, Luchinat E, Sideris D, Tokatlidis K (2010) Molecular chaperone function of Mia40 triggers consecutive induced folding steps of the substrate in mitochondrial protein import. Proc Natl Acad Sci U S A 107:20190–20195
14. Banci L, Bertini I, Ciofi-Baffoni S, Jaiswal D, Neri S, Peruzzini R, Winkelmann J (2012) Structural characterization of CHCHD5 and CHCHD7: two atypical human twin CX9C proteins. J Struct Biol 180:190–200
15. Beckervordersandforth R, Ebert B, Schäffner I, Moss J, Fiebig C, Shin J, Moore DL, Ghosh L, Trinchero MF, Stockburger C, Friedland K, Steib K, von Wittgenstein J, Keiner S, Redecker C, Hölter SM, Xiang W, Wurst W, Jagasia R, Schinder AF, Ming G li, Toni N, Jessberger S, Song H, Lie DC (2017) Role of Mitochondrial Metabolism in the Control of Early Lineage Progression and Aging Phenotypes in Adult Hippocampal Neurogenesis. Neuron 93:560
16. Beltrán-Heredia E, Tsai FC, Salinas-Almaguer S, Cao FJ, Bassereau P, Monroy F (2019)

Membrane curvature induces cardiolipin sorting. Commun Biol 2:
17. Biedler JL, Helson L, Spengler BA Morphology and Growth, Tumorigenicity, and Cytogenetics of Human Neuroblastoma Cells in Continuous Culture1.
18. Biedler1 JL, Roffler-Tarlov S, Schachner M, Freedman LS Multiple Neurotransmitter Synthesis by Human Neuroblastoma Cell Lines and Clones.
19. Birker K, Ge S, Kirkland NJ, Theis JL, Marchant J, Fogarty ZC, Missinato MA, Kalvakuri S, Grossfeld P, Engler AJ, Ocorr K, Nelson TJ, Colas AR, Olson TM, Vogler G, Bodmer R (2023) Mitochondrial MICOS complex genes, implicated in hypoplastic left heart syndrome, maintain cardiac contractility and actomyosin integrity. Elife 12:83385
20. Blaza JN, Serreli R, Jones AJY, Mohammed K, Hirst J (2014) Kinetic evidence against partitioning of the ubiquinone pool and the catalytic relevance of respiratory-chain supercomplexes. Proc Natl Acad Sci U S A 111:15735–15740
21. Bock-Bierbaum T, Funck K, Wollweber F, Lisicki E, von der Malsburg K, von der Malsburg A, Laborenz J, Noel JK, Hessenberger M, Jungbluth S, Bernert C, Kunz S, Riedel D, Lilie H, Jakobs S, van der Laan M, Daumke O (2022) Structural insights into crista junction formation by the Mic60-Mic19 complex. Sci Adv 8:31
22. Bohnert M, Wenz LS, Zerbes RM, Horvath SE, Stroud DA, Von Der Malsburg K, Müller JM, Oeljeklaus S, Perschil I, Warscheid B, Chacinska A, Veenhuis M, Van Der Klei IJ, Daum G, Wiedemann N, Becker T, Pfanner N, Van Der Laan M (2012) Role of mitochondrial inner membrane organizing system in protein biogenesis of the mitochondrial outer membrane. Mol Biol Cell 23:3948–3956
23. Bohnert M, Zerbes RM, Davies KM, Mühleip AW, Rampelt H, Horvath SE, Boenke T, Kram A, Perschil I, Veenhuis M, Kühlbrandt W, van der Klei IJ, Pfanner N, van der Laan M (2015) Central Role of Mic10 in the Mitochondrial Contact Site and Cristae Organizing System. Cell Metab 21:747–755
24. Bornhövd C, Vogel F, Neupert W, Reichert AS (2006) Mitochondrial membrane potential is dependent on the oligomeric state of F1F0-ATP synthase supracomplexes. J Biol Chem 281:13990–13998
25. Cai A, Lin Z, Liu N, Li X, Wang J, Wu Y, Gao K, Jiang Y (2022) Neuroblastoma SH-SY5Y Cell Differentiation to Mature Neuron by AM580 Treatment. Neurochem Res 47:3723–3732
26. Callegari S, Müller T, Schulz C, Lenz C, Jans DC, Wissel M, Opazo F, Rizzoli SO, Jakobs S, Urlaub H, Rehling P, Deckers M (2019) A MICOS–TIM22 Association Promotes Carrier Import into Human Mitochondria. J Mol Biol 431:2835–2851
27. Carelli V, Musumeci O, Caporali L, Zanna C, La Morgia C, Del Dotto V, Porcelli AM, Rugolo M, Valentino ML, Iommarini L, Maresca A, Barboni P, Carbonelli M, Trombetta C, Valente EM, Patergnani S, Giorgi C, Pinton P, Rizzo G, Tonon C, Lodi R, Avoni P, Liguori R, Baruzzi A, Toscano A, Zeviani M (2015) Syndromic parkinsonism and dementia associated with OPA 1 missense mutations. Ann Neurol 78:21
28. Cason SE, Holzbaur ELF (2022) Selective motor activation in organelle transport along axons. Nature Reviews Molecular Cell Biology 2022 23:11 23:699–714
29. Cedergren R, Gray MW, Abel Y, Sankoff D (1988) The evolutionary relationships among known life forms. J Mol Evol 28:98–112
30. Chella Krishnan K, Kurt Z, Barrere-Cain R, Sabir S, Das A, Floyd R, Vergnes L, Zhao Y, Che N, Charugundla S, Qi H, Zhou Z, Meng Y, Pan C, Seldin MM, Norheim F, Hui S, Reue K, Lusis AJ, Yang X (2018) Integration of Multi-omics Data from Mouse Diversity Panel Highlights Mitochondrial Dysfunction in Non-Alcoholic Fatty Liver Disease. Cell Syst 6:103
31. Cheung YT, Lau WKW, Yu MS, Lai CSW, Yeung SC, So KF, Chang RCC (2009) Effects of all-trans-retinoic acid on human SH-SY5Y neuroblastoma as in vitro model in neurotoxicity research. Neurotoxicology 30:127–135
32. Choi SW, Gerencser AA, Nicholls DG (2009) Bioenergetic Analysis of Isolated Cerebrocortical Nerve Terminals on a Microgram Scale: Spare Respiratory Capacity and Stochastic Mitochondrial Failure. J Neurochem 109:1179
33. Choi YS, Kim S, Pak YK (2001) Mitochondrial transcription factor A (mtTFA) and diabetes. Diabetes Res Clin Pract 54:S3–S9
34. Chung C, Boterberg T, Lucas J, Panoff J, Valteau-Couanet D, Hero B, Bagatell R, Hill-Kayser

CE (2021) Neuroblastoma. Pediatr Blood Cancer 68:e28473
35. Cogliati S, Frezza C, Soriano ME, Varanita T, Quintana-Cabrera R, Corrado M, Cipolat S, Costa V, Casarin A, Gomes LC, Perales-Clemente E, Salviati L, Fernandez-Silva P, Enriquez JA, Scorrano L (2013) Mitochondrial Cristae Shape Determines Respiratory Chain Supercomplexes Assembly and Respiratory Efficiency. Cell 155:160
36. Cogliati S, Enriquez JA, Scorrano L (2016) Mitochondrial Cristae: Where Beauty Meets Functionality. Trends Biochem Sci 41:261–273
37. Crowley LC, Christensen ME, Waterhouse NJ (2016) Measuring Mitochondrial Transmembrane Potential by TMRE Staining. Cold Spring Harb Protoc 2016:1092–1096
38. ČUNÁTOVÁ K, REGUERA DP, HOUŠTĚK J, MRÁČEK T, PECINA P (2020) Role of cytochrome c oxidase nuclear-encoded subunits in health and disease. Physiol Res 69:947–965
39. Darshi M, Mendiola VL, Mackey MR, Murphy AN, Koller A, Perkins GA, Ellisman MH, Taylor SS (2011) ChChd3, an Inner Mitochondrial Membrane Protein, Is Essential for Maintaining Crista Integrity and Mitochondrial Function. J Biol Chem 286:2918
40. Darshi M, Trinh KN, Murphy AN, Taylor SS (2012) Targeting and import mechanism of coiled-coil helix coiled-coil helix domain-containing protein 3 (ChChd3) into the mitochondrial intermembrane space. J Biol Chem 287:39480–39491
41. Daum B, Walter A, Horst A, Osiewacz HD, Kühlbrandt W (2013) Age-dependent dissociation of ATP synthase dimers and loss of inner-membrane cristae in mitochondria. Proc Natl Acad Sci U S A 110:15301–15306
42. Davies KM, Strauss M, Daum B, Kief JH, Osiewacz HD, Rycovska A, Zickermann V, Kühlbrandt W (2011) Macromolecular organization of ATP synthase and complex I in whole mitochondria. Proc Natl Acad Sci U S A 108:14121–14126
43. Davies KM, Anselmi C, Wittig I, Faraldo-Gómez JD, Kühlbrandt W (2012) Structure of the yeast F 1F o-ATP synthase dimer and its role in shaping the mitochondrial cristae. Proc Natl Acad Sci U S A 109:13602–13607
44. Davies KM, Blum TB, Kühlbrandt W (2018) Conserved in situ arrangement of complex I and III2 in mitochondrial respiratory chain supercomplexes of mammals, yeast, and plants. Proc Natl Acad Sci U S A 115:3024–3029
45. de Medeiros LM, De Bastiani MA, Rico EP, Schonhofen P, Pfaffenseller B, Wollenhaupt-Aguiar B, Grun L, Barbé-Tuana F, Zimmer ER, Castro MAA, Parsons RB, Klamt F (2019) Cholinergic Differentiation of Human Neuroblastoma SH-SY5Y Cell Line and Its Potential Use as an In vitro Model for Alzheimer's Disease Studies. Mol Neurobiol 56:7355–7367
46. Del Prete D, Suski JM, Oulès B, Debayle D, Gay AS, Lacas-Gervais S, Bussiere R, Bauer C, Pinton P, Paterlini-Bréchot P, Wieckowski MR, Checler F, Chami M (2017) Localization and Processing of the Amyloid-β Protein Precursor in Mitochondria-Associated Membranes. J Alzheimers Dis 55:1549–1570
47. Ding C, Wu Z, Huang L, Wang Y, Xue J, Chen S, Deng Z, Wang L, Song Z, Chen S (2015) Mitofilin and CHCHD6 physically interact with Sam50 to sustain cristae structure. Sci Rep 5:
48. Divakaruni AS, Paradyse A, Ferrick DA, Murphy AN, Jastroch M (2014) Analysis and interpretation of microplate-based oxygen consumption and pH data. Methods Enzymol 547:309–354
49. Dolder M, Wendt S, Wallimann T (2001) Mitochondrial creatine kinase in contact sites: interaction with porin and adenine nucleotide translocase, role in permeability transition and sensitivity to oxidative damage. Biol Signals Recept 10:93–111
50. Dolezal P, Likic V, Tachezy J, Lithgow T (2006) Evolution of the molecular machines for protein import into mitochondria. Science (1979) 313:314–318
51. DuBoff B, Feany M, Götz J (2013) Why size matters – balancing mitochondrial dynamics in Alzheimer's disease. Trends Neurosci 36:325–335
52. Ehses S, Raschke I, Mancuso G, Bernacchia A, Geimer S, Tondera D, Martinou JC, Westermann B, Rugarli EI, Langer T (2009) Regulation of OPA1 processing and mitochondrial fusion by m-AAA protease isoenzymes and OMA1. J Cell Biol 187:1023
53. Encinas M, Iglesias M, Liu Y, Wang H, Muhaisen A, Ceña V, Gallego C, Comella JX (2000) Sequential Treatment of SH-SY5Y Cells with Retinoic Acid and Brain-Derived Neurotrophic Factor Gives Rise to Fully Differentiated, Neurotrophic Factor-Dependent, Human Neuron-

Like Cells. J Neurochem 75:991–1003
54. Feichtinger RG, Brunner-Krainz M, Alhaddad B, Wortmann SB, Kovacs-Nagy R, Stojakovic T, Erwa W, Resch B, Windischhofer W, Verheyen S, Uhrig S, Windpassinger C, Locker F, Makowski C, Strom TM, Meitinger T, Prokisch H, Sperl W, Haack TB, Mayr JA (2017) Combined Respiratory Chain Deficiency and UQCC2 Mutations in Neonatal Encephalomyopathy: Defective Supercomplex Assembly in Complex III Deficiencies. Oxid Med Cell Longev 2017:
55. Ferrick DA, Neilson A, Beeson C (2008) Advances in measuring cellular bioenergetics using extracellular flux. Drug Discov Today 13:268–274
56. Flippo KH, Strack S (2017) Mitochondrial dynamics in neuronal injury, development and plasticity. J Cell Sci 130:671
57. Frey TG, Renken CW, Perkins GA (2002) Insight into mitochondrial structure and function from electron tomography. Biochimica et Biophysica Acta (BBA) - Bioenergetics 1555:196–203
58. Friedman JR, Mourier A, Yamada J, Michael McCaffery J, Nunnari J (2015) MICOS coordinates with respiratory complexes and lipids to establish mitochondrial inner membrane architecture. Elife 4:1–61
59. Fritz S, Rapaport D, Klanner E, Neupert W, Westermann B (2001) Connection of the Mitochondrial Outer and Inner Membranes by Fzo1 Is Critical for Organellar Fusion. J Cell Biol 152:683
60. Fuloria S, Subramaniyan V, Karupiah S, Kumari U, Sathasivam K, Meenakshi DU, Wu YS, Sekar M, Chitranshi N, Malviya R, Sudhakar K, Bajaj S, Fuloria NK (2021) Comprehensive review of methodology to detect reactive oxygen species (Ros) in mammalian species and establish its relationship with antioxidants and cancer. Antioxidants 10:1–35
61. Gabaldón T, Huynen MA (2003) Reconstruction of the proto-mitochondrial metabolism. Science (1979) 301:609
62. Georgakopoulos ND, Wells G, Campanella M (2017) The pharmacological regulation of cellular mitophagy. Nat Chem Biol 13:136–146
63. Giacomello M, Pyakurel A, Glytsou C, Scorrano L (2020) The cell biology of mitochondrial membrane dynamics. Nature Reviews Molecular Cell Biology 2020 21:4 21:204–224
64. Gilkerson R, De La Torre P, St. Vallier S (2021) Mitochondrial OMA1 and OPA1 as Gatekeepers of Organellar Structure/Function and Cellular Stress Response. Front Cell Dev Biol 9:
65. Gödiker J, Grüneberg M, Duchesne I, Reunert J, Rust S, Westermann C, Wada Y, Classen G, Langhans CD, Schlingmann KP, Rodenburg RJ, Pohlmann R, Marquardt T (2018) QIL1-dependent assembly of MICOS complex-lethal mutation in C19ORF70 resulting in liver disease and severe neurological retardation. J Hum Genet 63:707–716
66. Gold VAM, Ieva R, Walter A, Pfanner N, Van Der Laan M, Kühlbrandt W (2014) Visualizing active membrane protein complexes by electron cryotomography. Nat Commun 5:
67. Gomkale R, Cruz-Zaragoza LD, Suppanz I, Guiard B, Montoya J, Callegari S, Pacheu-Grau D, Warscheid B, Rehling P (2020) Defining the Substrate Spectrum of the TIM22 Complex Identifies Pyruvate Carrier Subunits as Unconventional Cargos. Current Biology 30:1119
68. Gorman GS, Chinnery PF, DiMauro S, Hirano M, Koga Y, McFarland R, Suomalainen A, Thorburn DR, Zeviani M, Turnbull DM (2016) Mitochondrial diseases. Nat Rev Dis Primers 2:
69. Gray MW (1982) Mitochondrial genome diversity and the evolution of mitochondrial DNA. Can J Biochem 60:157–171
70. Gray MW, Sankoff D, Cedergren RJ (1984) On the evolutionary descent of organisms and organelles: a global phylogeny based on a highly conserved structural core in small subunit ribosomal RNA. Nucleic Acids Res 12:5837–5852
71. Gray MW (1989) The evolutionary origins of organelles. Trends Genet 5:294–299
72. Gray MW (2012) Mitochondrial Evolution. Cold Spring Harb Perspect Biol 4:
73. Griparic L, Kanazawa T, Van Der Bliek AM (2007) Regulation of the mitochondrial dynamin-like protein Opa1 by proteolytic cleavage. J Cell Biol 178:757
74. Grodums EI (1977) Ultrastructural changes in the mitochondria of brown adipose cells during

the hibernation cycle of Citellus lateralis. Cell Tissue Res 185:231–237
75. Gu X, Ma Y, Liu Y, Wan Q (2021) Measurement of mitochondrial respiration in adherent cells by Seahorse XF96 Cell Mito Stress Test. STAR Protoc 2:
76. Guarani V, McNeill EM, Paulo JA, Huttlin EL, Fröhlich F, Gygi SP, Vactor D Van, Wade Harper J (2015) QIL1 is a novel mitochondrial protein required for MICOS complex stability and cristae morphology. Elife 4:1–23
77. Guarani V, Jardel C, Chrétien D, Lombès A, Bénit P, Labasse C, Lacène E, Bourillon A, Imbard A, Benoist JF, Dorboz I, Gilleron M, Goetzman ES, Gaignard P, Slama A, Elmaleh-Bergès M, Romero NB, Rustin P, de Baulny HO, Paulo JA, Harper JW, Schiff M (2016) QIL1 mutation causes MICOS disassembly and early onset fatal mitochondrial encephalopathy with liver disease. Elife 5:
78. Hahn A, Parey K, Bublitz M, Mills DJ, Zickermann V, Vonck J, Kühlbrandt W, Meier T (2016) Structure of a Complete ATP Synthase Dimer Reveals the Molecular Basis of Inner Mitochondrial Membrane Morphology. Mol Cell 63:445
79. Hansen KG, Herrmann JM (2019) Transport of Proteins into Mitochondria. The Protein Journal 2019 38:3 38:330–342
80. Harner M, Körner C, Walther D, Mokranjac D, Kaesmacher J, Welsch U, Griffith J, Mann M, Reggiori F, Neupert W (2011) The mitochondrial contact site complex, a determinant of mitochondrial architecture. EMBO J 30:4356–4370
81. Harner ME, Unger AK, Izawa T, Walther DM, Özbalci C, Geimer S, Reggiori F, Brügger B, Mann M, Westermann B, Neupert W (2014) Aim24 and MICOS modulate respiratory function, tafazzin-related cardiolipin modification and mitochondrial architecture. Elife 3:1684
82. Hartley CL, Johnston HB, Nicol S, Chan KM, Baines AJ, Anderton BH, Thomas SM (1996) Phenotypic morphology and the expression of cytoskeletal markers during long-term differentiation of human SH-SY5Y neuroblastoma cells. Toxicology in Vitro 10:539–550
83. Head B, Griparic L, Amiri M, Gandre-Babbe S, Van Der Bliek AM (2009) Inducible proteolytic inactivation of OPA1 mediated by the OMA1 protease in mammalian cells. J Cell Biol 187:959–966
84. Hessenberger M, Zerbes RM, Rampelt H, Kunz S, Xavier AH, Purfürst B, Lilie H, Pfanner N, Van Der Laan M, Daumke O (2017) Regulated membrane remodeling by Mic60 controls formation of mitochondrial crista junctions. Nat Commun 8:
85. Hirokawa N (1982) Cross-linker System between Neurofilaments, Microtubules, and Membranous Organelles in Frog Axons Revealed by the Quick-freeze, Deep-etching Method. THE JOURNAL OF CELl BIOLOGY • 94:129–142
86. Höhr AIC, Lindau C, Wirth C, Qiu J, Stroud DA, Kutik S, Guiard B, Hunte C, Becker T, Pfanner N, Wiedemann N (2018) Membrane protein insertion through a mitochondrial β-barrel gate. Science 359:
87. Hoppins S, Collins SR, Cassidy-Stone A, Hummel E, DeVay RM, Lackner LL, Westermann B, Schuldiner M, Weissman JS, Nunnari J (2011) A mitochondrial-focused genetic interaction map reveals a scaffold-like complex required for inner membrane organization in mitochondria. J Cell Biol 195:323–340
88. Hüttemann M, Jaradat S, Grossman LI (2003) Cytochrome c oxidase of mammals contains a testes-specific isoform of subunit VIb--the counterpart to testes-specific cytochrome c? Mol Reprod Dev 66:8–16
89. Huynen MA, Mühlmeister M, Gotthardt K, Guerrero-Castillo S, Brandt U (2016) Evolution and structural organization of the mitochondrial contact site (MICOS) complex and the mitochondrial intermembrane space bridging (MIB) complex. Biochimica et Biophysica Acta (BBA) - Molecular Cell Research 1863:91–101
90. Ikon N, Ryan RO (2017) Cardiolipin and mitochondrial cristae organization. Biochim Biophys Acta 1859:1156
91. Ioakeimidis F, Ott C, Kozjak-Pavlovic V, Violitzi F, Rinotas V, Makrinou E, Eliopoulos E, Fasseas C, Kollias G, Douni E (2014) A Splicing Mutation in the Novel Mitochondrial Protein DNAJC11 Causes Motor Neuron Pathology Associated with Cristae Disorganization, and Lymphoid Abnormalities in Mice. PLoS One 9:104237
92. Ishihara N, Fujita Y, Oka T, Mihara K (2006) Regulation of mitochondrial morphology

through proteolytic cleavage of OPA1. EMBO J 25:2966
93. Iwata R, Casimir P, Vanderhaeghen P (2020) Mitochondrial dynamics in postmitotic cells regulate neurogenesis. Science (1979) 369:858–862
94. Janer A, Prudent J, Paupe V, Fahiminiya S, Majewski J, Sgarioto N, Rosiers C Des, Forest A, Lin Z, Gingras A, Mitchell G, McBride HM, Shoubridge EA (2016) SLC25A46 is required for mitochondrial lipid homeostasis and cristae maintenance and is responsible for Leigh syndrome. EMBO Mol Med 8:1019
95. Janesick A, Wu SC, Blumberg B (2015) Retinoic acid signaling and neuronal differentiation. Cell Mol Life Sci 72:1559–1576
96. Jans DC, Wurm CA, Riedel D, Wenzel D, Stagge F, Deckers M, Rehling P, Jakobs S (2013) STED super-resolution microscopy reveals an array of MINOS clusters along human mitochondria. Proc Natl Acad Sci U S A 110:8936–8941
97. Jastroch M, Divakaruni AS, Mookerjee S, Treberg JR, Brand MD (2010) Mitochondrial proton and electron leaks. Essays Biochem 47:53
98. Jiang X, Jiang H, Shen Z, Wang X (2014) Activation of mitochondrial protease OMA1 by Bax and Bak promotes cytochrome c release during apoptosis. Proc Natl Acad Sci U S A 111:14782–14787
99. John GB, Shang Y, Li L, Renken C, Mannella CA, Selker JML, Rangell L, Bennett MJ, Zha J (2005) The Mitochondrial Inner Membrane Protein Mitofilin Controls Cristae Morphology. Mol Biol Cell 16:1543
100. Johnson DT, Harris RA, French S, Blair P V., You J, Bemis KG, Wang M, Balaban RS (2007) Tissue heterogeneity of the mammalian mitochondrial proteome. Am J Physiol Cell Physiol 292:689–697
101. Jonikas M, Madill M, Mathy A, Zekoll T, Zois CE, Wigfield S, Kurzawa-Akanbi M, Browne C, Sims D, Chinnery PF, Cowley SA, Tofaris GK (2018) Stem cell modeling of mitochondrial parkinsonism reveals key functions of OPA1. Ann Neurol 83:915–925
102. Jores T, Klinger A, Groß LE, Kawano S, Flinner N, Duchardt-Ferner E, Wöhnert J, Kalbacher H, Endo T, Schleiff E, Rapaport D (2016) Characterization of the targeting signal in mitochondrial β-barrel proteins. Nat Commun 7:
103. Kalpage HA, Bazylianska V, Recanati MA, Fite A, Liu J, Wan J, Mantena N, Malek MH, Podgorski I, Heath EI, Vaishnav A, Edwards BF, Grossman LI, Sanderson TH, Lee I, Hüttemann M (2019) Tissue-specific regulation of cytochrome c by post-translational modifications: respiration, the mitochondrial membrane potential, ROS, and apoptosis. The FASEB Journal 33:1540
104. Kampinga HH, Craig EA (2010) The HSP70 chaperone machinery: J proteins as drivers of functional specificity. Nat Rev Mol Cell Biol 11:579–592
105. Kang HT, Hwang ES (2006) 2-Deoxyglucose: An anticancer and antiviral therapeutic, but not any more a low glucose mimetic. Life Sci 78:1392–1399
106. Kasahara A, Scorrano L (2014) Mitochondria: from cell death executioners to regulators of cell differentiation. Trends Cell Biol 24:761–770
107. Khacho M, Clark A, Svoboda DS, Azzi J, MacLaurin JG, Meghaizel C, Sesaki H, Lagace DC, Germain M, Harper ME, Park DS, Slack RS (2016) Mitochondrial Dynamics Impacts Stem Cell Identity and Fate Decisions by Regulating a Nuclear Transcriptional Program. Cell Stem Cell 19:232–247
108. Khacho M, Harris R, Slack RS (2018) Mitochondria as central regulators of neural stem cell fate and cognitive function. Nature Reviews Neuroscience 2018 20:1 20:34–48
109. Khalifat N, Puff N, Bonneau S, Fournier JB, Angelova MI (2008) Membrane Deformation under Local pH Gradient: Mimicking Mitochondrial Cristae Dynamics. Biophys J 95:4924
110. Kondadi AK, Anand R, Hänsch S, Urbach J, Zobel T, Wolf DM, Segawa M, Liesa M, Shirihai OS, Weidtkamp-Peters S, Reichert AS (2020) Cristae undergo continuous cycles of membrane remodelling in a MICOS-dependent manner. EMBO Rep 21:
111. Koob S, Barrera M, Anand R, Reichert AS (2015) The non-glycosylated isoform of MIC26 is a constituent of the mammalian MICOS complex and promotes formation of crista junctions. Biochimica et Biophysica Acta (BBA) - Molecular Cell Research 1853:1551–1563
112. Korshunov SS, Skulachev VP, Starkov AA (1997) High protonic potential actuates a

mechanism of production of reactive oxygen species in mitochondria. FEBS Lett 416:15–18
113. Kovalevich J, Langford D (2013) Considerations for the use of SH-SY5Y neuroblastoma cells in neurobiology. Methods Mol Biol 1078:9–21
114. Križ J, Zhu Q, Julien JP, Padjen AL (2000) Electrophysiological properties of axons in mice lacking neurofilament subunit genes: disparity between conduction velocity and axon diameter in absence of NF-H. Brain Res 885:32–44
115. Kumar A, Waingankar TP, D'Silva P (2023) Functional crosstalk between the TIM22 complex and YME1 machinery maintains mitochondrial proteostasis and integrity. J Cell Sci 136:
116. Laemmli UK (1970) Cleavage of Structural Proteins during the Assembly of the Head of Bacteriophage T4. Nature 1970 227:5259 227:680–685
117. Leterrier J, Eyer J, Weiss DG, Lindén M (2008) In vitro studies of the physical interactions between neurofilaments, microtubules and mitochondria isolated from the central nervous system. AIP Conf Proc 226:91
118. Leterrier JF, Rusakov DA, Nelson BD, Linden M (1994) Interactions between brain mitochondria and cytoskeleton: evidence for specialized outer membrane domains involved in the association of cytoskeleton-associated proteins to mitochondria in situ and in vitro. Microsc Res Tech 27:233–261
119. Li H, Ruan Y, Zhang K, Jian F, Hu C, Miao L, Gong L, Sun L, Zhang X, Chen S, Chen H, Liu D, Song Z (2016) Mic60/Mitofilin determines MICOS assembly essential for mitochondrial dynamics and mtDNA nucleoid organization. Cell Death Differ 23:380–392
120. Liesa M, Shirihai OS (2013) Mitochondrial dynamics in the regulation of nutrient utilization and energy expenditure. Cell Metab 17:491–506
121. Lopes FM, Schröder R, Júnior MLC da F, Zanotto-Filho A, Müller CB, Pires AS, Meurer RT, Colpo GD, Gelain DP, Kapczinski F, Moreira JCF, Fernandes M da C, Klamt F (2010) Comparison between proliferative and neuron-like SH-SY5Y cells as an in vitro model for Parkinson disease studies. Brain Res 1337:85–94
122. Lopez-Fabuel I, Le Douce J, Logan A, James AM, Bonvento G, Murphy MP, Almeida A, Bolaños JP (2016) Complex I assembly into supercomplexes determines differential mitochondrial ROS production in neurons and astrocytes. Proc Natl Acad Sci U S A 113:13063–13068
123. Ly JD, Grubb DR, Lawen A (2003) The mitochondrial membrane potential (δψm) in apoptosis; an update. Apoptosis 8:115–128
124. MacVicar T, Langer T (2016) OPA1 processing in cell death and disease - the long and short of it. J Cell Sci 129:2297–2306
125. Maffezzini C, Calvo-Garrido J, Wredenberg A, Freyer C (2020) Metabolic regulation of neurodifferentiation in the adult brain. Cellular and Molecular Life Sciences 77:2483
126. Mannella CA, Marko M, Penczek P, Barnard D, Frank J (1994) The internal compartmentation of rat-liver mitochondria: Tomographic study using the high-voltage transmission electron microscope. Microsc Res Tech 27:278–283
127. Mannella CA, Pfeiffer DR, Bradshaw PC, Moraru II, Slepchenko B, Loew LM, Hsie CE, Buttle K, Marko M (2001) Topology of the mitochondrial inner membrane: Dynamics and bioenergetic implications. IUBMB Life 52:93–100
128. Mannella CA, Lederer WJ, Jafri MS (2013) The connection between inner membrane topology and mitochondrial function. J Mol Cell Cardiol 62:51
129. Martinez MM, Reif RD, Pappas D (2010) Detection of apoptosis : A review of conventional and novel techniques. Analytical Methods 2:996–1004
130. Matrella ML, Valletti A, Gigante I, De Rasmo D, Signorile A, Russo S, Lobasso S, Lobraico D, Dibattista M, Pacelli C, Cocco T (2024) High OXPHOS efficiency in RA-FUdr-differentiated SH-SY5Y cells: involvement of cAMP signalling and respiratory supercomplexes. Scientific Reports 2024 14:1 14:1–18
131. Mesecke N, Terziyska N, Kozany C, Baumann F, Neupert W, Hell K, Herrmann JM (2005) A disulfide relay system in the intermembrane space of mitochondria that mediates protein import. Cell 121:1059–1069
132. Mils V, Bosch S, Roy J, Bel-Vialar S, Belenguer P, Pituello F, Miquel MC (2015)

Mitochondrial Reshaping Accompanies Neural Differentiation in the Developing Spinal Cord. PLoS One 10:
133. Minauro-Sanmiguel F, Wilkens S, Garcia JJ (2005) Structure of dimeric mitochondrial ATP synthase: Novel F0 bridging features and the structural basis of mitochondrial cristae biogenesis. Proc Natl Acad Sci U S A 102:12356
134. Mishra P, Carelli V, Manfredi G, Chan DC (2014) Proteolytic Cleavage of Opa1 Stimulates Mitochondrial Inner Membrane Fusion and Couples Fusion to Oxidative Phosphorylation. Cell Metab 19:630–641
135. Mishra P, Chan DC (2016) Metabolic regulation of mitochondrial dynamics. J Cell Biol 212:379–387
136. Mühlenbein N, Hofmann S, Rothbauer U, Bauer MF (2004) Organization and function of the small Tim complexes acting along the import pathway of metabolite carriers into mammalian mitochondria. J Biol Chem 279:13540–13546
137. Mukherjee I, Ghosh M, Meinecke M (2021) MICOS and the mitochondrial inner membrane morphology – when things get out of shape. FEBS Lett 595:1159–1183
138. Muñoz-Gómez SA, Slamovits CH, Dacks JB, Baier KA, Spencer KD, Wideman JG (2015) Ancient homology of the mitochondrial contact site and cristae organizing system points to an endosymbiotic origin of mitochondrial cristae. Curr Biol 25:1489–1495
139. Muñoz-Gómez SA, Wideman JG, Roger AJ, Slamovits CH, Agashe D (2017) The Origin of Mitochondrial Cristae from Alphaproteobacteria. Mol Biol Evol 34:943–956
140. Murphy MP, Bayir H, Belousov V, Chang CJ, Davies KJA, Davies MJ, Dick TP, Finkel T, Forman HJ, Janssen-Heininger Y, Gems D, Kagan VE, Kalyanaraman B, Larsson NG, Milne GL, Nyström T, Poulsen HE, Radi R, Van Remmen H, Schumacker PT, Thornalley PJ, Toyokuni S, Winterbourn CC, Yin H, Halliwell B (2022) Guidelines for measuring reactive oxygen species and oxidative damage in cells and in vivo. Nat Metab 4:651–662
141. Neupert W (2003) PROTEIN IMPORT INTO MITOCHONDRIA. https://doi.org/101146/annurev.biochem661863 66:863–917
142. Ni X, Hu G, Cai X (2019) The success and the challenge of all-trans retinoic acid in the treatment of cancer. Crit Rev Food Sci Nutr 59:S71–S80
143. Nirody JA, Budin I, Rangamani P (2020) ATP synthase: Evolution, energetics, and membrane interactions. J Gen Physiol 152:
144. Nunnari J, Suomalainen A (2012) Mitochondria: In Sickness and in Health. Cell 148:1145
145. Olichon A, Emorine LJ, Descoins E, Pelloquin L, Brichese L, Gas N, Guillou E, Delettre C, Valette A, Hamel CP, Ducommun B, Lenaers G, Belenguer P (2002) The human dynamin-related protein OPA1 is anchored to the mitochondrial inner membrane facing the inter-membrane space. FEBS Lett 523:171–176
146. Otera H, Ishihara N, Mihara K (2013) New insights into the function and regulation of mitochondrial fission. Biochimica et Biophysica Acta (BBA) - Molecular Cell Research 1833:1256–1268
147. Ott C, Ross K, Straub S, Thiede B, Götz M, Goosmann C, Krischke M, Mueller MJ, Krohne G, Rudel T, Kozjak-Pavlovic V (2012) Sam50 Functions in Mitochondrial Intermembrane Space Bridging and Biogenesis of Respiratory Complexes. Mol Cell Biol 32:1173
148. Ott C, Dorsch E, Fraunholz M, Straub S, Kozjak-Pavlovic V (2015) Detailed Analysis of the Human Mitochondrial Contact Site Complex Indicate a Hierarchy of Subunits. PLoS One 10:
149. Overly CC, Rieff HI, Hollenbeck PJ (1996) Organelle motility and metabolism in axons vs dendrites of cultured hippocampal neurons. J Cell Sci 109 (Pt 5):971–980
150. Pagliarini DJ, Calvo SE, Chang B, Sheth SA, Vafai SB, Ong SE, Walford GA, Sugiana C, Boneh A, Chen WK, Hill DE, Vidal M, Evans JG, Thorburn DR, Carr SA, Mootha VK (2008) A mitochondrial protein compendium elucidates complex I disease biology. Cell 134:112
151. Påhlman S, Ruusala AI, Abrahamsson L, Mattsson MEK, Esscher T (1984) Retinoic acid-induced differentiation of cultured human neuroblastoma cells: a comparison with phorbolester-induced differentiation. Cell Differ 14:135–144
152. Palmieri F (2013) The mitochondrial transporter family SLC25: identification, properties and physiopathology. Mol Aspects Med 34:465–484
153. Patten DA, Wong J, Khacho M, Soubannier V, Mailloux RJ, Pilon-Larose K, MacLaurin JG,

Park DS, McBride HM, Trinkle-Mulcahy L, Harper M-E, Germain M, Slack RS (2014) OPA1-dependent cristae modulation is essential for cellular adaptation to metabolic demand. EMBO J 33:2676
154. Paumard P, Vaillier J, Coulary B, Schaeffer J, Soubannier V, Mueller DM, Brèthes D, Rago J-P di, Velours J (2002) The ATP synthase is involved in generating mitochondrial cristae morphology. EMBO J 21:221
155. Pavlov PF, Wiehager B, Sakai J, Frykman S, Behbahani H, Winblad B, Ankarcrona M (2011) Mitochondrial γ-secretase participates in the metabolism of mitochondria-associated amyloid precursor protein. FASEB J 25:78–88
156. Peleh V, Cordat E, Herrmann JM (2016) Mia40 is a trans-site receptor that drives protein import into the mitochondrial intermembrane space by hydrophobic substrate binding. Elife 5:
157. Pernas L, Scorrano L (2016) Mito-Morphosis: Mitochondrial Fusion, Fission, and Cristae Remodeling as Key Mediators of Cellular Function. https://doi.org/101146/annurev-physiol-021115-105011 78:505–531
158. Pfanner N, van der Laan M, Amati P, Capaldi RA, Caudy AA, Chacinska A, Darshi M, Deckers M, Hoppins S, Icho T, Jakobs S, Ji J, Kozjak-Pavlovic V, Meisinger C, Odgren PR, Park SK, Rehling P, Reichert AS, Sheikh MS, Taylor SS, Tsuchida N, van der Bliek AM, van der Klei IJ, Weissman JS, Westermann B, Zha J, Neupert W, Nunnari J (2014) Uniform nomenclature for the mitochondrial contact site and cristae organizing system. J Cell Biol 204:1083
159. Prasai K (2017) Regulation of mitochondrial structure and function by protein import: A current review. Pathophysiology 24:107–122
160. Presgraves SP, Ahmed T, Borwege S, Joyce JN (2004) Terminally differentiated SH-SY5Y cells provide a model system for studying neuroprotective effects of dopamine agonists. Neurotox Res 5:579–598
161. Prince FP (2002) Lamellar and tubular associations of the mitochondrial cristae: unique forms of the cristae present in steroid-producing cells. Mitochondrion 1:381–389
162. Rabl R, Soubannier V, Scholz R, Vogel F, Mendl N, Vasiljev-Neumeyer A, Körner C, Jagasia R, Keil T, Baumeister W, Cyrklaff M, Neupert W, Reichert AS (2009) Formation of cristae and crista junctions in mitochondria depends on antagonism between Fcj1 and Su e/g. J Cell Biol 185:1047
163. Rampelt H, Zerbes RM, van der Laan M, Pfanner N (2017) Role of the mitochondrial contact site and cristae organizing system in membrane architecture and dynamics. Biochimica et Biophysica Acta (BBA) - Molecular Cell Research 1864:737–746
164. Rampelt H, Wollweber F, Gerke C, de Boer R, van der Klei IJ, Bohnert M, Pfanner N, van der Laan M (2018) Assembly of the Mitochondrial Cristae Organizer Mic10 Is Regulated by Mic26–Mic27 Antagonism and Cardiolipin. J Mol Biol 430:1883–1890
165. Rampelt H, Sucec I, Bersch B, Horten P, Perschil I, Martinou JC, Van Der Laan M, Wiedemann N, Schanda P, Pfanner N (2020) The mitochondrial carrier pathway transports non-canonical substrates with an odd number of transmembrane segments. BMC Biol 18:
166. Rampelt H, Wollweber F, Licheva M, de Boer R, Perschil I, Steidle L, Becker T, Bohnert M, van der Klei I, Kraft C, van der Laan M, Pfanner N (2022) Dual role of Mic10 in mitochondrial cristae organization and ATP synthase-linked metabolic adaptation and respiratory growth. Cell Rep 38:
167. Rao VS, Srinivas K, Sujini GN, Kumar GNS (2014) Protein-Protein Interaction Detection: Methods and Analysis. Int J Proteomics 2014:1–12
168. Reichert AS, Neupert W (2002) Contact sites between the outer and inner membrane of mitochondria—role in protein transport. Biochimica et Biophysica Acta (BBA) - Molecular Cell Research 1592:41–49
169. Revel JP, Fawcett DW, Philpott CW OBSERVATIONS ON MITOCHONDRIAL STRUCTURE Angular Configurations of the Cristae.
170. Rosano TG, Jones DH (1976) Developmental changes in mitochondria during the transition into lactation in the mouse mammary gland. J Cell Biol 69:573–580
171. Rose S, Frye RE, Slattery J, Wynne R, Tippett M, Pavliv O, Melnyk S, James SJ (2014) Oxidative Stress Induces Mitochondrial Dysfunction in a Subset of Autism Lymphoblastoid

Cell Lines in a Well-Matched Case Control Cohort. PLoS One 9:85436
172. Ross2 RA, Biedler JL (1985) Presence and Regulation of Tyrosinase Activity in Human Neuroblastoma Cell Variants in Vitro1. Cancer Res 45:1628–1632
173. Rottenberg H, Covian R, Trumpower BL (2009) Membrane potential greatly enhances superoxide generation by the cytochrome bc1 complex reconstituted into phospholipid vesicles. J Biol Chem 284:19203–19210
174. Rottenberg H (2023) The Reduction in the Mitochondrial Membrane Potential in Aging: The Role of the Mitochondrial Permeability Transition Pore. Int J Mol Sci 24:12295
175. Russell BE, Whaley KG, Bove KE, Labilloy A, Lombardo RC, Hopkin RJ, Leslie ND, Prada C, Assouline Z, Barcia G, Bouchereau J, Chomton M, Debray D, Dorboz I, Durand P, Gaignard P, Habes D, Jardel C, Labarthe F, Lévy J, Lombès A, Mehler-Jacob C, Melki J, Menvielle L, Munnich A, Mussini C, Pichard S, Rio M, Rötig A, Sissaoui S, Slama A, Miethke AG, Schiff M (2019) Expanding and Underscoring the Hepato-Encephalopathic Phenotype of QIL1/MIC13. Hepatology 70:1066–1070
176. Saddar S, Stuart RA (2005) The yeast F(1)F(0)-ATP synthase: analysis of the molecular organization of subunit g and the importance of a conserved GXXXG motif. J Biol Chem 280:24435–24442
177. Sakowska P, Jans DC, Mohanraj K, Riedel D, Jakobs S, Chacinska A (2015) The Oxidation Status of Mic19 Regulates MICOS Assembly. Mol Cell Biol 35:4222
178. Salewskij K, Rieger B, Hager F, Arroum T, Duwe P, Villalta J, Colgiati S, Richter CP, Psathaki OE, Enriquez JA, Dellmann T, Busch KB (2020) The spatio-temporal organization of mitochondrial F1FO ATP synthase in cristae depends on its activity mode. Biochim Biophys Acta Bioenerg 1861:
179. Sánchez E, Lobo T, Fox JL, Zeviani M, Winge DR, Fernández-Vizarra E (2013) LYRM7/MZM1L is a UQCRFS1 chaperone involved in the last steps of mitochondrial Complex III assembly in human cells. Biochim Biophys Acta Bioenerg 1827:285–293
180. Sastri M, Darshi M, Mackey M, Ramachandra R, Ju S, Phan S, Adams S, Stein K, Douglas CR, Kim JJ, Ellisman MH, Taylor SS, Perkins GA (2017) Sub-mitochondrial localization of the genetic-tagged mitochondrial intermembrane space-bridging components Mic 19, Mic60 and Sam50. J Cell Sci 130:3248–3260
181. Schäfer E, Seelert H, Reifschneider NH, Krause F, Dencher NA, Vonck J (2006) Architecture of Active Mammalian Respiratory Chain Supercomplexes. Journal of Biological Chemistry 281:15370–15375
182. Schägger H, Pfeiffer K (2000) Supercomplexes in the respiratory chains of yeast and mammalian mitochondria. EMBO J 19:1777–1783
183. Schindelin J, Arganda-Carreras I, Frise E, Kaynig V, Longair M, Pietzsch T, Preibisch S, Rueden C, Saalfeld S, Schmid B, Tinevez JY, White DJ, Hartenstein V, Eliceiri K, Tomancak P, Cardona A (2012) Fiji - an Open Source platform for biological image analysis. Nat Methods 9:676–682
184. Serricchio M, Bütikofer P (2021) A Conserved Mitochondrial Chaperone-Protease Complex Involved in Protein Homeostasis. Front Mol Biosci 8:
185. Shang Y, Sun X, Chen X, Wang Q, Wang EJ, Miller E, Xu R, Pieper AA, Qi X (2022) A CHCHD6–APP axis connects amyloid and mitochondrial pathology in Alzheimer's disease. Acta Neuropathol 144:911
186. Sheng ZH (2014) Mitochondrial trafficking and anchoring in neurons: New insight and implications. J Cell Biol 204:1087
187. Shiota T, Imai K, Qiu J, Hewitt VL, Tan K, Shen HH, Sakiyama N, Fukasawa Y, Hayat S, Kamiya M, Elofsson A, Tomii K, Horton P, Wiedemann N, Pfanner N, Lithgow T, Endo T (2015) Molecular architecture of the active mitochondrial protein gate. Science 349:1544–1548
188. Shipley MM, Mangold CA, Szpara ML (2016) Differentiation of the SH-SY5Y Human Neuroblastoma Cell Line. J Vis Exp 2016:
189. Smith Eble K, Coleman WB, Hantgan RR, Cunningham CC (1990) Tightly associated cardiolipin in the bovine heart mitochondrial ATP synthase as analyzed by 31P nuclear magnetic resonance spectroscopy. Journal of Biological Chemistry 265:19434–19440

190. Smith RA, Ord MJ (1983) Mitochondrial form and function relationships in vivo: their potential in toxicology and pathology. Int Rev Cytol 83:63–134
191. SOLS A, CRANE RK (1954) SUBSTRATE SPECIFICITY OF BRAIN HEXOKINASE. Journal of Biological Chemistry 210:581–595
192. Steffen J, Vashisht AA, Wan J, Jen JC, Claypool SM, Wohlschlegel JA, Koehler CM (2017) Rapid degradation of mutant SLC25A46 by the ubiquitin-proteasome system results in MFN1/2-mediated hyperfusion of mitochondria. Mol Biol Cell 28:600
193. Stephan T, Brüser C, Deckers M, Steyer AM, Balzarotti F, Barbot M, Behr TS, Heim G, Hübner W, Ilgen P, Lange F, Pacheu-Grau D, Pape JK, Stoldt S, Huser T, Hell SW, Möbius W, Rehling P, Riedel D, Jakobs S (2020) MICOS assembly controls mitochondrial inner membrane remodeling and crista junction redistribution to mediate cristae formation. EMBO J 39:
194. Stojanovski D, Milenkovic D, Müller JM, Gabriel K, Schulze-Specking A, Baker MJ, Ryan MT, Guiard B, Pfanner N, Chacinska A (2008) Mitochondrial protein import: precursor oxidation in a ternary complex with disulfide carrier and sulfhydryl oxidase. J Cell Biol 183:195–202
195. Stoldt S, Wenzel D, Hildenbeutel M, Wurm CA, Herrmann JM, Jakobs S (2012) The inner-mitochondrial distribution of Oxa1 depends on the growth conditions and on the availability of substrates. Mol Biol Cell 23:2292
196. Stoll EA, Makin R, Sweet IR, Trevelyan AJ, Miwa S, Horner PJ, Turnbull DM (2015) Neural Stem Cells in the Adult Subventricular Zone Oxidize Fatty Acids to Produce Energy and Support Neurogenic Activity. Stem Cells 33:2306–2319
197. Stroh A, Anderka O, Pfeiffer K, Yagi T, Finel M, Ludwig B, Schägger H (2004) Assembly of respiratory complexes I, III, and IV into NADH oxidase supercomplex stabilizes complex I in Paracoccus denitrificans. J Biol Chem 279:5000–5007
198. Stroud DA, Surgenor EE, Formosa LE, Reljic B, Frazier AE, Dibley MG, Osellame LD, Stait T, Beilharz TH, Thorburn DR, Salim A, Ryan MT (2016) Accessory subunits are integral for assembly and function of human mitochondrial complex I. Nature 2016 538:7623 538:123–126
199. Tang J, Zhang K, Dong J, Yan C, Hu C, Ji H, Chen L, Chen S, Zhao H, Song Z (2019) Sam50–Mic19–Mic60 axis determines mitochondrial cristae architecture by mediating mitochondrial outer and inner membrane contact. Cell Death & Differentiation 2019 27:1 27:146–160
200. Tateo I, Tohoru I, Yukie M, Fumio H, Kazuhiko K, Nobuo T (1994) A novel human gene that is preferentially transcribed in heart muscle. Gene 144:301–306
201. Urbach J, Kondadi AK, David C, Naha R, Deinert K, Reichert AS, Anand R (2021) Conserved GxxxG and WN motifs of MIC13 are essential for bridging two MICOS subcomplexes. Biochimica et Biophysica Acta (BBA) - Biomembranes 1863:183683
202. Vafai SB, Mootha VK (2012) Mitochondrial disorders as windows into an ancient organelle. Nature 2012 491:7424 491:374–383
203. van der Laan M, Horvath SE, Pfanner N (2016) Mitochondrial contact site and cristae organizing system. Curr Opin Cell Biol 41:33–42
204. Varabyova A, Topf U, Kwiatkowska P, Wrobel L, Kaus-Drobek M, Chacinska A (2013) Mia40 and MINOS act in parallel with Ccs1 in the biogenesis of mitochondrial Sod1. FEBS J 280:4943–4959
205. Vercellino I, Sazanov LA (2021) The assembly, regulation and function of the mitochondrial respiratory chain. Nature Reviews Molecular Cell Biology 2021 23:2 23:141–161
206. Violitzi F, Perivolidi VI, Thireou T, Grivas I, Haralambous S, Samiotaki M, Panayotou G, Douni E (2019) Mapping Interactome Networks of DNAJC11, a Novel Mitochondrial Protein Causing Neuromuscular Pathology in Mice. J Proteome Res 18:3896–3912
207. Vogel F, Bornhövd C, Neupert W, Reichert AS (2006) Dynamic subcompartmentalization of the mitochondrial inner membrane. J Cell Biol 175:237
208. von der Malsburg K, Müller JM, Bohnert M, Oeljeklaus S, Kwiatkowska P, Becker T, Loniewska-Lwowska A, Wiese S, Rao S, Milenkovic D, Hutu DP, Zerbes RM, Schulze-Specking A, Meyer HE, Martinou JC, Rospert S, Rehling P, Meisinger C, Veenhuis M,

Warscheid B, van der Klei IJ, Pfanner N, Chacinska A, van der Laan M (2011) Dual role of mitofilin in mitochondrial membrane organization and protein biogenesis. Dev Cell 21:694–707
209. Wagner OI, Lifshitz J, Janmey PA, Linden M, McIntosh TK, Leterrier JF (2003) Mechanisms of Mitochondria-Neurofilament Interactions. The Journal of Neuroscience 23:9046
210. Wai T, Langer T (2016) Mitochondrial Dynamics and Metabolic Regulation. Trends in Endocrinology and Metabolism 27:105–117
211. Walker JE, Walker JE (1998) ATP Synthesis by Rotary Catalysis (Nobel lecture)**. Angew Chem Int Ed 37:
212. Wallace DC (1982) Structure and evolution of organelle genomes. Microbiol Rev 46:208–240
213. Weber TA, Koob S, Heide H, Wittig I, Head B, van der Bliek A, Brandt U, Mittelbronn M, Reichert AS (2013) APOOL Is a Cardiolipin-Binding Constituent of the Mitofilin/MINOS Protein Complex Determining Cristae Morphology in Mammalian Mitochondria. PLoS One 8:63683
214. Weckbecker D, Longen S, Riemer J, Herrmann JM (2012) Atp23 biogenesis reveals a chaperone-like folding activity of Mia40 in the IMS of mitochondria. EMBO J 31:4348–4358
215. Weinhäupl K, Lindau C, Hessel A, Wang Y, Schütze C, Jores T, Melchionda L, Schönfisch B, Kalbacher H, Bersch B, Rapaport D, Brennich M, Lindorff-Larsen K, Wiedemann N, Schanda P (2018) Structural Basis of Membrane Protein Chaperoning through the Mitochondrial Intermembrane Space. Cell 175:1365-1379.e25
216. Wheatley DN (1968) Mitochondrial tubules in the rat adrenal cortex. J Anat 103:151–154
217. Wiedemann N, Kozjak V, Chacinska A, Schönfisch B, Rospert S, Ryan MT, Pfanner N, Meisinger C (2003) Machinery for protein sorting and assembly in the mitochondrial outer membrane. Nature 424:565–571
218. Wilkins HM, Swerdlow RH (2017) Amyloid Precursor Protein Processing and Bioenergetics. Brain Res Bull 133:71
219. Wilkins HM, Troutwine BR, Menta BW, Manley SJ, Strope TA, Lysaker CR, Swerdlow RH (2022) Mitochondrial Membrane Potential Influences Amyloid Precursor Protein Localization and Aβ Secretion. J Alzheimers Dis 85:381
220. Williams KP, Sobral BW, Dickerman AW (2007) A robust species tree for the alphaproteobacteria. J Bacteriol 189:4578–4586
221. Williams RJP (2000) Mitochondria and chloroplasts: localized and delocalized bioenergetic transduction. Trends Biochem Sci 25:479
222. Wilson R, Gundamaraju R, Vemuri R, Angelucci C, Geraghty D, Gueven N, Eri RD (2020) Identification of Key Pro-Survival Proteins in Isolated Colonic Goblet Cells of Winnie, a Murine Model of Spontaneous Colitis. Inflamm Bowel Dis 26:80–92
223. Wittig I, Braun HP, Schägger H (2006) Blue native PAGE. Nat Protoc 1:418–428
224. Wollweber F, von der Malsburg K, van der Laan M (2017) Mitochondrial contact site and cristae organizing system: A central player in membrane shaping and crosstalk. Biochimica et Biophysica Acta (BBA) - Molecular Cell Research 1864:1481–1489
225. Wurm CA, Jakobs S (2006) Differential protein distributions define two sub-compartments of the mitochondrial inner membrane in yeast. FEBS Lett 580:5628–5634
226. Xicoy H, Wieringa B, Martens GJM (2017) The SH-SY5Y cell line in Parkinson's disease research: a systematic review. Mol Neurodegener 12:1–11
227. Xie HR, Hu L Sen, Li GY (2010) SH-SY5Y human neuroblastoma cell line: In vitro cell model of dopaminergic neurons in Parkinson's disease. Chin Med J (Engl) 123:1086–1092
228. Xie J, Marusich MF, Souda P, Whitelegge J, Capaldi RA (2007) The mitochondrial inner membrane protein Mitofilin exists as a complex with SAM50, metaxins 1 and 2, coiled-coil-helix coiled-coil-helix domain-containing protein 3 and 6 and DnaJC11. FEBS Lett 581:3545–3549
229. Yamamoto H, Fukui K, Takahashi H, Kitamura S, Shiota T, Terao K, Uchida M, Esaki M, Nishikawa SI, Yoshihisa T, Yamano K, Endo T (2009) Roles of Tom70 in import of presequence-containing mitochondrial proteins. J Biol Chem 284:31635–31646
230. Yan C, Duanmu X, Zeng L, Liu B, Song Z (2019) Mitochondrial DNA: Distribution, Mutations, and Elimination. Cells 8:

231. Ylikallio E, Suomalainen A (2012) Mechanisms of mitochondrial diseases. https://doi.org/103109/078538902011598547 44:41–59
232. Youle RJ, Van Der Bliek AM (2012) Mitochondrial fission, fusion, and stress. Science 337:1062–1065
233. Youle RJ, Van Der Bliek AM (2012) Mitochondrial Fission, Fusion, and Stress. Science 337:1062
234. Yuan A, Rao M V., Veeranna, Nixon RA (2012) Neurofilaments at a glance. J Cell Sci 125:3257–3263
235. Yuan A, Rao M V., Veeranna, Nixon RA (2017) Neurofilaments and Neurofilament Proteins in Health and Disease. Cold Spring Harb Perspect Biol 9:
236. Zeharia A, Friedman JR, Tobar A, Saada A, Konen O, Fellig Y, Shaag A, Nunnari J, Elpeleg O (2016) Mitochondrial hepato-encephalopathy due to deficiency of QIL1/MIC13 (C19orf70), a MICOS complex subunit. Eur J Hum Genet 24:1778–1782
237. Zerbes RM, Der Klei IJV, Veenhuis M, Pfanner N, Laan M Van Der, Bohnert M (2012) Mitofilin complexes: Conserved organizers of mitochondrial membrane architecture. Biol Chem 393:1247–1261
238. Zerbes RM, Höß P, Pfanner N, Van Der Laan M, Bohnert M (2016) Distinct Roles of Mic12 and Mic27 in the Mitochondrial Contact Site and Cristae Organizing System. J Mol Biol 428:1485–1492
239. Zhang H, Chen P, Zeng H, Zhang Y, Peng H, Chen Y, He Z (2013) Protective Effect of Demethylation Treatment on Cigarette Smoke Extract–Induced Mouse Emphysema Model. J Pharmacol Sci 123:159–166
240. Zhang YW, Thompson R, Zhang H, Xu H (2011) APP processing in Alzheimer's disease. Mol Brain 4:3
241. Zheng X, Boyer L, Jin M, Mertens J, Kim Y, Ma L, Ma L, Hamm M, Gage FH, Hunter T (2016) Metabolic reprogramming during neuronal differentiation from aerobic glycolysis to neuronal oxidative phosphorylation. Elife 5:
242. Zheng Y, Gibb AA, Xu H, Liu S, Hill BG (2023) The metabolic state of the heart regulates mitochondrial supercomplex abundance in mice. Redox Biol 63:
243. Immt - MICOS complex subunit Mic60 - Mus musculus (Mouse) | UniProtKB | UniProt. URL: https://www.uniprot.org/uniprotkb/Q8CAQ8/entry#sequences
244. IMMT - MICOS complex subunit MIC60 - Homo sapiens (Human) | UniProtKB | UniProt. URL: https://www.uniprot.org/uniprotkb/Q16891/entry#sequences

7. Abbreviations

$\Delta\psi_m$	mitochondrial membrane potential
F_1	F_1 fraction of the mitochondrial ATP synthase
F_o	ooligomycin-sensitive fraction the the mitochondrial ATP synthase
µg	microgram
µl	microliters
µM	micromoles per liter
a.u.	arbitrary units
AD	Alzheimer's disease
ADOA	autosomal dominant optic atrophy
ADP	adenosine diphosphate
AML12	alpha mouse liver 12
ANT	adenine nucleotide translocase
APP	amyloid precursor protein
ATP	adenosine triphosphate
ATRA	all-trans retinoic acid
Aβ	β-amyloid
BDNF	brain-derived neurotrophic factor
BN-PAGE	blue native polyacrylamide gel electrophoresis
CC	coiled-coil domain
CCDC127	coiled-coil domain containing 127
CHCH	coiled-coil helix coiled-coil helix domain
CJ	crista junction
CL	cardiolipin
CM	crista membrane
Cx9C	coiled-coil helix coiled-coil helix domain
df	degree of freedom
DMEM	Dulbecco's Modified Eagle Medium
DNA	deoxyribonucleic acid
DNAJC11	DnaJ Heat Shock Protein Family Member C11
DRP1	Dynamin-related protein 1
DUF	domain of unknown function
e.g.	exempli gratia
ECAR	extracellular acidification rate
EPR	electron paramagnetic resonance

ER	endoplasmic reticulum
ESR	electron spin resonance
FCCP	carbonyl cyanide-p-trifluoromethoxy phenylhydrazone
FLAG	octapeptide (DYKDDDDK) protein tag for affinity purification
GDP-DH	Glyceraldehyde 3-phosphate dehydrogenase
GFP	green fluorescent protein
GTP	guanosine triphosphate
h	hours
HEK	human embryonic kidney
HK	hexokinase
Hsp	heat shock protein
IBM	inner boundary membrane
IF	Intermediate filament
IgG	immunoglobulin G
IMM	inner mitochondrial membrane
IMS	intermembrane space
iPSC	induced pluripotent stem cell
kDa	kilo-Dalton
KO	knockout
KSS	Kearns-Sayre syndrome
LDH	lactate dehydrogenase
LHON	Leber's hereditary optic neuropathy
LS	Leigh syndrome
M	moles per liter
mA	milliampere
MAP2	microtubule-associated protein 2
MELAS	Mitochondrial encephalomyopathy, lactic acidosis, and stroke-like episodes
MFN	Mitofusin
Mgm1	mitochondrial genome maintenance protein 1
MIA	mitochondrial intermembrane space import and assembly pathway
MIB	mitochondrial intermembrane space bridging complex
MICOS	mitochondrial contact site and cristae organising system
MICx	subunit of the MICOS complex, x = molecular weight in kDa
min	minutes
mM	millimoles per liter
MM	mitochondrial matrix
mPh	milipotential/-power of hydrogen

mRNA	messenger ribonucleic acid
mtCK	mitochondrial creatine kinase
mtDNA	mitochondrial DNA
mtTFA	mitochondrial transcription factor A
mV	millivolt
NAD	Nicotinamide adenine dinucleotide
NAFLD	non-alcoholic fatty liver disease
NeuN	neuronal nuclear antigen
NF	Neurofilament
NFH	Neurofilament H
NGF	Nerve growth factor
nm	nanometres
NSE	neuron-specific enolase
OCR	oxygen consumption rate
OMA1	overlapping activity with m-AAA protease 1
OMM	outer mitochondrial membrane
OPA1	optic atrophy 1 protein
Oxa1	oxidase assembly protein 1
OXPHOS	oxidative phosphorylation
p value	probability value
PBS	phosphate buffer saline
PC	phosphatidylcholine
PE	phosphatidylethanolamine
pH	potential/power of hydrogen
PI	phosphatidylinositol
PKM	pyruvate kinase muscle
pmol	picomoles
POTRA	polypeptide transport-associated domain
Protein A	C-terminal protein tag for affinity purifications, also contains TEV cleavage site and hepta-histidine tag
PS	phosphatidylserine
PTP	permeability transition pore
px	pixel
RA	retinoic acid
RKO	colorectal cancer
RNA	ribonucleic acid
ROS	reactive oxygen species

rpm	revolutions per minute
rRNA	ribosomal ribonucleic acid
SAM	sorting and assembly machinery
SD	standard deviation
SDH	Succinyl dehydrogenase
SDS-PAGE	sodium dodecyl sulphate polyacrylamide gel electrophoresis
sgRNA	single guide ribonucleic acid
siRNA	small interfering ribonucleic acid
SLC25A46	Solute Carrier Family 25 Member 46
TBS	Tris-buffered saline
TCA cycle	tricarboxylic acid cycle
TIM	translocase of the inner membrane
TMRE	Tetramethylrhodamine
TOM	translocase of the outer membrane
tRNA	transfer ribonucleic acid
V	Volt
v/v	volume per volume
VDAC	voltage-dependent anion channel
w/v	weight per volume
WT	wildtype
x g	unit of relative centrifugal force
YME1L	yeast mitochondrial escape 1-like ATPase

8. List of figures

9. List of tables

10. Acknowledgements

First and foremost, this thesis results from work conducted in the research laboratory of Prof. Dr. Martin van der Laan at Saarland University Medical Centre in Homburg. I am deeply grateful for providing the opportunity to pursue my thesis without any previous research experience whatsoever and giving the chance to prove myself.

Thank you to all members of the van der Laan lab, without you, this work would not have been possible. I would like to express my greatest appreciation for Dr. Karina von der Malsburg, who provided guidance at all steps along the way. Thank you for all your kindness, patience and time, no matter how mundane or absurd the matter. Sincere thanks to Dr. Alexander von der Malsburg who greatly boosted my immunofluorescence skills and was always happy to jump into content discussions. Eva Bohnert, who acquainted me with crucial lab competencies right in the beginning of my journey, thank you for not losing hope after seeing my lack of talent for calculating rules of three. I had the pleasure to work with two amazing lab technicians, Sybille Jungbluth and Katja Noll, who do an incredible job at keeping the lab running smoothly and saved my experiments more than once from stupid mistakes. In addition, thanks to Lina, who joined my journey along the way as my office mate, with whom I could discuss major and minor issues of daily lab-life. I'd like to appreciate all the members of the Mick-lab, with whom we shared our facilities with, for providing a great working atmosphere, sharing equipment, and solving the occasional software problem.

Moreover, I would like to express profound gratitude to Annika, Amrei, and Geraldine, who never failed to lift my spirits when my cells died once over again. Not to mention my roommates, who leniently listened to my daily progress reports about two newly written sentences. Daniela, I am eternally grateful for your ability to always believe in me. And most importantly, huge thank you to my parents and my sister, who partied all my highs and suffered through all my lows with me never losing trust in my abilities and faith in me.

Finally, one last sushi for everyone:

11. Curriculum vitae

Aus datenschutzrechtlichen Gründen wird der Lebenslauf in der elektronischen Fassung der Dissertation nicht veröffentlicht.